NUMERICAL MODELLING OF THE DEFORMATION OF ELASTIC MATERIAL BY THE TLM METHOD

PHILIP LANGLEY

PhD

HULL UNIVERSITY

1997

NAME...*P. Langley*...DEPARTMENT...*E. Eng*...DEGREE...*PhD*

THE UNIVERSITY OF HULL

Deposit of thesis in accordance with Senate Minute 131, 1955/56,

141, 1970/1 and 343, 1988/89

I...*Philip Langley*...hereby give my consent that a copy of my thesis

Numerical modelling of the Deformation of Geologic materials by the Tlm method.

If accepted for the degree of---*PhD*---in the University of Hull and thereafter deposited in the University Library shall be available for consultation, interlibrary loan and photocopying at the discretion of the University Librarian

Signature...*P. Langley*

If, by reason of special circumstances, the author wishes to withold for a period of not more than five years from the date of the degree being awarded the consent required by Senate, and if for similar reasons he or she does not wish details of the thesis to be included in the University Library's catalogues or forwarded to any indexing or abstraction organisation, he or she should complete and sign sections (1) and (2) below, as appropriate

(1) I wish access to my thesis to be witheld until...for

the following reason..

Signature...............................

(2) I further wish that full details of the title and subject of my thesis are not to be included in the University Library's catalogues or forwarded to any indexing or abstracting organisation until...for the following reason

....

Signature...............................

IN THE EVENT OF THIS FORM NOT BEING RETURNED TO THE POSTGRADUATE OFFICE WITH THE THESIS, IT WILL BE ASSUMED THAT THE AUTHOR CONSENTS TO THE THESIS BEING MADE AVAILABLE, FULLY CATALOGUED AND DETAILS NOTED TO ANY APPROPRIATE INDEXING OR ABSTRACTING ORGANISATIONS

Abstract

The transmission line matrix (TLM) method is a numerical tool for the solution of wave and diffusion type equations. The application of TLM to physical phenomena such as heat flow and electromagnetic wave propagation is well established. A previous attempt to apply TLM models to the area of elastic wave propagation and elastic deformation had limited success. The work of this thesis extends the application base of TLM to the area of elastic deformation modelling and validates the model for several two-dimensional situations. In doing this it has been necessary to develop new nodal structures which facilitate the scaling of differential coefficients and incorporation of cross derivatives. Nodal structures which allow the modelling of two and three-dimensional, and anisotropic, elastic deformation are described.

The technique is demonstrated by applying the elastic deformation model to several elastic problems. These include two-dimensional isotropic models and models of anisotropic elastic deformation. Provision is also made for the application of various boundary conditions which include displacement, force and frictional boundaries.

Keywords: TLM, elastic deformation, anisotropic elasticity.

Acknowledgements

To Ellie Langley,

whose love and friendship render the rest of the world insignificant.

Contents

Appendix

Introduction

The aim of this work is to extend the application of TLM to modelling the deformation of elastic material. Previous work, modelling transient stress waves by the TLM method, showed limited success [Boston I E, 1992], and TLM models of bending via a viscoelastic mechanism have shown excellent agreement with experimental data [Newton H R, 1994].

This thesis presents a method of elastic deformation modelling using TLM and contains the following chapters.

Chapter one, entitled, TLM - History, Theory and Applications, gives a thorough introduction to the TLM method in terms of its history, theoretical development and applications.

Chapter two lays the theoretical groundwork for elastic deformation. The fundamental quantities, elasticity, stress and strain are examined. Consideration of generalised Hooke's law and Newton's second law of motion leads to the development of the equations of motion for elastic bodies. Mathematical description is given also to the boundaries of bodies.

Chapter three records the development of the standard two-dimensional TLM wave nodal structure to one that is applicable to modelling the equations of motion for elastic bulk material. This includes the incorporation of scaled impedance transmission lines which allow the modelling of scaled spatial derivatives, and the incorporation of additional transmission lines configured so that spacial cross derivatives may be modelled. Both enhancements are prerequisite for modelling the

elastic equations of motion using TLM. The technique is extended to include models of anisotropic materials.

Chapter four describes the implementation of boundary conditions in the TLM elastic deformation model. Consideration is given to displacement, force and frictional boundary conditions. Since the implementation of the force boundary condition described requires discretisation of the boundary equations through the use of difference equations, the effects on the stability of such boundaries are investigated.

Having described the TLM elastic deformation model in chapters three and four, the solutions to several elastic problems, as modelled by the TLM method, are presented in chapter five. The examples chosen illustrate the application of the TLM model to a variety of problems including a semi-infinite plate, a two-dimensional problem with frictional contact and several anisotropic examples.

Chapter six, provides an extension to the technique for three dimensional analysis and concludes the thesis with a summary and evaluation of the work, together with a discussion of what future enhancements might be appropriate to the TLM elastic deformation model.

1

TLM - History, Theory and Applications

1.1 Introduction

This chapter presents an overview of the TLM method in terms of its history, theoretical background, and applications. The historical overview presents developments made in TLM modelling from the time of its conception to present day. Principal researchers in various fields of TLM are identified, and the section gives an insight into the application of TLM. The theoretical overview describes the general TLM algorithm and analyses the two-dimensional shunt nodal structure to demonstrate its application in wave and diffusion problems. Analysis is carried out using lumped network analysis and the discrete TLM-state space analogy. The application of TLM to two physical processes, electromagnetic wave propagation and heat diffusion, is demonstrated.

1.2 Historical Overview

The TLM (Transmission Line Matrix or Transmission Line Modelling) method originated in the early nineteen seventies and is a development of the use of electrical networks, network analysers, to solve electromagnetic field problems [Johns P B, Beurle R L, 1971]. The major difference between the network analyser method and TLM is that the network analyser is only spatially discretised whereas TLM is discretised in time and space and as such the method can easily be implemented on digital computer. The first publication concerning TLM is a paper entitled "Numerical solution of 2-dimensional scattering problems using a transmission-line matrix", by Johns and Beurle which appeared in the Proceedings of the Institution of

Electrical Engineers in September 1971. The paper deals with the solution of Maxwell's equations in two dimensions by TLM, and solutions to some waveguide problems are presented. Thus, TLM found initial application in the area of electromagnetics following on from which numerous developments have been reported in this area. For example: extension to three-dimensional electromagnetic field analysis [Akhtarzad S, Johns P B, 1974]; the solution of inhomogeneous waveguide problems [Johns P B, 1974]; consideration of anisotropic media [Mariki G E, Yeh C, 1985]; alternative nodal structures [Johns P B, 1987] and dispersion analysis [Huber C, Krumpholz M, Russer P, 1995]. Further application for the TLM wave equation model came with the extension to modelling acoustic waves [Orme E A, Johns P B, Arnold J M, 1988], [Saleh A H M, Blanchfield P, 1990], and ultrasonics [Pomeroy S C, Williams H R, Blanchfield P B, 1991] and [Zhang G, Wykes C, Pomeroy S C, 1991]. The first published work on modelling elastic deformation appeared in 1992 [Boston I E, 1992]. This work gave a valuable insight into the problems associated with modelling elastic deformation and led to the present work and associated papers [Langley P, Pulko S H, Wilkinson A J, 1994], [Langley P, Wilkinson A J, Pulko S H, 1995] and [Langley P, Pulko S H, Wilkinson A J, 1996], which describe a new method of modelling the elastic deformation of materials using an extended TLM wave model.

A major development in expanding the application of TLM came with the work entitled "A simple explicit and unconditionally stable numerical routine for the solution of the diffusion equation" by Johns which was published in the International Journal of Numerical Methods in 1977. This paper describes how the TLM technique can be used to model the diffusion equation, as a result of which the modelling of various diffusion processes by Johns and other researchers was undertaken. Examples of such work are, the solution of moving boundary heat problems [Butler G, Johns P B, 1979], modelling of heat transfer in foodstuffs [Johns P B, Pulko S H, 1987], thermal distributions in electronic components [de

Cogan D, Henini M, 1987], mass diffusion in semiconductors [Pulko S H, Phizacklea C P, 1989] and modelling the deformation of vitreous china ware during firing [Newton H R *et al*, 1994]. As in the case of the wave application, the technique has been extended to three-dimensions [Pulko S H, Johns P B, 1987] and consideration given to anisotropic media [Witwit A R M, 1994]. The modelling of coupled phenomena has been reported, whereby coupled heat and mass diffusion models are used to describe the interdependence of aqueous diffusivity and temperature in a drying process [Newton H R, Pulko S H, 1991].

Complementing the work produced by researchers in the fields of waves and diffusion is the work undertaken by many researchers in the area of meshing. Much of this work is concerned with allowing the TLM mesh more accurately to approximate the dimensions of the modelled region. Examples of such work for electromagnetic applications include: the modelling of waveguides with curved boundaries [Johns P B, Slater G F, 1973], orthogonal curvilinear meshes [Meliani H, de Cogan D, Johns P B, 1988] and new boundary descriptions [Chen Z, Ney M M, Hoefer W J R, 1991] and [Jaycocks R, Pomeroy S C, 1996]. Similarly, in the area of diffusion modelling examples include: general curvilinear orthogonal meshes [Austin J D, Pulko S H, 1993] and new nodal structures and boundary treatments [Witwit A R M, Pulko S H, 1996]. Other work has concentrated on reducing the computational effort required for models, either by reducing the number of nodes for a given problem, or by manipulation of the time step over the course of the modelling period. Work by Al-Mukhtar and Sitch describes TLM models of waveguides with irregular graded space so that corner regions and slot lines can be modelled by a suitably fine mesh, while the remaining regions are modelled by an appropriate coarse mesh [Al-Mukhtar D A, Sitch J E, 1981]. In the area of diffusion, variable meshing has been described such that the temperature of bodies of complex geometry can be modelled efficiently while retaining the accuracy of the standard fine meshes [Pulko S H, Mallik A, Johns P B, 1986]. Substructuring of

diffusion models in both time and space is another technique in this area. Spatial substructuring is similar to variable meshing without the limitation of the necessity for continuous transmission lines in the modelled region. Temporal substructuring allows a more appropriate choice of time step for particular regions within the body [Pulko S H, Halleron I A, Phizacklea C P, 1990]. Automatic time stepping has been described and parameters relating to monitoring of timestepping errors have been devised [Pulko S H, Mallik A, Allen R, Johns P B, 1990], [Enders P, de Cogan D, 1993] and [Russell I A D, Webb P W, 1996].

TLM has found application in the area of network analysis of electrical circuits. Network components, capacitors and inductors, are modelled by open and short circuit stub transmission lines and non-linear components such as transistors by transmission lines [Johns P B, O'Brien M, 1980]. Development of this technique has lead, for example, to the simulation of an induction motor and associated drive circuitry [Selhi H, Christopoulos C, Howe A F, 1995] and to models of distributed amplifiers [Stubbs D M, Pulko S H, Wilson B, 1995] and [Stubbs D M, Pulko S H, Wilson B, 1996]. The diversity of application of the TLM technique is demonstrated by the many engineering applications referred to above and also by several none engineering applications. Such work includes modelling the dynamics of populations of simple species [S H Pulko *et al*, 1992]. Research has been carried out also into the accuracy of the TLM method and its relationship to other numerical techniques [P B Johns, 1977][P B Johns, G Butler, 1983], [Simons N R S, Bridges E, 1991] and [Simons N R S, Sebak A A, 1992]. General texts on the theory and application of TLM can be found in [Johns P B, 1979], [Hoefer W J R, 1989] and [Christopoulos C, 1995].

Presently there is a strong research community in the area of TLM. Publications suggest that work continues in several areas: developing new applications for the technique, as in this work; versatile meshing and analysis tools [Witwit A R M,

Wilkinson A J, Pulko S H, 1995]; distributed and parallel implementations [So P P M, Eswarappa C, and Hoefer W J R, 1995] and [Parsons P J, Jaques S R, Pulko S H, Rabbi F A, 1996]; and TLM specific computer hardware [Stothard D, Pomeroy S C, Sillitoe I P W, 1995].

1.3 Theoretical Overview

1.3.1 Introduction

TLM is a numerical technique which is able to describe several classes of wave and diffusion phenomena. Initially the technique involves the discretisation of the modelled region by approximating that region with an array, or arrays, of transmission lines which intersect at nodes, the transmission lines being of length Δl, the space step. This is referred to as a TLM mesh. Frequently the TLM mesh is coincident with a reference co-ordinate frame and in general the space step may be different in each of the co-ordinate directions.

The computational routine involves an iterative process, whereby temporal discretisation is achieved by incrementing the time variable at each iteration by Δt, the time step. During each time increment, pulses are transmitted along the transmission lines such that they become incident on adjacent nodes. Each node has associated with it a potential which is calculated in terms of the incident pulses according to equation (1.1).

$$_k\Phi_n = \left[\sum_l \frac{2\,_kV_{n,l}^i}{(R_l + Z_l)} \right] \frac{1}{Y} \qquad \text{where } Y = \sum_l \frac{1}{(R_l + Z_l)} \qquad (1.1)$$

In expression (1.1), $_k\Phi_n$ is the potential of node n at iteration k, $_kV_{n,l}^i$ is the pulse incident on node n along transmission line l, R_l and Z_l are the resistance and impedance of transmission line l. The nodal potential is constant over the time step. Incident pulses instantaneously give rise to reflected pulses from nodes which are calculated in terms of the nodal potential and the incident pulse on the transmission line according to

$$_kV_{n,l}^r = {}_k\Phi_n \frac{Z_l}{(R_l + Z_l)} + {}_kV_{n,l}^i \frac{(R_l - Z_l)}{(R_l + Z_l)} \qquad (1.2)$$

$_kV_{n,l}^r$ is the pulse reflected from node n along transmission line l due to incident pulse $_kV_{n,l}^i$. The reflected pulses are transmitted to adjacent nodes in the TLM mesh. This completes one cycle of the iterative routine which is repeated until the desired modelling period is achieved. Thus the technique is discrete in both time and space. It is also apparent that models involving the fundamental node are, in their implementation, one step, explicit and unconditionally stable [Johns P B, 1977]. The TLM technique described above is implemented on a digital computer. Generally, array variables hold values of nodal potential, reflected and incident pulses. Scatter routines effect the transmission of reflected pulses to adjacent nodes. Nodal potentials and reflected pulses are calculated according to (1.1) and (1.2). Visualisation of the process as a mesh of interconnected transmission lines, aids our understanding of the process, and extensive use of transmission line connection and nodal structure illustrations are made throughout this thesis.

1.3.2 Lumped network analysis

In order to understand how the application of the above technique models various phenomena it is necessary to analyse the TLM building block - the transmission line.

A transmission line may be defined as a device for transmitting or guiding energy from one point to another and under this general definition there are many examples of transmission lines. Here we are concerned with two conductor transmission lines which can be modelled by the equivalent circuit shown in figure 1.1 [Kraus J D, 1989][1]. The equivalent circuit shows that a two conductor transmission line can be modelled by ideal conductors connecting distributed values of resistance, inductance and capacitance.
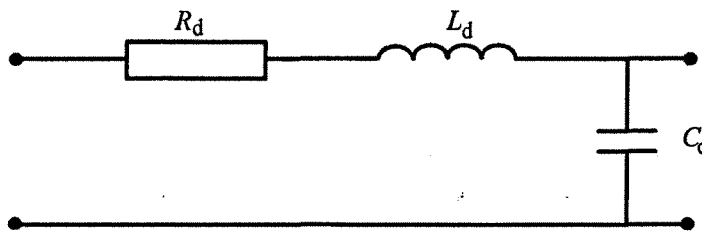
Figure 1.1 Equivalent Circuit of a section of Transmission Line

A TLM model consists of a number of transmission lines intersecting at nodes as illustrated in figure 1.2, where the inductance and capacitance of the equivalent circuit model are represented by link line impedance Z.

Figure 1.2 shows a typical two-dimensional TLM shunt nodal structure consisting of two transmission lines intersecting at a common node at position x = i, y = j, the

---

[1] A full model of a transmission line includes shunt conductance G. Here the analysis assumes no shunt conductance, however shunt conductance may be incorporated by use of stubs [Hoefer W J R, 1989].

transmission lines forming connections with adjacent nodes in the mesh. The equivalent circuit for this structure is shown in figure 1.3.
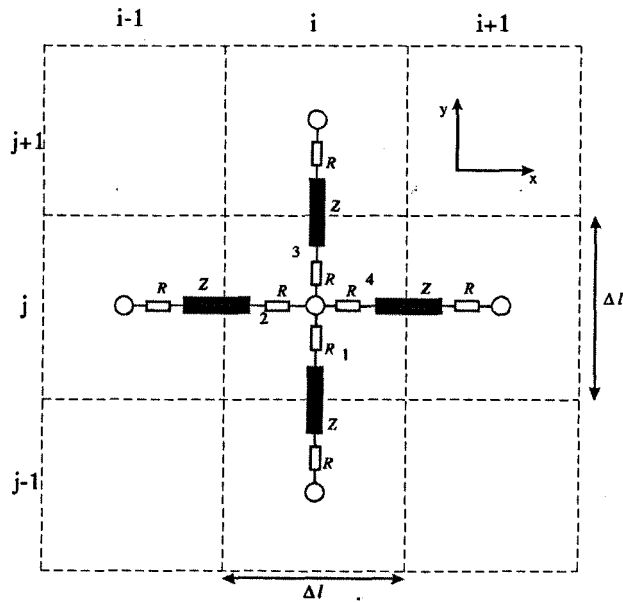
Figure 1.2 General two-dimensional TLM node

Figure 1.3 represents the lumped element model of the TLM node shown in figure 1.2 [Johns P B, 1977]. The following analysis of the lumped element circuit leads to equations which describe the dynamic behaviour of the nodal structure.

Considering the current flows indicated in figure 1.3 and applying Kirchoff's current law gives

$$I_x + \frac{\partial I_x}{\partial x} \Delta l - I_x + I_y + \frac{\partial I_y}{\partial y} \Delta l - I_y + I_c = 0 \qquad (1.3)$$
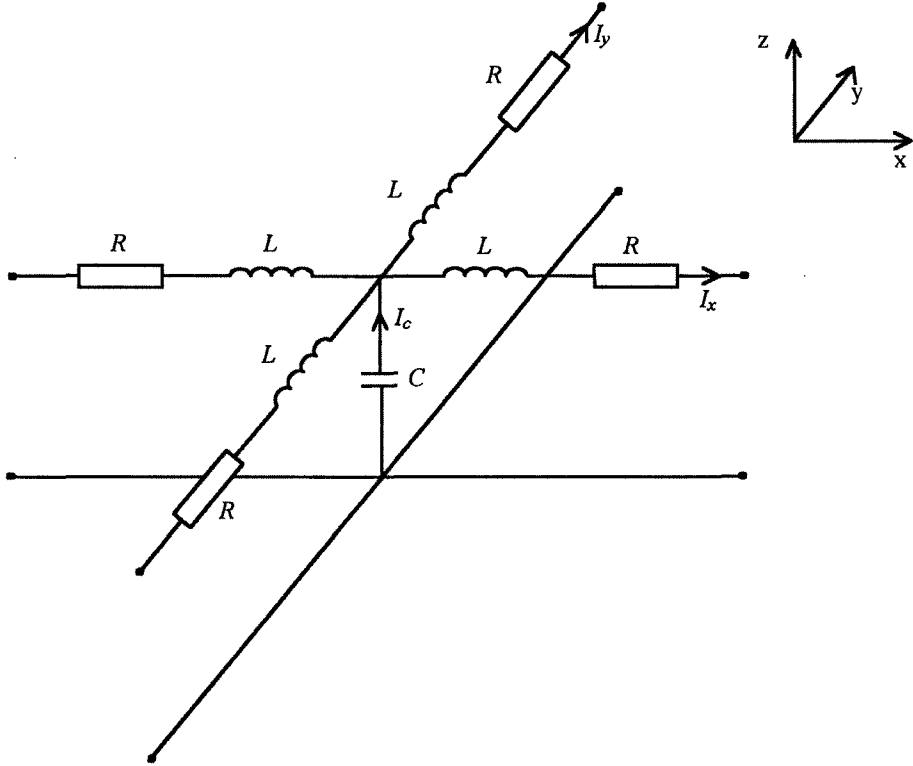
Figure 1.3 Equivalent circuit of the two-dimensional TLM shunt node

Simplifying (1.3) gives

$$\frac{\partial I_x}{\partial x}\Delta l + \frac{\partial I_y}{\partial y}\Delta l = -I_c \tag{1.4}$$

where Δl is the length of the transmission lines and corresponds to the elemental size of the TLM node.

Using the current/voltage relationship for a capacitor, the current through the capacitor can be expressed in terms of the voltage across it as

$$I_c = C\frac{\partial V_z}{\partial t} \tag{1.5}$$

11

where V_z is the voltage across the capacitor, and C is the sum of the capacitances of the individual transmission lines due to their parallel connection. If the capacitance per unit length of transmission line is C_d then the capacitance of a single transmission line is $C_d\Delta l$ and the total capacitance for the circuit, as represented by the single capacitor in figure 1.3, is given by

$$C = 2C_d\Delta l \tag{1.6}$$

Substituting (1.6) into (1.5) gives

$$I_c = 2C_d\Delta l \frac{\partial V_z}{\partial t} \tag{1.7}$$

and substituting (1.7) into (1.4) gives

$$\frac{\partial I_x}{\partial x} + \frac{\partial I_y}{\partial y} = -2C_d \frac{\partial V_z}{\partial t} \tag{1.8}$$

With reference to figure 1.3, the voltage drop across each transmission line is given by the sum of the voltages dropped across each of the inductors and resistors.

The voltage drop across an inductor is described by

$$V_l = L\frac{\partial I}{\partial t} \tag{1.9}$$

12

and the voltage drop across a resistor by

$$V_r = RI \qquad (1.10)$$

where R is the resistance, L is the inductance and I represents current.

Since each resistor and inductor represents the resistance and inductance of a transmission line of length $\Delta l/2$, and R_d and L_d are the resistance and inductance per unit length, L and R may be expressed in terms of their distributed quantities as

$$L = L_d \frac{\Delta l}{2} \qquad (1.11)$$

$$R = R_d \frac{\Delta l}{2} \qquad (1.12)$$

Applying these equations to the circuit of figure 1.3, and considering the voltage drop across each transmission line, the following expressions are obtained

$$\frac{\partial V_z}{\partial x} \Delta l = -L_d \Delta l \frac{\partial I_x}{\partial t} - R_d \Delta l I_x$$

$$\frac{\partial V_z}{\partial y} \Delta l = -L_d \Delta l \frac{\partial I_y}{\partial t} - R_d \Delta l I_y \qquad (1.13)$$

Having derived expressions which describe the behaviour of nodal voltage (V_z) with respect to time (1.8) and space (1.13), it is left to combine these equations to give the complete relationship in terms of nodal voltage only.

Differentiating (1.8) with respect to time

13

$$\frac{\partial^2 I_x}{\partial x \partial t} + \frac{\partial^2 I_y}{\partial y \partial t} = -2C_d \frac{\partial^2 V_z}{\partial t^2} \qquad (1.14)$$

and (1.13) with respect to x and y gives

$$\frac{\partial^2 V_z}{\partial x^2} \Delta l = -L_d \Delta l \frac{\partial^2 I_x}{\partial x \partial t} - R_d \Delta l \frac{\partial I_x}{\partial x}$$
$$\frac{\partial^2 V_z}{\partial y^2} \Delta l = -L_d \Delta l \frac{\partial^2 I_y}{\partial y \partial t} - R_d \Delta l \frac{\partial I_y}{\partial y} \qquad (1.15)$$

Expressions (1.14) and (1.15) can be combined to provide an equation which describes the spatial and temporal variation of nodal voltage, V_z. Rearranging (1.15)

$$\frac{\partial^2 I_x}{\partial x \partial t} = -\frac{R_d}{L_d} \frac{\partial I_x}{\partial x} - \frac{1}{L_d} \frac{\partial^2 V_z}{\partial x^2}$$
$$\frac{\partial^2 I_y}{\partial y \partial t} = -\frac{R_d}{L_d} \frac{\partial I_y}{\partial y} - \frac{1}{L_d} \frac{\partial^2 V_z}{\partial y^2} \qquad (1.16)$$

and substituting (1.16) into (1.14) gives

$$-\frac{1}{L_d}\left(\frac{\partial^2 V_z}{\partial x^2} + \frac{\partial^2 V_z}{\partial y^2}\right) - \frac{R_d}{L_d}\left(\frac{\partial I_x}{\partial x} + \frac{\partial I_y}{\partial y}\right) = -2C_d \frac{\partial^2 V_z}{\partial t^2} \qquad (1.17)$$

substituting (1.8) into expression (1.17) gives

$$-\frac{1}{L_d}\left(\frac{\partial^2 V_z}{\partial x^2} + \frac{\partial^2 V_z}{\partial y^2}\right) + 2\frac{R_d C_d}{L_d} \frac{\partial V_z}{\partial t} = -2C_d \frac{\partial^2 V_z}{\partial t^2} \qquad (1.18)$$

Rearranging,

$$\frac{\partial^2 V_z}{\partial x^2} + \frac{\partial^2 V_z}{\partial y^2} = 2 R_d C_d \frac{\partial V_z}{\partial t} + 2 L_d C_d \frac{\partial^2 V_z}{\partial t^2} \qquad (1.19)$$

Equation (1.19) is often referred to as the telegrapher's equation. It is of the form of a lossy wave equation, and describes the dynamic behaviour of the lumped parameter circuit of figure 1.3.

To relate the lumped parameter model (figure 1.3) to the two-dimensional TLM nodal structure (figure 1.2), a relationship between the fundamental parameters, link line impedance, space step and time step, of the TLM nodal structure, and the capacitive and inductive impedances of the lumped parameter model, must be derived.

The velocity of waves along a single transmission line is given by the equation [Kraus J D, 1989]

$$v = \frac{1}{\sqrt{L_d C_d}} \qquad (1.20)$$

The velocity of pulses from one node to the next in the TLM mesh is

$$v = \frac{\Delta l}{\Delta t} \qquad (1.21)$$

Thus

$$\frac{1}{\sqrt{L_d C_d}} = \frac{\Delta l}{\Delta t} \qquad (1.22)$$

15

From which can be obtained

$$L_d = \frac{\Delta t^2}{C_d \Delta l^2}$$

$$C_d = \frac{\Delta t^2}{L_d \Delta l^2}$$

(1.23)

The characteristic impedance of a transmission line is given by [Kraus J D, 1989]

$$Z = \sqrt{\frac{L_d}{C_d}}$$

(1.24)

from which the following equations for inductance and capacitance can be obtained

$$L_d = Z^2 C_d$$

$$C_d = \frac{L_d}{Z^2}$$

(1.25)

Substituting (1.25) into (1.23) gives

$$L_d = Z \frac{\Delta t}{\Delta l}$$

$$C_d = \frac{1}{Z} \frac{\Delta t}{\Delta l}$$

(1.26)

and the distributed parameters are expressed solely in terms of the TLM parameters Z, the link line impedance, Δt, the time step and Δl, the space step. Recalling also that $R_d = \frac{2R}{\Delta l}$ (derived from equation 1.12), the telegrapher's equation (1.19) can be expressed in terms of the TLM parameters as

16

$$\frac{\partial^2 V_z}{\partial x^2} + \frac{\partial^2 V_z}{\partial y^2} = 4 \frac{R}{Z} \frac{\Delta t}{\Delta l^2} \frac{\partial V_z}{\partial t} + 2 \frac{\Delta t^2}{\Delta l^2} \frac{\partial^2 V_z}{\partial t^2} \qquad (1.27)$$

Thus, the nodal structure shown in figure 1.2 is able to model phenomena with a mathematical description given by equation (1.27). The nodal potential (V_z) provides the solution variable for the network. The following section describes the application of the TLM nodal structure to wave and diffusion models.

1.3.2.1 Wave and diffusion equation models

Equation (1.27) is a lossy wave equation. By suitable choice of model parameters it is possible to model lossy waves, lossless waves and diffusion processes. Considering (1.27), it can be seen that if the first derivative with respect to time is small compared with the second derivative with respect to time, then the equation is predominantly a wave equation. If the resistance is zero, then the equation modelled by the standard two-dimensional nodal structure is

$$\frac{\partial^2 V_z}{\partial x^2} + \frac{\partial^2 V_z}{\partial y^2} = 2 \frac{\Delta t^2}{\Delta l^2} \frac{\partial^2 V_z}{\partial t^2} \qquad (1.28)$$

The mesh wave velocity is

$$v_m = \frac{1}{\sqrt{2 \frac{\Delta t^2}{\Delta l^2}}} = \frac{1}{\sqrt{2}} \frac{\Delta l}{\Delta t} \qquad (1.29)$$

which compares with an elementary transmission line wave velocity of

$$v = \frac{\Delta l}{\Delta t} \qquad (1.30)$$

Thus waves propagate across the TLM mesh at a velocity $1/\sqrt{2}$ times that of a single loss free transmission line [Johns P B, Beurle R L, 1971]. It can be seen from (1.29) that the model wave speed, v_m, is determined solely by the time and space step chosen for the model.

Returning to equation (1.27), it can be seen that if the second derivative with respect to time is small compared with the first derivative with respect to time, then the equation is predominantly a diffusion equation. To make the diffusion equation dominate, Δt must be small. Given that

$$4 \frac{R}{Z} \frac{\Delta t}{\Delta l^2} \frac{\partial V_z}{\partial t} >> 2 \frac{\Delta t^2}{\Delta l^2} \frac{\partial^2 V_z}{\partial t^2} \tag{1.31}$$

then

$$\frac{\partial^2 V_z}{\partial x^2} + \frac{\partial^2 V_z}{\partial y^2} \approx 4 \frac{R}{Z} \frac{\Delta t}{\Delta l^2} \frac{\partial V_z}{\partial t} \tag{1.32}$$

Thus, the TLM node of figure 1.2 is able to model both wave and diffusion processes. Although this analysis is two-dimensional, the same analysis carried out in one or three dimensions yields the one and three dimensional telegrapher's equation respectively.

1.3.2.2 Propagation analysis and dispersion

Propagation analysis has been carried out for the TLM routine when modelling wave [Johns P B, 1971] and diffusion processes [Johns P B, 1977]. The fundamental assumption when using lumped network analysis is that the voltages and currents are continuous across adjacent nodes. This assumption is valid only if the space step is small compared with the wavelength of the process being modelled [Hoefer W J R, 1989]. Johns and Beurle have shown that for one-dimensional wave propagation,

if the ratio of space step to wavelength approaches 1/4, then waves propagate at a velocity of 1/2 times that of a single transmission line, and not as indicated by the lumped network analysis, which predicts a mesh velocity of $1/\sqrt{2}$ times that of a single transmission line [Johns P B, Beurle R L, 1971]. In fact the lumped network analysis prediction is valid only if the space step is zero or the wavelength is infinite, and only for propagation in the direction of the transmission line. The velocity of propagation on the mesh is dependent upon the frequency and direction of the waves on the mesh, and as such is dispersive and anisotropic [Simons N R S, Sebak A A, 1992], this being a result of the discretising process. However, if the ratio of space step to wavelength is small (< 1/10) then the lumped network prediction is a valid approximation and velocity errors due to dispersion are small (<2%) [Christopoulos C, 1995].

The lumped network analysis of the previous section results in continuous space and time differential equations, yet TLM is discrete in both time and space. Hence this analysis represents a model of a model and is perhaps not the most appropriate for the TLM algorithm [Johns P B, 1979]. Discrete analysis of the TLM algorithm has been carried out and will be presented in the following section.

1.3.3 TLM-State space analysis

1.3.3.1 Introduction

The TLM method is discrete in both space and time. Lumped network analysis, as described previously, is based on a continuous space and time model of transmission lines and as such perhaps is not the most appropriate analysis tool for the TLM algorithm. Published work describes a discrete analysis tool and applies it to several

TLM nodal structures [Witwit A R M, Wilkinson A J, Pulko S H, 1995]. The following section summarises this work and applies it to the analysis of a two-dimensional TLM node.

1.3.3.2 Discrete state space analysis

Discrete state space analysis describes the behaviour of a discrete system in terms of state variables and inputs to the system. For a linear, time-invariant system the discrete state space description is [Cadzow J A, Martens H R, 1970].

$$\mathbf{x}(k+1) = \mathbf{A}\mathbf{x}(k) + \mathbf{B}\mathbf{u}(k) \tag{1.33}$$

$$y(k) = \mathbf{C}\mathbf{x}(k) + \mathbf{D}\mathbf{u}(k) \tag{1.34}$$

where $\mathbf{x}(k)$ is the state vector at iteration k, $\underline{\mathbf{u}}(k)$ is the input vector and $y(k)$ is the system output. $\mathbf{A}$ is the state transition or system matrix, $\mathbf{B}$ is the input or driving matrix, $\mathbf{C}$ is the output matrix and $\mathbf{D}$ is the direct transmission matrix. Eliminating the state vector from equation (1.34) allows definition of the transfer function of the system. This is achieved by introducing a time shift operator Q [Witwit A R M, 1995] such that (1.33) may be expressed as

$$Q\mathbf{I}\,\mathbf{x}(k) = \mathbf{A}\mathbf{x}(k) + \mathbf{B}\mathbf{u}(k) \tag{1.35}$$

where $\mathbf{I}$ is the unit matrix.

Solving for $\mathbf{x}(k)$ gives

$$\mathbf{x}(k) = (Q\mathbf{I} - \mathbf{A})^{-1}\mathbf{B}u(k) \qquad (1.36)$$

Substituting (1.36) into (1.34) gives

$$y(k) = \mathbf{C}(Q\mathbf{I} - \mathbf{A})^{-1}\mathbf{B}u(k) + \mathbf{D}u(k) \qquad (1.37)$$

or alternatively

$$y(k) = \mathbf{G}u(k) \qquad (1.38)$$

$\mathbf{G}$ is known as the transfer function matrix from which the characteristic equation of the system may be obtained. The characteristic equation describes the dynamic behaviour of the system and is obtained by equating to zero the denominator of the determinant of the transfer function matrix [Witwit A R M, Wilkinson A J, Pulko S H, 1995].

Since

$$\mathbf{G} = \mathbf{C}(Q\mathbf{I} - \mathbf{A})^{-1}\mathbf{B} + \mathbf{D} \qquad (1.39)$$

which can be written

$$\mathbf{G} = \frac{\mathbf{C}(Q\mathbf{I} - \mathbf{A})^{adj}\mathbf{B} + \mathbf{D}|(Q\mathbf{I} - \mathbf{A})|}{|(Q\mathbf{I} - \mathbf{A})|} \qquad (1.40)$$

21

the characteristic equation is given by

$$\left| (Q\mathbf{I} - \mathbf{A}) \right| = 0 \tag{1.41}$$

It can be seen that characteristic equation, and consequently the dynamic behaviour of the system, is governed by $\mathbf{A}$, the state transition matrix.

1.3.3.3 Matrix notation of the TLM equations

The TLM potential and pulse equations for a single node may be expressed in matrix form [Johns P B, 1977]. This notation is useful in developing the TLM-state space analysis and is described here.

Defining $_k\mathbf{V}_n^i$ as a $m \times 1$ column vector of pulses incident on node n at iteration k, where m is the number of transmission lines connected to the node,

$$_k\mathbf{V}_n^i = \begin{bmatrix} V_{n,1}^i \\ V_{n,2}^i \\ V_{n,3}^i \\ \vdots \\ _kV_{n,m}^i \end{bmatrix} \tag{1.42}$$

Also defining $\mathbf{q}$ as a $1 \times m$ row vector, the potential of the node in matrix notation is given by

$$_k\Phi_n = \mathbf{q}\,_k\mathbf{V}_n^i \tag{1.43}$$

Similarly, the equations describing the pulses reflected from the node are given by

$$_k\mathbf{V}_n^r = \mathbf{p}\,_k\Phi_n + \mathbf{r}\,_k\mathbf{V}_n^i \qquad\qquad (1.44)$$

where $_k\mathbf{V}_n^r$ is a $m \times 1$ column vector of pulses reflected from node n at iteration k, $\mathbf{p}$ is a $m \times 1$ column vector and $\mathbf{r}$ is a $m \times m$ diagonal matrix. Substituting expression (1.43) into (1.44), the reflected pulses may be expressed in terms of incident pulses only, giving

$$_k\mathbf{V}_n^r = (\mathbf{pq} + \mathbf{r})\,_k\mathbf{V}_n^i \qquad\qquad (1.45)$$

Alternatively, matrices of incident and reflected pulses may be considered to be related by

$$_k\mathbf{V}_n^r = \mathbf{S}\,_k\mathbf{V}_n^i \qquad\qquad (1.46)$$

where $\mathbf{S}$ is known as the scattering matrix. During the transmission of reflected pulses to adjacent nodes along transmission lines, time Δt elapses, and reflected pulses become incident on adjacent nodes at iteration $k + 1$. Thus, (1.46) may be written in terms of incident pulses,

$$_{k+1}\mathbf{V}_{n\pm1}^i = \mathbf{S}'\,_k\mathbf{V}_n^i \qquad\qquad (1.47)$$

In equation (1.47), $_{k+1}\mathbf{V}_{n\pm1}^i$ is a vector of pulses incident on nodes connected to node n via transmission lines, and $\mathbf{S}'$ is a modified scattering matrix which consists of scattering matrix $\mathbf{S}$ with rows interchanged dependent upon the scattering notation used. An alternative representation of equation (1.47) is possible with the introduction of a space and time shift operator matrix $\mathbf{T}$, giving,

$$T_k V_n^i = S' {}_k V_n^i \qquad (1.48)$$

where **T** is a matrix which describes the direction of scatter of reflected pulses in terms of spatial forward and backward shift operators in each of the co-ordinate directions. It also describes the time increment in terms of a forward shift operator in time. A similar representation is used in [Russer P, Krumpholz M, 1993].

Having stated the state space equations and the matrix notation for the TLM algorithm, the TLM-state space analogy can be described.

Considering the state space equations, summarised for convenience in equations (1.49) and (1.50), and comparing with the TLM matrix equations (1.51) and (1.52), then the TLM-state space analogy is apparent.

$$Q\mathbf{I}\,\mathbf{x}(k) = \mathbf{A}\mathbf{x}(k) + \mathbf{B}\mathbf{u}(k) \qquad (1.49)$$

$$y(k) = \mathbf{C}\mathbf{x}(k) + \mathbf{D}\mathbf{u}(k) \qquad (1.50)$$

$$\mathbf{T}_k V_n^i = \mathbf{S}' {}_k V_n^i \qquad (1.51)$$

$$_k \Phi_n = \mathbf{q}\,_k V_n^i \qquad (1.52)$$

Selecting $_k V_n^i$ as the state vector in the state space analysis and comparing equation (1.49) with (1.51) the following equivalencies may be made:

$$\mathbf{x}(k) \equiv {}_k V_n^i \qquad (1.53)$$

24

$$\mathbf{A} \equiv \mathbf{S'} \tag{1.54}$$

$$Q\mathbf{I} \equiv \mathbf{T} \tag{1.55}$$

Comparing the output equations, (1.50) and (1.52), the following equivalencies may be made:

$$y(k) \equiv {}_k\Phi_n \tag{1.56}$$

$$\mathbf{C} \equiv \mathbf{q} \tag{1.57}$$

It can be seen that the input vector $\mathbf{u}(k)$ is zero.

The characteristic equation corresponding to the TLM structure can be obtained by use of equation (1.41), giving

$$|(\mathbf{T} - \mathbf{S'})| = 0 \tag{1.58}$$

This describes the discrete dynamic behaviour of the nodal structure. The TLM-state space analogy as set out above can be used to verify the discrete representation of nodal structures and is thus a useful tool in the development of new nodal structures.

1.3.3.4 Analysis of a two-dimensional TLM node using state space analysis

To demonstrate the application of the TLM-state space analogy, state space analysis and TLM matrix notation are applied to the same nodal structure considered using lumped network analysis of section 1.3.2.

The template used for numbering of link lines is illustrated in figure 1.4.
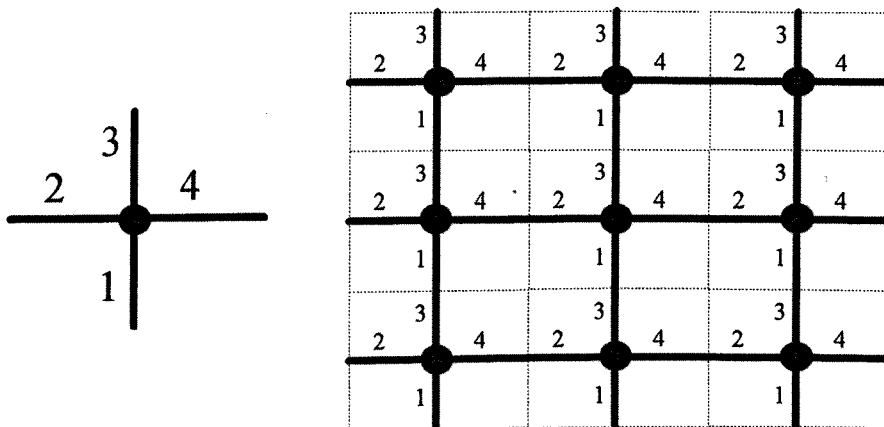
Figure 1.4 Notation used for identification of link lines

This notation is applied to the link lines of the two-dimensional shunt node shown in figure 1.5. Figure 1.5 illustrates a node at position x = *i*, y = *j* with associated transmission lines numbered 1, 2, 3 and 4. Also shown are adjacent nodes which connect to the central node via transmission lines, which again are numbered according to the template described in figure 1.4.
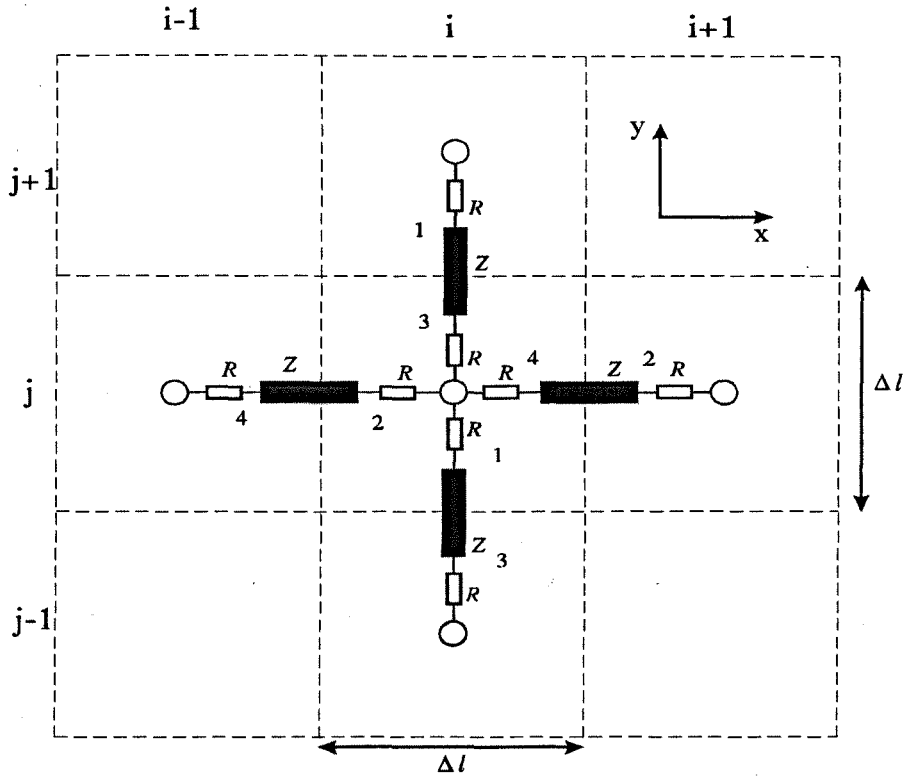
Figure 1.5 Two-dimensional TLM shunt node showing connecting nodes

Each transmission lines has associated with it an incident pulse. The notation for the pulses incident on the node at position (i,j) at iteration k is demonstrated in (1.59).

$$_k\mathbf{V}_{i,j}^i = \begin{bmatrix} V_{i,j,1}^i \\ V_{i,j,2}^i \\ V_{i,j,3}^i \\ V_{i,j,4}^i \end{bmatrix}_k \tag{1.59}$$

Given that, for the node illustrated in figure 1.5, $R_l = R$ and $Z_l = Z$ $(l = 1$ to $4)$, the nodal potential equation, (1.1), may be expressed as

$$_k\Phi_{i,j} = \frac{1}{2}\begin{bmatrix} 1 & 1 & 1 & 1 \end{bmatrix} \begin{bmatrix} V^i_{i,j,1} \\ V^i_{i,j,2} \\ V^i_{i,j,3} \\ V^i_{i,j,4} \end{bmatrix}_k \tag{1.60}$$

from which, when compared with (1.43), $\mathbf{q}$, the output vector, can be identified as

$$\mathbf{q} = \frac{1}{2}\begin{bmatrix} 1 & 1 & 1 & 1 \end{bmatrix} \tag{1.61}$$

Each transmission line has associated with it a reflected pulse. The reflected pulse vector is defined as

$$_k\mathbf{V}^r_{i,j} = \begin{bmatrix} V^r_{i,j,1} \\ V^r_{i,j,2} \\ V^r_{i,j,3} \\ V^r_{i,j,4} \end{bmatrix}_k \tag{1.62}$$

With reference to equation (1.2), the reflected pulse equation for this node structure can be written

$$\begin{bmatrix} V^r_{i,j,1} \\ V^r_{i,j,2} \\ V^r_{i,j,3} \\ V^r_{i,j,4} \end{bmatrix}_k = {}_k\Phi_{i,j} \begin{bmatrix} \dfrac{Z}{R+Z} \\ \dfrac{Z}{R+Z} \\ \dfrac{Z}{R+Z} \\ \dfrac{Z}{R+Z} \end{bmatrix} + \begin{bmatrix} \dfrac{R-Z}{R+Z} & 0 & 0 & 0 \\ 0 & \dfrac{R-Z}{R+Z} & 0 & 0 \\ 0 & 0 & \dfrac{R-Z}{R+Z} & 0 \\ 0 & 0 & 0 & \dfrac{R-Z}{R+Z} \end{bmatrix} \begin{bmatrix} V^i_{i,j,1} \\ V^i_{i,j,2} \\ V^i_{i,j,3} \\ V^i_{i,j,4} \end{bmatrix}_k \tag{1.63}$$

and, when compared with (1.44), $\mathbf{p}$ and $\mathbf{r}$ can be identified as

28

$$\mathbf{p} = \begin{bmatrix} \dfrac{Z}{R+Z} \\[2mm] \dfrac{Z}{R+Z} \\[2mm] \dfrac{Z}{R+Z} \\[2mm] \dfrac{Z}{R+Z} \end{bmatrix} \tag{1.64}$$

and

$$\mathbf{r} = \begin{bmatrix} \dfrac{R-Z}{R+Z} & 0 & 0 & 0 \\[2mm] 0 & \dfrac{R-Z}{R+Z} & 0 & 0 \\[2mm] 0 & 0 & \dfrac{R-Z}{R+Z} & 0 \\[2mm] 0 & 0 & 0 & \dfrac{R-Z}{R+Z} \end{bmatrix} \tag{1.65}$$

With reference to equations (1.45) and (1.46), the state transition or scattering matrix is obtained from $\mathbf{S} = (\mathbf{pq} + \mathbf{r})$, giving

$$\mathbf{S} = \frac{1}{2}\left(\frac{Z}{R+Z}\right)\begin{bmatrix} 1+\dfrac{2}{Z}(R-Z) & 1 & 1 & 1 \\[2mm] 1 & 1+\dfrac{2}{Z}(R-Z) & 1 & 1 \\[2mm] 1 & 1 & 1+\dfrac{2}{Z}(R-Z) & 1 \\[2mm] 1 & 1 & 1 & 1+\dfrac{2}{Z}(R-Z) \end{bmatrix}$$

$$\tag{1.66}$$

Reflected pulses are calculated from expression (1.46), which for this structure may be written

$$\begin{bmatrix} V^r_{i,j,1} \\ V^r_{i,j,2} \\ V^r_{i,j,3} \\ V^r_{i,j,4} \end{bmatrix}_k = \frac{1}{2}\left(\frac{Z}{R+Z}\right)\begin{bmatrix} 1+\frac{2}{Z}(R-Z) & 1 & 1 & 1 \\ 1 & 1+\frac{2}{Z}(R-Z) & 1 & 1 \\ 1 & 1 & 1+\frac{2}{Z}(R-Z) & 1 \\ 1 & 1 & 1 & 1+\frac{2}{Z}(R-Z) \end{bmatrix}\begin{bmatrix} V^i_{i,j,1} \\ V^i_{i,j,2} \\ V^i_{i,j,3} \\ V^i_{i,j,4} \end{bmatrix}_k$$

$$(1.67)$$

After time step Δt, reflected pulses become incident on adjacent nodes. Considering figure 1.5, at iteration k, a reflected pulse from node i,j, on link line number 1, will become incident on link line number 3 of node i,j-1, at iteration $k + 1$. Similarly, a reflected pulse on link line number 2 of node i,j, becomes incident on link line number 4 of node i-1,j, and so on. Thus, the reflected pulses scatter according to

$$\begin{bmatrix} V^i_{i,j-1,3} \\ V^i_{i-1,j,4} \\ V^i_{i,j+1,1} \\ V^i_{i+1,j,2} \end{bmatrix}_{k+1} = \begin{bmatrix} V^r_{i,j,1} \\ V^r_{i,j,2} \\ V^r_{i,j,3} \\ V^r_{i,j,4} \end{bmatrix}_k$$

$$(1.68)$$

Expression (1.67) can now be written as

$$\begin{bmatrix} V^i_{i,j-1,3} \\ V^i_{i-1,j,4} \\ V^i_{i,j+1,1} \\ V^i_{i+1,j,2} \end{bmatrix}_{k+1} = \frac{1}{2}\left(\frac{Z}{R+Z}\right)\begin{bmatrix} 1+\frac{2}{Z}(R-Z) & 1 & 1 & 1 \\ 1 & 1+\frac{2}{Z}(R-Z) & 1 & 1 \\ 1 & 1 & 1+\frac{2}{Z}(R-Z) & 1 \\ 1 & 1 & 1 & 1+\frac{2}{Z}(R-Z) \end{bmatrix}\begin{bmatrix} V^i_{i,j,1} \\ V^i_{i,j,2} \\ V^i_{i,j,3} \\ V^i_{i,j,4} \end{bmatrix}_k \quad (1.69)$$

Rearranging such that the incident pulse link line indices are the same on both sides of the equation, gives

$$
\begin{bmatrix} V^i_{i,j+1,1} \\ V^i_{i+1,j,2} \\ V^i_{i,j-1,3} \\ V^i_{i-1,j,4} \end{bmatrix}_{k+1} = \frac{1}{2}\left(\frac{Z}{R+Z}\right) \begin{bmatrix} 1 & 1 & 1+\frac{2}{Z}(R-Z) & 1 \\ 1 & 1 & 1 & 1+\frac{2}{Z}(R-Z) \\ 1+\frac{2}{Z}(R-Z) & 1 & 1 & 1 \\ 1 & 1+\frac{2}{Z}(R-Z) & 1 & 1 \end{bmatrix}_k \begin{bmatrix} V^i_{i,j,1} \\ V^i_{i,j,2} \\ V^i_{i,j,3} \\ V^i_{i,j,4} \end{bmatrix}_k
$$

<div align="right">(1.70)</div>

from which, with reference to (1.47), the modified scattering matrix, $\mathbf{S}'$, can be identified as

$$
\mathbf{S}' = \frac{1}{2}\left(\frac{Z}{R+Z}\right) \begin{bmatrix} 1 & 1 & 1+\frac{2}{Z}(R-Z) & 1 \\ 1 & 1 & 1 & 1+\frac{2}{Z}(R-Z) \\ 1+\frac{2}{Z}(R-Z) & 1 & 1 & 1 \\ 1 & 1+\frac{2}{Z}(R-Z) & 1 & 1 \end{bmatrix}
$$

<div align="right">(1.71)</div>

Pulses incident on adjacent nodes at iteration $k + 1$, can be related to incident pulses on node i,j, at iteration k, by the expression

$$
\begin{bmatrix} V^i_{i,j+1,1} \\ V^i_{i+1,j,2} \\ V^i_{i,j-1,3} \\ V^i_{i-1,j,4} \end{bmatrix}_{k+1} = \begin{bmatrix} QJ & 0 & 0 & 0 \\ 0 & QI & 0 & 0 \\ 0 & 0 & QJ^{-1} & 0 \\ 0 & 0 & 0 & QI^{-1} \end{bmatrix}_k \begin{bmatrix} V^i_{i,j,1} \\ V^i_{i,j,2} \\ V^i_{i,j,3} \\ V^i_{i,j,4} \end{bmatrix}_k
$$

<div align="right">(1.72)</div>

Q is the time shift operator, representing the time shift from iteration k to $k + 1$. I is the forward shift operator, representing a shift in the x direction from i to $i + 1$. J is the forward shift operator in the y direction from j to $j + 1$. I^{-1} and J^{-1} are the shift operators in the negative direction of x and y respectively.

From (1.72), the space and time shift operator matrix, T, is identified as

$$
\mathbf{T} = \begin{bmatrix} QJ & 0 & 0 & 0 \\ 0 & QI & 0 & 0 \\ 0 & 0 & QJ^{-1} & 0 \\ 0 & 0 & 0 & QI^{-1} \end{bmatrix}
$$

(1.73)

With reference to (1.48), **T** may be incorporated into equation (1.70) giving

$$
\begin{bmatrix} QJ & 0 & 0 & 0 \\ 0 & QI & 0 & 0 \\ 0 & 0 & QJ^{-1} & 0 \\ 0 & 0 & 0 & QI^{-1} \end{bmatrix} \begin{bmatrix} V_{i,j,1}^{i} \\ V_{i,j,2}^{i} \\ V_{i,j,3}^{i} \\ V_{i,j,4}^{i} \end{bmatrix}_{k} = \frac{1}{2}\left(\frac{Z}{R+Z}\right) \begin{bmatrix} 1 & 1 & 1+\frac{2}{Z}(R-Z) & 1 \\ 1 & 1 & 1 & 1+\frac{2}{Z}(R-Z) \\ 1+\frac{2}{Z}(R-Z) & 1 & 1 & 1 \\ 1 & 1+\frac{2}{Z}(R-Z) & 1 & 1 \end{bmatrix} \begin{bmatrix} V_{i,j,1}^{i} \\ V_{i,j,2}^{i} \\ V_{i,j,3}^{i} \\ V_{i,j,4}^{i} \end{bmatrix}_{k}
$$

(1.74)

Having identified the matrices, **T** and **S′**, it is possible to obtain the characteristic equation by use of expression (1.58), which for the nodal structure under consideration is

$$
\left| \begin{bmatrix} QJ & 0 & 0 & 0 \\ 0 & QI & 0 & 0 \\ 0 & 0 & QJ^{-1} & 0 \\ 0 & 0 & 0 & QI^{-1} \end{bmatrix} - \frac{1}{2}\left(\frac{Z}{R+Z}\right) \begin{bmatrix} 1 & 1 & 1+\frac{2}{Z}(R-Z) & 1 \\ 1 & 1 & 1 & 1+\frac{2}{Z}(R-Z) \\ 1+\frac{2}{Z}(R-Z) & 1 & 1 & 1 \\ 1 & 1+\frac{2}{Z}(R-Z) & 1 & 1 \end{bmatrix} \right| = 0
$$

(1.75)

Manipulation of (1.75) by the symbolic mathematics software Mathematica, yields the characteristic equation

$$\left(Q^2(R+Z)^2 - (R-Z)^2\right)$$
$$\left(Q^2 2IJ(R+Z) - QZ\left(J+I+IJ^2 + I^2J\right) + 2IJ(Z-R)\right) = 0$$

$$(1.76)$$

for which there are four solutions, roots of the quadratics

$$\left(Q^2 2IJ(R+Z) - QZ\left(J+I+IJ^2 + I^2J\right) + 2IJ(Z-R)\right) = 0$$

$$(1.77)$$

and

$$\left(Q^2(R+Z)^2 - (R-Z)^2\right) = 0 \qquad (1.78)$$

Considering (1.77), and dividing by QIJ gives

$$\left(2Q(R+Z) - Z\left(J+I+J^{-1}+I^{-1}\right) + 2Q^{-1}(Z-R)\right) = 0 \qquad (1.79)$$

Rearranging so that

$$2R\left(Q-Q^{-1}\right) + 2Z\left(Q+Q^{-1}\right) = Z\left(J+I+J^{-1}+I^{-1}\right) \qquad (1.80)$$

Dividing by Z and subtracting 4 from each side of the equation gives

$$2\frac{R}{Z}\left(Q-Q^{-1}\right) + 2\left(Q-2+Q^{-1}\right) = \left(I-2+I^{-1}\right) + \left(J-2+J^{-1}\right)$$

$$(1.81)$$

33

Recognising the continuous time and discrete time equivalencies, as described in Appendix 1,

$$(I - 2 + I^{-1}) \equiv (\Delta l)^2 \frac{\partial^2}{\partial x^2}$$

$$(J - 2 + J^{-1}) \equiv (\Delta l)^2 \frac{\partial^2}{\partial y^2}$$

$$\left(Q - 2 + Q^{-1}\right) \equiv (\Delta t)^2 \frac{\partial^2}{\partial t^2}$$

$$\left(Q - Q^{-1}\right) \equiv 2 \Delta t \frac{\partial}{\partial t} \tag{1.82}$$

(1.81) can be expressed in continuous time equivalent form as

$$2 \frac{(\Delta t)^2}{(\Delta l)^2} \frac{\partial^2}{\partial t^2} + 4 \frac{(\Delta t)}{(\Delta l)^2} \frac{R}{Z} \frac{\partial}{\partial t} = \frac{\partial^2}{\partial x^2} + \frac{\partial^2}{\partial y^2} \tag{1.83}$$

Equation (1.83) represents a lossy wave equation and is derived by consideration of the TLM algorithm and associated parameters. This is in contrast to the lumped network analysis which utilises an electrical model of the TLM algorithm. The equation resulting from the TLM-state space analogy corresponds to that derived using lumped network analysis, (1.27), and the wave speed and diffusion coefficient are in agreement.

The TLM-state space analogy yields a further solution, that specified in expression (1.78). This solution contains no spacial operators. Factoring (1.78) gives

$$\left(Q + \frac{(R-Z)}{(R+Z)}\right)\left(Q - \frac{(R-Z)}{(R+Z)}\right) \tag{1.84}$$

34

These factors are additional poles of the characteristic equation and represent "spurious solutions". These solutions, resulting from the discretisation process, have been reported by workers investigating dispersion in TLM structures, for example, [Trenkic V, Benson T M, Christopoulos C, 1995] and [Huber C, Krumpholz M, Russer P, 1995], and are common to a number of numerical techniques [Schroeder W, Wolff I, 1994]. The knowledge of the accuracy of these TLM nodal structures in the solution of wave and diffusion type equations, suggests that the solution representing the discretised wave/diffusion equation, specified in (1.80), is dominant, and the additional poles have little or no effect on the behaviour of TLM in solving diffusion and wave type problems. However, a full analysis of these solutions may provide additional information about the TLM method.

1.3.4 Stub transmission lines

Stub transmission lines were introduced by Johns for the solution of inhomogeneous waveguide problems, and have become widely used in both wave [Johns P B, 1974] and diffusion [Pulko S H, Johns P B, 1987] TLM applications. Incorporation of stub lines into a model allows flexibility in choice of time and space step for a given problem, and enables the convenient modelling of inhomogenity. An open circuit stub line placed at a node represents additional shunt capacitance for the node. A stub length of $\Delta l/2$ ensures time synchronisation with the rest of the TLM network, since a pulse transmitted from a node along a stub transmission line, is reflected from the open circuit end, to become incident on the node from which it was transmitted, time Δt later.

Considering the wave application of the stub loaded node only, figure 1.6 illustrates a two-dimensional TLM shunt node with stub line. The stub resistance is shown only for generality and has the value zero [Johns P B, 1977].
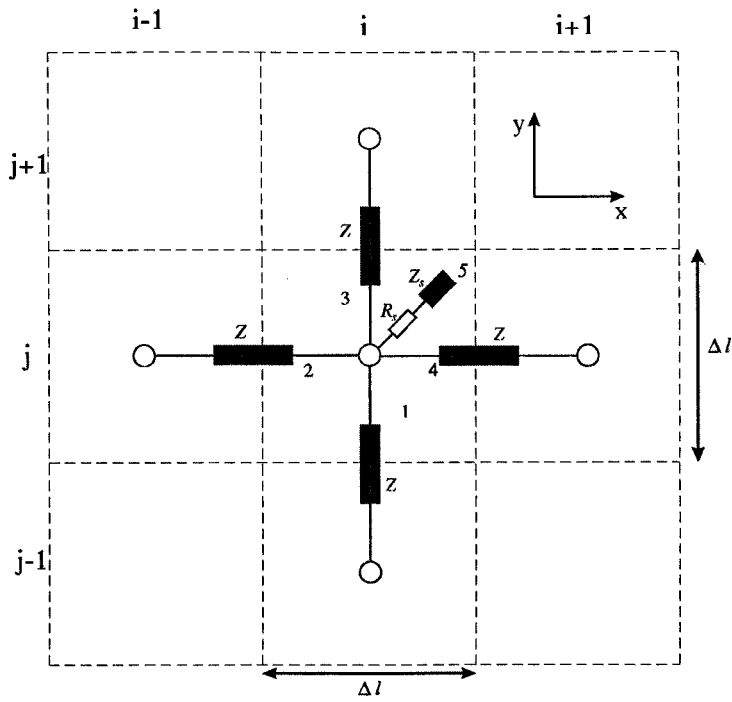
Figure 1.6 Two-dimensional shunt node with stub

Analysis of this nodal structure, using TLM matrix notation and state space analysis, yields the following expressions.

The output matrix:

$$\mathbf{q} = \frac{2}{(4+y_0)}\begin{bmatrix} 1 & 1 & 1 & 1 & y_0 \end{bmatrix} \qquad (1.85)$$

where y_0 is the normalised characteristic admittance, defined as $\dfrac{Z}{Z_s}$.

Vector **p**:

$$\mathbf{p} = \begin{bmatrix} 1 \\ 1 \\ 1 \\ 1 \\ 1 \end{bmatrix} \qquad (1.86)$$

36

Matrix **r**:

$$\mathbf{r} = \begin{bmatrix} -1 & 0 & 0 & 0 & 0 \\ 0 & -1 & 0 & 0 & 0 \\ 0 & 0 & -1 & 0 & 0 \\ 0 & 0 & 0 & -1 & 0 \\ 0 & 0 & 0 & 0 & -1 \end{bmatrix} \qquad (1.87)$$

The scattering matrix:

$$\mathbf{S} = \frac{1}{4+y_0} \begin{bmatrix} -(2+y_0) & 2 & 2 & 2 & 2y_0 \\ 2 & -(2+y_0) & 2 & 2 & 2y_0 \\ 2 & 2 & -(2+y_0) & 2 & 2y_0 \\ 2 & 2 & 2 & -(2+y_0) & 2y_0 \\ 2 & 2 & 2 & 2 & -(4-y_0) \end{bmatrix} \qquad (1.88)$$

Specifying the notation which describes the scatter of pulses along transmission lines as

$$\begin{bmatrix} V^i_{i,j-1,3} \\ V^i_{i-1,j,4} \\ V^i_{i,j+1,1} \\ V^i_{i+1,j,2} \\ V^i_{i,j,5} \end{bmatrix}_{k+1} = \begin{bmatrix} V^r_{i,j,1} \\ V^r_{i,j,2} \\ V^r_{i,j,3} \\ V^r_{i,j,4} \\ V^r_{i,j,5} \end{bmatrix}_{k} \qquad (1.89)$$

the space and time shift operator matrix, **T**, is

$$\mathbf{T} = \begin{bmatrix} QJ & 0 & 0 & 0 & 0 \\ 0 & QI & 0 & 0 & 0 \\ 0 & 0 & QJ^{-1} & 0 & 0 \\ 0 & 0 & 0 & QI^{-1} & 0 \\ 0 & 0 & 0 & 0 & Q \end{bmatrix} \qquad (1.90)$$

37

The modified scattering matrix is

$$
\mathbf{S'} = \frac{1}{4+y_0}
\begin{bmatrix}
2 & 2 & -(2+y_0) & 2 & 2y_0 \\
2 & 2 & 2 & -(2+y_0) & 2y_0 \\
-(2+y_0) & 2 & 2 & 2 & 2y_0 \\
2 & -(2+y_0) & 2 & 2 & 2y_0 \\
2 & 2 & 2 & 2 & -(4-y_0)
\end{bmatrix}
\tag{1.91}
$$

Having obtained expressions for **T** and **S'** the characteristic equation is obtained by use of the symbolic mathematics package, Mathematica, as

$$
(Q-1)(Q+1)^2\left((Q^2+1)(y_0+4)-2Q(I+I^{-1}+y_0+J+J^{-1})\right)=0
$$

$$\tag{1.92}$$

to which there are five solutions, roots of the quadratic

$$
\left((Q^2+1)(y_0+4)-2Q(I+I^{-1}+y_0+J+J^{-1})\right)=0
\tag{1.93}
$$

and the following "spurious solutions"

$$
(Q+1)^2 = 0
\tag{1.94}
$$

$$
(Q-1) = 0
\tag{1.95}
$$

The quadratic solution contains spacial and temporal differences and yields the equivalent continuous time and space wave equation

$$\frac{\left(4+y_0\right)}{2}\frac{(\Delta t)^2}{(\Delta l)^2}\frac{\partial^2}{\partial t^2}=\frac{\partial^2}{\partial x^2}+\frac{\partial^2}{\partial y^2} \qquad (1.96)$$

for which the wave speed is given by

$$v_m=\frac{\Delta l}{\Delta t}\sqrt{\frac{2}{4+y_0}} \qquad (1.97)$$

Inclusion of the stub line for the wave application allows flexibility in the choice of time and space step since these are no longer determined by the wave speed of the problem being modelled.

The "spurious solutions" to the characteristic equation are similar to those obtained when analysing the node without a stub. In fact setting R to zero in (1.84) gives the same poles as those for the node with stub, as indicated in (1.94) and (1.95). However, it appears that the incorporation of the stub results in an additional pole at $Q = -1$.

1.4 Application of TLM to wave and diffusion models

1.4.1 Introduction

It has been shown that TLM is able to solve wave and diffusion type equations. Many physical phenomena exhibit wave or diffusion type behaviour, and as such can be modelled using the TLM method. To illustrate how such models are applied, the method will be demonstrated for electromagnetic wave propagation and heat

diffusion problems. Consideration is also given to the treatment of boundaries in these applications

1.4.2 Electromagnetic wave propagation model

By consideration of Maxwell's curl equations it can be shown that the equation which describes the electric field in a rectangular waveguide operating in TE_{n0} mode is given by [Johns P B, Beurle R L, 1971]

$$\mu\varepsilon\frac{\partial^2 E_z}{\partial t^2} = \frac{\partial^2 E_z}{\partial x^2} + \frac{\partial^2 E_z}{\partial y^2} \qquad (1.98)$$

where E_z is the transverse electric field, μ is the permeability and ε the permittivity of the medium in which the wave travels.

The equation modelled by the two-dimensional stub loaded node shown in figure 1.6 is

$$\frac{(4+y_0)}{2}\frac{(\Delta t)^2}{(\Delta l)^2}\frac{\partial^2 \Phi}{\partial t^2} = \frac{\partial^2 \Phi}{\partial x^2} + \frac{\partial^2 \Phi}{\partial y^2} \qquad (1.99)$$

Comparing (1.98) with (1.99), it can be seen that the nodal potential, Φ, in the TLM model is equivalent to the electric field, E_z. The stub impedance in the TLM model is chosen to ensure that the correct wave speed is modelled for a given time and space step according to (1.100).

$$y_0 = \frac{Z}{Z_s} = 2\mu\varepsilon\left(\frac{\Delta l}{\Delta t}\right)^2 - 4 \qquad (1.100)$$

The transmission line impedance, Z, is generally set to unity. Physical meaning often can be interpreted from the TLM model. In this case, the nodal potential is equivalent to the electric field intensity, and the current along transmission line is equivalent to the magnetic field intensity [Johns P B, Beurle R L, 1971].

1.4.3 Thermal diffusion model

Heat propagation through certain materials may be described by the two-dimensional thermal diffusion equation

$$\frac{S\rho}{K} \frac{\partial T}{\partial t} = \frac{\partial^2 T}{\partial x^2} + \frac{\partial^2 T}{\partial y^2} \tag{1.101}$$

where T is temperature, S is specific heat, ρ is density and K is the thermal conductivity of the material.

It has been shown that TLM is able to model equations of the form

$$4\frac{(\Delta t)}{(\Delta l)^2} \frac{R}{Z} \frac{\partial \Phi}{\partial t} = \frac{\partial^2 \Phi}{\partial x^2} + \frac{\partial^2 \Phi}{\partial y^2} \tag{1.102}$$

assuming condition (1.31) is satisfied by appropriate choice of time step, Δt.

Comparing (1.101) with (1.102), it can be seen that the nodal potential, Φ, is equivalent to the temperature, T. The values for R and Z are obtained by equating the diffusion constants in each of the equations.

$$4\frac{(\Delta t)}{(\Delta l)^2}\frac{R}{Z} = \frac{S\rho}{K} \tag{1.103}$$

The resistance and impedance may be calculated in such a way that physical meaning is given to these transmission line parameters. For example, the resistance to heat flow is inversely proportional to the thermal conductivity (K) and the area through which it travels (Δl^2). The thermal resistance is proportional to the distance of flow (Δl) in a given time, (Δt). Thus, the link line resistors, of which there are two in each line, can be specified as

$$2R = \frac{1}{K\Delta l} \tag{1.104}$$

Substituting (1.104) into (1.103) enables the link line impedance to be specified as

$$Z = \frac{2\Delta t}{S\rho\Delta l^3} \tag{1.105}$$

Since the impedance of a TLM diffusion model is assumed to consist of capacitance only (inductance is negligible due to the choice of time step), (1.105) may be written in terms of capacitance. The capacity of the body to store heat is proportional to the specific heat of the body and the mass, from which the capacitance can be expressed as

$$C = s\rho(\Delta l)^3 \tag{1.106}$$

Substituting this into (1.105) gives

$$Z = \frac{2\Delta t}{C}$$

(1.107)

The following section describes the treatment of boundaries in TLM models.

1.4.4 Boundary descriptions

Boundaries terminate meshes and often are the sources of input to the model. Figure 1.7 illustrates a general one-dimensional TLM mesh terminated at a boundary [Johns P B, Pulko, S H, 1986]. The boundary node has only one port which connects to its internal neighbouring node via a transmission line and boundary resistor R_b.

The current flow across the boundary, and through the resistor may be specified by

$$I_b = \frac{\left(V^i - V^r\right)}{Z}$$

(1.108)

and the voltage drop across the resistor by

$$V_d = R_b \frac{\left(V^i - V^r\right)}{Z}$$

(1.109)

and

$$V_d = V^i + V^r - \Phi_b \qquad (1.110)$$
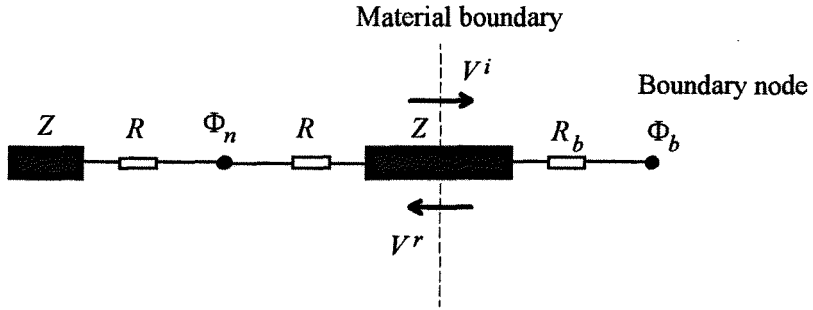
Figure 1.7 Termination of a one-dimensional TLM mesh

Combining (1.109) and (1.110) to derive an expression for the reflected pulse from the boundary yields

$$V^r = \frac{(R_B - Z)}{(R_B + Z)} V^i + \frac{Z}{(R_B + Z)} \Phi_b \qquad (1.111)$$

For the case $R_b = 0$,

$$V_r = \Phi_b - V_i \qquad (1.112)$$

for which, in thermal applications, the boundary represents an infinite sink, or in electromagnetic waves applications represents a short circuit boundary.

44

For the case of R_b infinitely large then

$$V_r = V_i \qquad\qquad (1.113)$$

and the boundary represents a perfect insulator in thermal applications, or in electromagnetic waves applications represents an open circuit boundary. This boundary condition is used also to simulate symmetry boundary conditions within the bulk of a body. For example, with reference to figure 1.7, if $R_b = R$, and $\Phi_b = \Phi_n$, which represents a symmetry boundary condition, then $V_r = V_i$.

Thus, the boundary conditions for a given problem are, in general, represented in TLM by the reflection of pulses from nodes external to the region being modelled, such that the boundary lies half way between an internal node and external node. However, other boundary representations have been reported, both for electromagnetic and diffusion problems, which allow nodes to be positioned directly on the boundary [Chen Z, Ney M M, Hoefer W J R, 1991] and [Witwit A R M, Pulko S H, 1996].

1.5 Summary

This chapter provides an introduction to the TLM technique in terms of its history, theory and applications. The use of the TLM technique in the solution of wave and diffusion equations has been described. Tools have been presented for the analysis of nodal structures, in the form of lumped network analysis and the TLM-state space analogy. These tools are used extensively in the development of a nodal structure suitable for elastic wave application. The following chapter develops the equations

45

relevant to elastic deformation, for which TLM nodal structures, suitable for the solution of these equations, will be developed in subsequent chapters.

2

Elasticity and the Equations of Motion for an Elastic Solid

2.1 Introduction

This chapter presents a definition of elastic materials and ultimately derives the equations of motion for an elastic body. Consideration is given also to boundary conditions which describe how finite elastic bodies interface to their surrounding medium. In developing the equations of motion for an elastic body it is necessary to define the fundamental quantities which describe the deformation of materials, namely, stress and strain.

2.2 Elasticity

When a body is subjected to an applied force the body will deform. The ability of a body to recover from this deformation is called its elasticity. In this thesis consideration is given to materials which recover completely from a deformed shape, that is, bodies which are perfectly elastic [Timoshenko S, 1934]. Many engineering materials can be assumed to be perfectly elastic if the elastic limit of the material is not exceeded. If this limit is exceeded then plastic deformation occurs and the original shape of the body cannot be recovered [Wang C T, 1953].

2.3 Stress

Stress describes the force acting on a part of a body. It is defined as the force per unit area acting on a body which may be expressed as

$$\text{stress} = \lim_{\Delta A \longrightarrow 0} \frac{\Delta F}{\Delta A} \qquad\qquad (2.1)$$

where ΔF is the force acting on the area ΔA. In order to define a stress completely, it is necessary to specify its magnitude, direction and the plane in which it acts. In practical terms, stress is measured relative to a reference co-ordinate frame and, in the general case, will have components along each of the reference axes. Throughout this thesis the Cartesian co-ordinate system will be used since it is appropriate for the rectangular meshes used in the TLM models. Resolving the stresses into components along the co-ordinate axes results in stresses which lie normal to the area under consideration, the *normal* stresses, and stresses which lie in the plane of the area under consideration, the *shear* stresses. The notation used for identification of the stress components is demonstrated in figure 2.1. The normal stresses are denoted by σ_i where i represents the co-ordinate direction in which the stress acts. The shear stresses are denoted by τ_{ij} where i represents the direction of the normal to the plane in which the stress acts, and j represents the direction of the stress [Timoshenko S, 1934].
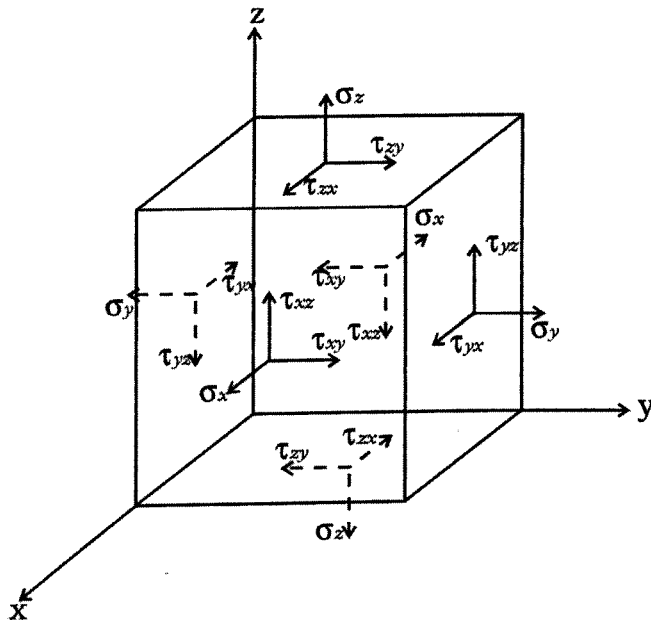
Figure 2.1 Notation for stress components in the Cartesian co-ordinate system

If the cubic element in figure 2.1 is in equilibrium, by considering moments about the centre of the cube, it can be shown that the nine stress components of figure 2.1 are reduced to six components [Mal A K, Singh S J, 1991]. Consider moments about the x axis as shown in figure 2.2.
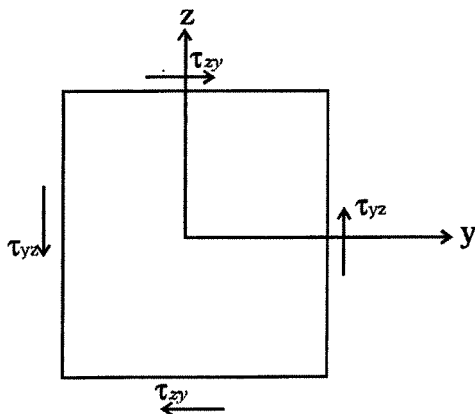
Figure 2.2 Shear stresses on a plane

Under equilibrium the sum of the moments is zero giving

$$2\tau_{zy}(dydx)\frac{dz}{2} - 2\tau_{yz}(dzdx)\frac{dy}{2} = 0 \qquad (2.2)$$

where dx, dy and dz correspond to the dimensions of the cube in each of the co-ordinate directions. Simplifying gives

$$\tau_{zy} = \tau_{yz} \qquad (2.3)$$

Similar analysis applied to equilibrium conditions about the y and z axes results in

$$\tau_{yx} = \tau_{xy} \qquad (2.4)$$

and

$$\tau_{zx} = \tau_{xz} \qquad (2.5)$$

Consequently, the number of stress components is reduced to six.

2.4 Strain

Strain describes the deformation of a body. It quantifies the relative displacement of points in the body. The displacement at a point may have components in each of the reference co-ordinate frame directions. Let the displacement of a point in a body in the x, y and z directions be u, v and w respectively. Then the strains are defined as [Timoshenko S, 1934]

$$\varepsilon_x = \frac{\partial u}{\partial x}, \quad \varepsilon_y = \frac{\partial v}{\partial y}, \quad \varepsilon_z = \frac{\partial w}{\partial z} \qquad (2.6)$$

$$\gamma_{xy} = \frac{\partial v}{\partial x} + \frac{\partial u}{\partial y}, \quad \gamma_{yz} = \frac{\partial v}{\partial z} + \frac{\partial w}{\partial y}, \quad \gamma_{xz} = \frac{\partial w}{\partial x} + \frac{\partial u}{\partial z} \qquad (2.7)$$

where ε_x, ε_y, ε_z are the longitudinal or normal strain components, and γ_{xy}, γ_{yz}, γ_{zx} are the shearing strain components. The fundamental assumption in the derivation of these equations is that the deformation of the body is small [Wang C T, 1953].

50

2.5 Generalised Hooke's Law

2.5.1 Anisotropic materials

Generalised Hooke's Law relates the deformation of an elastic body to the applied forces, through the stresses and strains of the body and its elastic properties. The law is applicable within the proportional elastic limit of the material [Mal A K, Singh S J, 1991]. Generalised Hooke's Law, (2.8) states that each of the six stress components may be expressed as a function of the six components of strain.

$$\sigma_x = c_{11}\varepsilon_x + c_{12}\varepsilon_y + c_{13}\varepsilon_z + c_{14}\gamma_{yz} + c_{15}\gamma_{xz} + c_{16}\gamma_{xy}$$

$$\sigma_y = c_{21}\varepsilon_x + c_{22}\varepsilon_y + c_{23}\varepsilon_z + c_{24}\gamma_{yz} + c_{25}\gamma_{xz} + c_{26}\gamma_{xy}$$

$$\sigma_z = c_{31}\varepsilon_x + c_{32}\varepsilon_y + c_{33}\varepsilon_z + c_{34}\gamma_{yz} + c_{35}\gamma_{xz} + c_{36}\gamma_{xy}$$

$$\tau_{yz} = c_{41}\varepsilon_x + c_{42}\varepsilon_y + c_{43}\varepsilon_z + c_{44}\gamma_{yz} + c_{45}\gamma_{xz} + c_{46}\gamma_{xy} \qquad (2.8)$$

$$\tau_{xz} = c_{51}\varepsilon_x + c_{52}\varepsilon_y + c_{53}\varepsilon_z + c_{54}\gamma_{yz} + c_{55}\gamma_{xz} + c_{56}\gamma_{xy}$$

$$\tau_{xy} = c_{61}\varepsilon_x + c_{62}\varepsilon_y + c_{63}\varepsilon_z + c_{64}\gamma_{yz} + c_{65}\gamma_{xz} + c_{66}\gamma_{xy}$$

The coefficients, c_{ij}, describe the elastic properties of the material. These may be dependent upon position within the body, if the material is inhomogeneous, and may also describe elastic nonlinearity. It can be seen from (2.8) that for the most general case of an anisotropic elastic material, 36 elastic constants are required to describe the stress-strain relationship. Many engineering materials do not possess such anisotropic characteristics since the materials exhibit elastic symmetry and, as will be shown, for an isotropic elastic material, only two independent elastic coefficients are required. The number of elastic constants may be reduced if the material is hyperelastic. This is the case when deformation takes place isothermally or adiabatically [Lekhnitskii S G, 1981]. Then the elastic constants are symmetrical

such that $c_{ij} = c_{ji}$, and the number of elastic constants is reduced to 21 [Shames I H, Cozzarelli F A, 1992].

2.5.2 Elastic symmetry

When the elastic properties are different for every path taken from a given point within a material, the material is said to be anisotropic. However, there is a class of anisotropic materials which exhibit some degree of elastic symmetry, such that the elastic properties on certain paths taken from a given point are the same. Elastic symmetry is identified by comparing the elastic constants, c_{ij}, with the elastic constants of the same material which has undergone a co-ordinate transformation, $c_{i'j'}$ [Shames I H, Cozzarelli F A, 1992]. If $c_{ij} = c_{i'j'}$, then elastic symmetry exists for that particular transformation. The degree of anisotropy of an elastic body is determined by how few of these transformations exist.

2.5.2.1 Orthotropic materials

Anisotropic materials which exhibits three mutually perpendicular (orthogonal) planes of elastic symmetry are known as orthotropic materials. Due to elastic symmetry the number of elastic constants, when compared with the anisotropic material of the most general kind, is reduced, since it is found that [Lekhnitskii S G, 1981]

$$c_{14} = c_{24} = c_{34} = c_{46} = c_{15} = c_{25} = c_{35} = c_{45} = c_{16} = c_{26} = c_{36} = c_{56} = 0 \qquad (2.9)$$

Thus generalised Hooke's law for an orthotropic hyperelastic material reduces to

$$\sigma_x = c_{11}\varepsilon_x + c_{12}\varepsilon_y + c_{13}\varepsilon_z$$

$$\sigma_y = c_{12}\varepsilon_x + c_{22}\varepsilon_y + c_{23}\varepsilon_z$$

$$\sigma_z = c_{13}\varepsilon_x + c_{23}\varepsilon_y + c_{33}\varepsilon_z$$

$$\tau_{yz} = c_{44}\gamma_{yz}$$

$$\tau_{xz} = c_{55}\gamma_{xz}$$

$$\tau_{xy} = c_{66}\gamma_{xy}$$

(2.10)

An example assumed to belong to this category of elastic material is wood.

2.5.2.2 Isotropic materials

An isotropic elastic material has the characteristic that the elastic properties of the material are the same whichever path is taken from a given point in the material. In such a material, any arbitrary co-ordinate transform results in no change to the elastic constants. Due to this symmetry, the number of independent elastic constants is reduced to two since the only non zero elastic constants and their relationships are [Shames I H, Cozzarelli F A, 1992]

$$c_{11} = c_{22} = c_{33}, \quad c_{23} = c_{13} = c_{12}, \quad c_{44} = c_{55} = c_{66} = \frac{1}{2}\left(c_{11} - c_{12}\right) \quad (2.11)$$

Replacing $c_{23} = c_{13} = c_{12}$ and $c_{44} = c_{55} = c_{66} = \dfrac{1}{2}\left(c_{11} - c_{12}\right)$ with their more common representations, λ and G respectively, the stress strain relationships for an isotropic material are

$$
\begin{aligned}
\sigma_x &= (2G+\lambda)\varepsilon_x + & \lambda\varepsilon_y + & & \lambda\varepsilon_z \\
\sigma_y &= \lambda\varepsilon_x + (2G+\lambda)\varepsilon_y + & & & \lambda\varepsilon_z \\
\sigma_z &= \lambda\varepsilon_x + & \lambda\varepsilon_y + (2G+\lambda)\varepsilon_z \\
\tau_{yz} &= & & & G\gamma_{yz} \\
\tau_{xz} &= & & & G\gamma_{xz} \\
\tau_{xy} &= & & & G\gamma_{xy}
\end{aligned}
\tag{2.12}
$$

where λ is the Lamé constant and G is the shear modulus, both of which can be expressed in terms of the fundamental engineering parameters, Young's modulus, E, and Poisson's ratio, ν, giving

$$
\lambda = \frac{\nu E}{(1+\nu)(1-2\nu)}
\tag{2.13}
$$

and

$$
G = \frac{E}{2(1+\nu)}
\tag{2.14}
$$

As an example of such a material, typical values for Young's modulus and Poisson's ratio for mild steel are $E = 2.1 \times 10^{10}$ N/m^2 and $\nu = 0.3$.

2.6 Equations of Motion

In order to model the transient deformation of an elastic body, it is necessary to formulate the equations of motion which describe such deformation.

Consider the variation of stress across a small cubic element whose sides coincide with the rectangular axes x, y and z, as shown in figure 2.3.
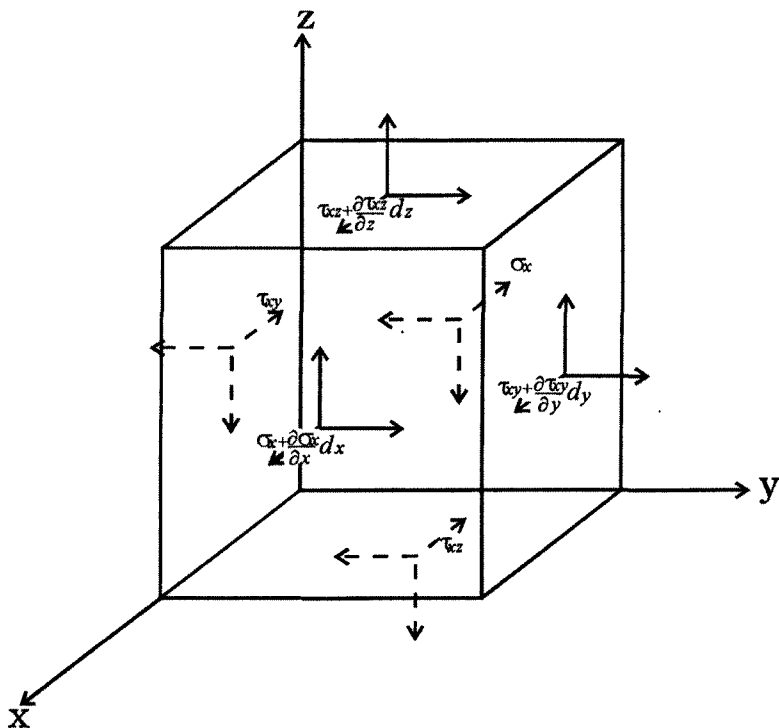
Figure 2.3 Stress variation in the x direction on a small element of material

Figure 2.3 shows the variation of stresses in the x direction, which is assumed to be continuous over the element. Summing the forces to obtain the total force acting in the x direction, and equating this to Newton's second law of motion, which relates the force acting on a body to its mass and acceleration gives [Mal A K, Singh S J, 1991]

$$\left(\sigma_x + \frac{\partial \sigma_x}{\partial x} dx\right) dydz - \sigma_x dydz + Xdxdydz + \left(\tau_{xy} + \frac{\partial \tau_{xy}}{\partial y} dy\right) dxdz - \tau_{xy} dxdz$$

$$+\left(\tau_{xz} + \frac{\partial \tau_{xz}}{\partial z} dz\right) dxdy - \tau_{xz} dxdy = \rho dxdydz \frac{\partial^2 u}{\partial t^2}$$

(2.15)

where ρ is the density of the element, and X is the body force, resolved in the x direction. A body force is a force which acts on every part of the body, as would be experienced, for example, under gravitational or centrifugal forces.

After simplification (2.15) reduces to

$$\rho \frac{\partial^2 u}{\partial t^2} = X + \frac{\partial \sigma_x}{\partial x} + \frac{\partial \tau_{xy}}{\partial y} + \frac{\partial \tau_{xz}}{\partial z}$$

(2.16)

Repeating the above procedure for the forces acting in the y and z directions of the small element in figure 2.3, yields a similar set of equations for motion in the y and z directions. The equations which describe motion in each direction are

$$\rho \frac{\partial^2 u}{\partial t^2} = X + \frac{\partial \sigma_x}{\partial x} + \frac{\partial \tau_{xy}}{\partial y} + \frac{\partial \tau_{xz}}{\partial z}$$

$$\rho \frac{\partial^2 v}{\partial t^2} = Y + \frac{\partial \tau_{xy}}{\partial x} + \frac{\partial \sigma_y}{\partial y} + \frac{\partial \tau_{yz}}{\partial z}$$

(2.17)

$$\rho \frac{\partial^2 w}{\partial t^2} = Z + \frac{\partial \tau_{xz}}{\partial x} + \frac{\partial \tau_{yz}}{\partial y} + \frac{\partial \sigma_z}{\partial z}$$

where Y and Z are the body forces in the y and z directions respectively.

These equations describe the transient deformation of a body, given the stress state of the body. The equations also hold for the steady state deformation since the steady state condition simply results in the accelerations, $\frac{\partial^2 u}{\partial t^2}$, $\frac{\partial^2 v}{\partial t^2}$ and $\frac{\partial^2 w}{\partial t^2}$ equating to zero. Substituting the stresses as defined by generalised Hooke's Law (2.8) into equation (2.17), and replacing the strains with their small strain differential form (2.6) and (2.7), the equations of motion can be written in terms of the elastic constants of the material, and in terms of differentials of displacements. Thus, for an anisotropic elastic body the equations of motion which describe motion in the x, y and z directions are [Lekhnitskii S G, 1981]

$$\rho\frac{\partial^2 u}{\partial t^2} = c_{11}\frac{\partial^2 u}{\partial x^2} + c_{66}\frac{\partial^2 u}{\partial y^2} + c_{55}\frac{\partial^2 u}{\partial z^2} + \left(c_{16}+c_{61}\right)\frac{\partial^2 u}{\partial x\partial y} + \left(c_{15}+c_{51}\right)\frac{\partial^2 u}{\partial x\partial z} + \left(c_{65}+c_{56}\right)\frac{\partial^2 u}{\partial y\partial z}$$

$$+ c_{16}\frac{\partial^2 v}{\partial x^2} + c_{62}\frac{\partial^2 v}{\partial y^2} + c_{54}\frac{\partial^2 v}{\partial z^2} + \left(c_{12}+c_{66}\right)\frac{\partial^2 v}{\partial x\partial y} + \left(c_{14}+c_{56}\right)\frac{\partial^2 v}{\partial x\partial z} + \left(c_{64}+c_{52}\right)\frac{\partial^2 v}{\partial y\partial z}$$

$$+ c_{15}\frac{\partial^2 w}{\partial x^2} + c_{64}\frac{\partial^2 w}{\partial y^2} + c_{53}\frac{\partial^2 w}{\partial z^2} + \left(c_{14}+c_{65}\right)\frac{\partial^2 w}{\partial x\partial y} + \left(c_{13}+c_{55}\right)\frac{\partial^2 w}{\partial x\partial z} + \left(c_{63}+c_{54}\right)\frac{\partial^2 w}{\partial y\partial z}$$

$$\rho\frac{\partial^2 v}{\partial t^2} = c_{66}\frac{\partial^2 v}{\partial x^2} + c_{22}\frac{\partial^2 v}{\partial y^2} + c_{44}\frac{\partial^2 v}{\partial z^2} + \left(c_{62}+c_{26}\right)\frac{\partial^2 v}{\partial x\partial y} + \left(c_{64}+c_{46}\right)\frac{\partial^2 v}{\partial x\partial z} + \left(c_{24}+c_{42}\right)\frac{\partial^2 v}{\partial y\partial z}$$

$$+ c_{61}\frac{\partial^2 u}{\partial x^2} + c_{26}\frac{\partial^2 u}{\partial y^2} + c_{45}\frac{\partial^2 u}{\partial z^2} + \left(c_{21}+c_{66}\right)\frac{\partial^2 u}{\partial x\partial y} + \left(c_{41}+c_{65}\right)\frac{\partial^2 u}{\partial x\partial z} + \left(c_{46}+c_{25}\right)\frac{\partial^2 u}{\partial y\partial z}$$

$$+ c_{65}\frac{\partial^2 w}{\partial x^2} + c_{24}\frac{\partial^2 w}{\partial y^2} + c_{43}\frac{\partial^2 w}{\partial z^2} + \left(c_{25}+c_{64}\right)\frac{\partial^2 w}{\partial x\partial y} + \left(c_{63}+c_{45}\right)\frac{\partial^2 w}{\partial x\partial z} + \left(c_{23}+c_{44}\right)\frac{\partial^2 w}{\partial y\partial z}$$

$$\rho\frac{\partial^2 w}{\partial t^2} = c_{55}\frac{\partial^2 w}{\partial x^2} + c_{44}\frac{\partial^2 w}{\partial y^2} + c_{33}\frac{\partial^2 w}{\partial z^2} + \left(c_{54}+c_{45}\right)\frac{\partial^2 w}{\partial x\partial y} + \left(c_{35}+c_{53}\right)\frac{\partial^2 w}{\partial x\partial z} + \left(c_{34}+c_{43}\right)\frac{\partial^2 w}{\partial y\partial z}$$

$$+ c_{51}\frac{\partial^2 u}{\partial x^2} + c_{46}\frac{\partial^2 u}{\partial y^2} + c_{35}\frac{\partial^2 u}{\partial z^2} + \left(c_{41}+c_{56}\right)\frac{\partial^2 u}{\partial x\partial y} + \left(c_{31}+c_{55}\right)\frac{\partial^2 u}{\partial x\partial z} + \left(c_{45}+c_{36}\right)\frac{\partial^2 u}{\partial y\partial z}$$

$$+ c_{56}\frac{\partial^2 v}{\partial x^2} + c_{42}\frac{\partial^2 v}{\partial y^2} + c_{34}\frac{\partial^2 v}{\partial z^2} + \left(c_{52}+c_{46}\right)\frac{\partial^2 v}{\partial x\partial y} + \left(c_{36}+c_{54}\right)\frac{\partial^2 v}{\partial x\partial z} + \left(c_{32}+c_{44}\right)\frac{\partial^2 v}{\partial y\partial z}$$

(2.18)

Where elastic symmetry exists, the above equations are simplified since there are fewer elastic constants. Thus for an isotropic material the equations of motion are

$$\rho \frac{\partial^2 u}{\partial t^2} = (2G + \lambda) \frac{\partial^2 u}{\partial x^2} + G \left(\frac{\partial^2 u}{\partial y^2} + \frac{\partial^2 u}{\partial z^2} \right) + (G + \lambda) \left(\frac{\partial^2 v}{\partial x \partial y} + \frac{\partial^2 w}{\partial x \partial z} \right)$$

$$\rho \frac{\partial^2 v}{\partial t^2} = (2G + \lambda) \frac{\partial^2 v}{\partial y^2} + G \left(\frac{\partial^2 v}{\partial x^2} + \frac{\partial^2 v}{\partial z^2} \right) + (G + \lambda) \left(\frac{\partial^2 u}{\partial x \partial y} + \frac{\partial^2 w}{\partial y \partial z} \right) \quad (2.19)$$

$$\rho \frac{\partial^2 w}{\partial t^2} = (2G + \lambda) \frac{\partial^2 w}{\partial z^2} + G \left(\frac{\partial^2 w}{\partial x^2} + \frac{\partial^2 w}{\partial y^2} \right) + (G + \lambda) \left(\frac{\partial^2 x}{\partial x \partial z} + \frac{\partial^2 v}{\partial y \partial z} \right)$$

In (2.18) and (2.19), the body forces X, Y and Z have been omitted. Often it is appropriate to neglect the body forces terms, since the deformation as a result of body forces, such as gravitational force, is negligible when compared with the deformation as a result of the applied surface forces. Gravitational body forces have been applied to TLM models of viscous bending [Newton H R, Pulko S H, Langley P, Wallis R, 1994], and it is possible that a similar approach could be taken to apply body forces in elastic deformation models. However, all the models developed in the work of this thesis are such that body forces are negligible compared with the applied loads, hence no further consideration will be given to them.

2.7 Boundary Conditions

Various boundary conditions may be applied to elastic bodies to effect some constraint, movement or deformation of the body. These include force, displacement, clamped and frictional boundaries. If a boundary is neither loaded in any way nor restrained it is called a free boundary. Since stresses are continuous throughout the bulk of the material, the external forces applied at the boundary are

considered to be a continuation of the internal stress distribution. Figure 2.4 illustrates a force acting on a body, the components of the force are resolved in each co-ordinate direction.
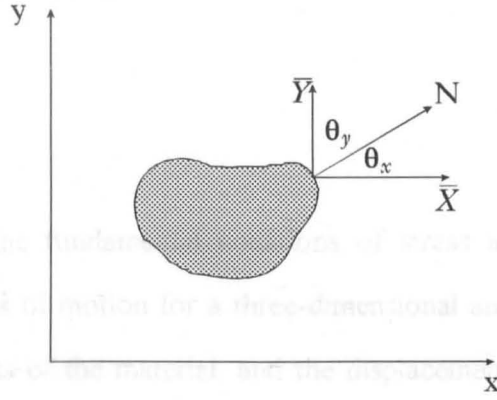
Figure 2.4 Surface forces on an arbitrary boundary

Equation (2.20) defines the surface forces in terms of the stresses on the boundary of the material, and the direction cosines of the normal to the surface [Wang, 1953].

$$\overline{X} = l\sigma_x + m\tau_{xy} + n\tau_{xz}$$
$$\overline{Y} = l\tau_{xy} + m\sigma_y + n\tau_{yz} \qquad (2.20)$$
$$\overline{Z} = l\tau_{xz} + m\tau_{yz} + n\sigma_z$$

$\overline{X}$, $\overline{Y}$ and $\overline{Z}$ are the surface forces per unit area on the boundary in the x, y and z directions respectively, and l, m and n, the direction cosines, are defined as

$$l = cos\theta_x$$
$$m = cos\theta_y \qquad (2.21)$$
$$n = cos\theta_z$$

The equations contained in (2.20) enable force boundary conditions to be implemented in a TLM elastic deformation model. Free boundary conditions may be implemented with the simplification that the surface forces in (2.20) are zero. Chapter four gives a full account of the implementation of boundary conditions in the TLM elastic deformation model.

2.8 Summary

Initially considering the fundamental equations of stress and strain, this chapter develops the equations of motion for a three-dimensional anisotropic body in terms of the elastic constants of the material, and the displacements within the body. In materials where elastic symmetry exists the number of elastic constants is reduced from that of the fully anisotropic material. Consideration is given to applying loads to elastic bodies, for which the boundary equations are presented. The following chapters describe the TLM elastic deformation model.

3

Solution of the elastic equations by TLM

3.1 Introduction

This chapter describes the TLM technique as applied to modelling the bulk deformation of elastic materials. The extensions to existing TLM nodal structures for the purpose of modelling elastic deformation are presented. A description of the nodal structure for modelling two-dimensional isotropic elastic deformation is given, together with an analysis of this structure using the TLM - state space analogy. Extension to the modelling of two-dimensional, anisotropic elastic materials is also presented.

3.2 Development of the standard two-dimensional TLM wave model

The equations which describe the transient deformation of elastic material are derived in chapter two. They are stated in their most general form for a fully anisotropic elastic material in (2.18). For an isotropic elastic material, the equations of elastic deformation in two-dimensions may be extracted from (2.19),

$$\rho\frac{\partial^2 u}{\partial t^2} = (2G+\lambda)\frac{\partial^2 u}{\partial x^2} + G\frac{\partial^2 u}{\partial y^2} + (G+\lambda)\frac{\partial^2 v}{\partial x \partial y}$$

$$\rho\frac{\partial^2 v}{\partial t^2} = G\frac{\partial^2 v}{\partial x^2} + (2G+\lambda)\frac{\partial^2 v}{\partial y^2} + (G+\lambda)\frac{\partial^2 u}{\partial x \partial y}$$

(3.1)

The TLM nodal structure for two-dimensional wave applications, is illustrated in figure 1.6, for which the continuous time equation is specified in (1.96). The

extensions to this nodal structure for the modelling of two-dimensional elastic deformation will now be examined.

The continuous time equation for the two-dimensional stub loaded shunt node structure, (1.96), is repeated below in (3.2). Comparing (3.2) with the elastic deformation equation for the x direction, (3.3), the extensions required to the existing two-dimensional TLM nodal structure to facilitate the modelling of elastic deformation can be identified.

$$\frac{\left(4+y_0\right)}{2}\frac{(\Delta t)^2}{(\Delta l)^2}\frac{\partial^2 \Phi}{\partial t^2} = \frac{\partial^2 \Phi}{\partial x^2} + \frac{\partial^2 \Phi}{\partial y^2} \tag{3.2}$$

$$\rho\frac{\partial^2 u}{\partial t^2} = (2G+\lambda)\frac{\partial^2 u}{\partial x^2} + G\frac{\partial^2 u}{\partial y^2} + (G+\lambda)\frac{\partial^2 v}{\partial x\partial y} \tag{3.3}$$

It is apparent that the proposed TLM scheme must be able to incorporate scaled spacial cross derivatives of the form $h\frac{\partial^2}{\partial x\partial y}$. This arises due to the expression $(G+\lambda)\frac{\partial^2 v}{\partial x\partial y}$ in (3.3), for which there is no equivalent expression in equation, (3.2). It is also apparent that the spacial derivatives in (3.2), $\frac{\partial^2 \Phi}{\partial x^2}$ and $\frac{\partial^2 \Phi}{\partial y^2}$, require scaling of the form $h_1\frac{\partial^2}{\partial x^2}$ and $h_2\frac{\partial^2}{\partial y^2}$ respectively, where h_1 corresponds to $(2G+\lambda)$, and h_2 corresponds to G in (3.3). Given these extensions, the comparison suggests that the TLM nodal potential, Φ, will be equivalent to the displacement variable u.

In considering a TLM implementation of the elastic deformation equations, it is reasonable to conclude that, since two equations containing two displacement variables are required to describe the elastic deformation in each of the co-ordinate

directions, then two TLM meshes will be required to model the two displacement variables. A conceptual model is illustrated in figure 3.1.

Φ_x

y

x

Φ_y

2-D Elastic Body   TLM model
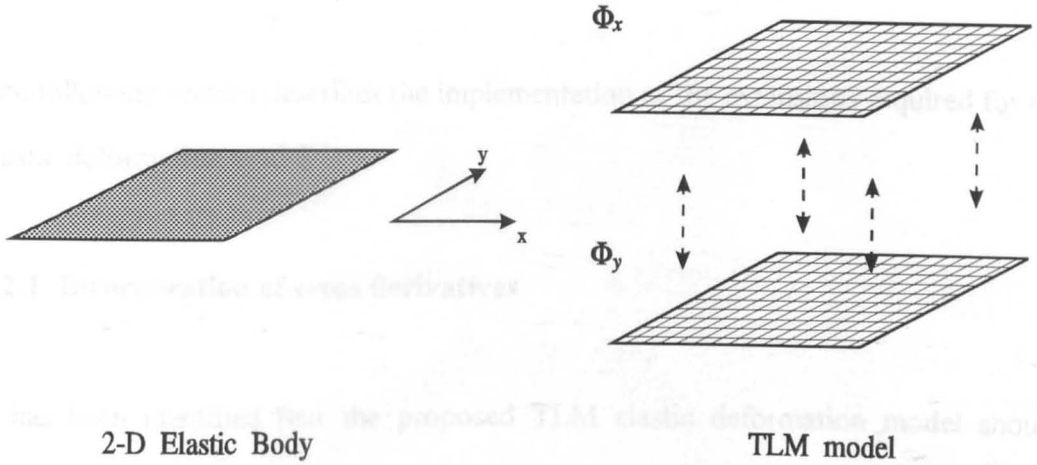
Figure 3.1 Conceptual model of the two-dimensional elastic deformation TLM scheme - two

interdependent meshes describe deformation in each of the co-ordinate directions

Thus, two interdependent meshes, say Φ_x, which describes displacement in the x direction, and Φ_y, which describes displacement in the y direction, will form the basis of the TLM elastic deformation model. The meshes must be considered interdependent since, from (3.1)

$$u = f(u,v) \quad \text{and} \quad v = f(u,v)$$

which implies   (3.4)

$$\Phi_x = f(\Phi_x,\Phi_y) \quad \text{and} \quad \Phi_y = f(\Phi_x,\Phi_y)$$

This interdependence is apparent from (3.1), where the dependence of u on v, and v on u, is through the scaled spacial cross derivatives. Connections between the two meshes will provide information routes for interchange of data between the two meshes.

The following section describes the implementation of the extensions required for the elastic deformation model.

3.2.1 Incorporation of cross derivatives

It has been identified that the proposed TLM elastic deformation model should incorporate scaled spacial cross derivatives. Work by Witwit *et al* describes the TLM-state space analogy for analysis of TLM nodal structures, and applies it to a number of nodal structures [Witwit, A R M, Wilkinson A J, Pulko S H, 1995]. One of the structures considered, is a mesh to model the two-dimensional wave equation incorporating a scaled spacial cross derivative of the form

$$M\frac{\partial^2}{\partial t^2} = \frac{\partial^2}{\partial x^2} + \frac{\partial^2}{\partial y^2} + h\frac{\partial^2}{\partial x \partial y} \qquad (3.5)$$

for which the corresponding nodal structure, identified by Witwit *et al*, is shown in figure 3.2.

The nodal structure consists of a central node at location (i,j) with associated transmission lines, numbered 1 to 9. The transmission lines numbered 1, 2, 3, 4, of impedance Z, and 5, of impedance Z_s, are those of the standard TLM wave nodal structure (figure 1.6) incorporating a stub line. The additional transmission lines, numbered 6, 7, 8 and 9, connect the central node to adjacent diagonal nodes in the same mesh at positions $(i - 1, j + 1)$, $(i + 1, j + 1)$, $(i + 1, j - 1)$ and $(i -1, j - 1)$

respectively. This connection of nodes is similar to the template used in finite difference implementations of cross derivatives [Leigh J R, 1983].
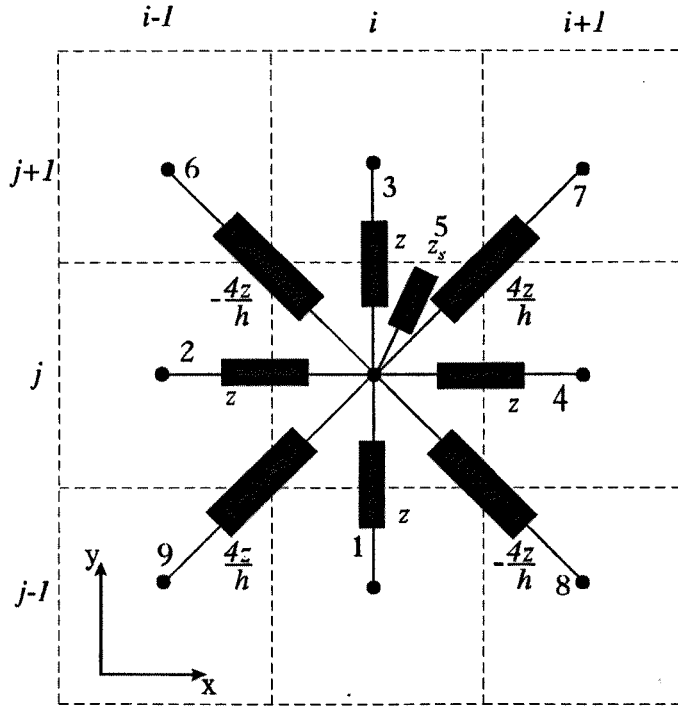
Figure 3.2 Nodal structure for incorporating scaled cross derivative [Witwit, A R M, Wilkinson A J, Pulko S H, 1995]

These diagonal transmission lines have an impedance of magnitude Z scaled by the factor $(4/h)$. The sign of the impedance is dependent upon the link lines position within the structure, such that impedances of link lines 6 and 8 are negative, and those of 7 and 9 are positive. Analysis of this nodal structure, by Witwit *et al*, using TLM-state space analysis yields a solution for the characteristic equation of

$$\frac{4+y_0}{2}\left(Q-2+Q^{-1}\right) = \left(I-2+I^{-1}\right) + \left(J-2+J^{-1}\right) + \frac{h}{4}\left(IJ - IJ^{-1} - I^{-1}J + I^{-1}J^{-1}\right)$$

(3.6)

for which, with reference to Appendix 1, the corresponding continuous time equation is

$$\frac{4+y_0}{2}\frac{(\Delta t)^2}{(\Delta l)^2}\frac{\partial^2\Phi}{\partial t^2}=\frac{\partial^2\Phi}{\partial x^2}+\frac{\partial^2\Phi}{\partial y^2}+h\frac{\partial^2\Phi}{\partial x\partial y} \qquad (3.7)$$

where

$$\frac{\partial^2\Phi}{\partial y^2}\equiv\frac{\left(I-2+I^{-1}\right)}{\Delta l^2}, \qquad \frac{\partial^2\Phi}{\partial y^2}\equiv\frac{\left(J-2+J^{-1}\right)}{\Delta l^2},$$

$$\frac{\partial^2\Phi}{\partial t^2}\equiv\frac{\left(Q-2+Q^{-1}\right)}{\Delta t^2} \quad\text{and}\quad \frac{\partial^2\Phi}{\partial x\partial y}\equiv\frac{\left(IJ-IJ^{-1}-I^{-1}J+I^{-1}J^{-1}\right)}{4(\Delta l)^2}.$$

The analysis demonstrates that scaling the impedance by the value 4, ensures consistency of spacial discretisation, and scaling the impedance by ($1/h$) ensures the correct scaling of the cross derivative. Thus, scaled spacial cross derivatives may be incorporated into a TLM model by inclusion, in a standard wave nodal structure, of appropriately scaled diagonally connected transmission lines. However, there is one fundamental difference between the nodal structure described by Witwit, and that required for the TLM elastic deformation model. This relates to the interdependence of the two meshes required in the proposed elastic deformation model, as described in (3.4). The nodal structure illustrated in figure 3.2 models the equation specified in (3.7), which has a single solution variable (nodal potential), Φ. Having identified that the proposed TLM model will consist of two interdependent meshes, with solution variables Φ_x and Φ_y, the following representation of the equations to be modelled can be written.

$$M\frac{\partial^2\Phi_x}{\partial t^2}=h_1\frac{\partial^2\Phi_x}{\partial x^2}+h_2\frac{\partial^2\Phi_x}{\partial y^2}+h\frac{\partial^2\Phi_y}{\partial x\partial y}$$

$$M\frac{\partial^2\Phi_y}{\partial t^2}=h_2\frac{\partial^2\Phi_y}{\partial x^2}+h_1\frac{\partial^2\Phi_y}{\partial y^2}+h\frac{\partial^2\Phi_x}{\partial x\partial y}$$

$$(3.8)$$

It is apparent from equations (3.8) that the interdependence of the two meshes is through the cross derivatives. Extending the work of Witwit *et al* to accommodate cross derivatives related to other meshes, the nodal structure illustrated in figure 3.3 is proposed.
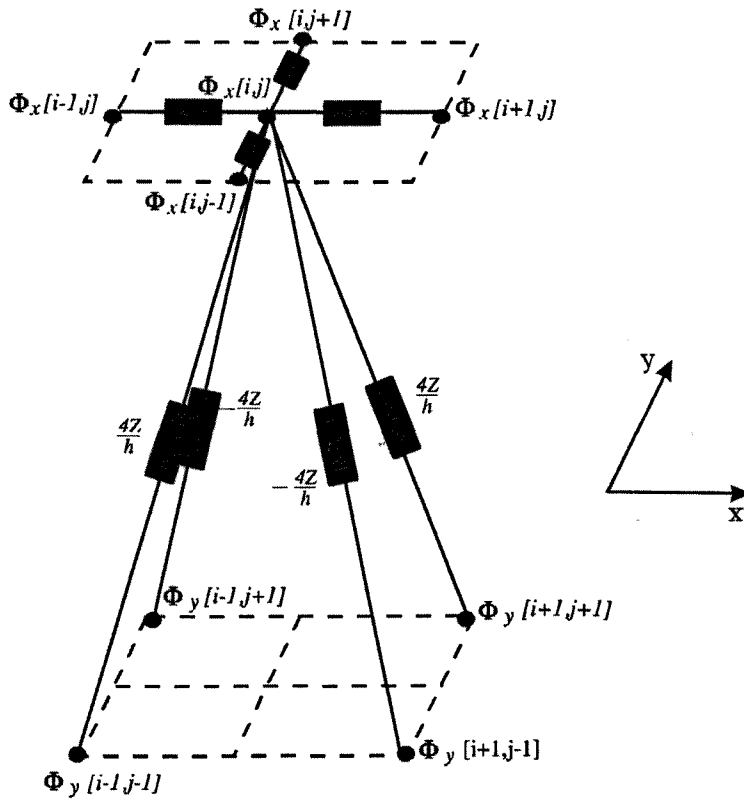
Figure 3.3 Connections for implementation of cross derivatives (Φ_x mesh)

Figure 3.3 illustrates the connections and scaled impedances of the proposed nodal structure for incorporation of scaled spacial cross derivatives of Φ_y into the Φ_x mesh. Since the sum of the impedances of the cross derivative link lines is zero, the overall nodal impedance is not changed because of these additional transmission lines.

3.2.2 Scaling of the spacial derivatives

The previous section described the incorporation of scaled spacial cross derivatives. It is shown that by multiplying the cross derivative link line impedances by the factor, $(4/h)$, the cross derivative is scaled by h. It is shown also that the factor 4 is required only to ensure consistency of spacial discretisation for the implementation of cross derivatives. Extending this implementation, it is anticipated that the scaling of the spatial derivatives $\dfrac{\partial^2 \Phi}{\partial x^2}$ and $\dfrac{\partial^2 \Phi}{\partial y^2}$, is accomplished by scaling the appropriate standard transmission line impedances by the reciprocal of the desired coefficient. For example, to scale $\dfrac{\partial^2 \Phi}{\partial x^2}$ by h_1, the transmission line impedance Z along the x direction is scaled by $(1/h_1)$.

Having proposed methods by which cross derivatives and scaling can be incorporated into TLM models, the corresponding nodal structure for modelling the elastic deformation equations (3.1), is illustrated in figure 3.4a and figure 3.4b. Figure 3.4c shows the connectivity between the two meshes.

For clarity the stub transmission lines at each node in figures 3.4a 3.4b and 3.4c are not shown, the impedances also are omitted from figure 3.4c. The proposed model therefore consists of two interdependent, two dimensional meshes, one with solution variable (nodal potential) Φ_x, and one with solution variable Φ_y, corresponding to displacements, u and v, in the x and y co-ordinate directions respectively. Each node in the Φ_x mesh has four transmission lines each of which connects with one neighbouring node in the Φ_x mesh, four transmission lines each of which connects with its diagonal spacial neighbouring node in the Φ_y mesh. A stub transmission line is included also.

Figure 3.4a Nodal structure for solution of Φx

Figure 3.4b Nodal structure for solution of Φy
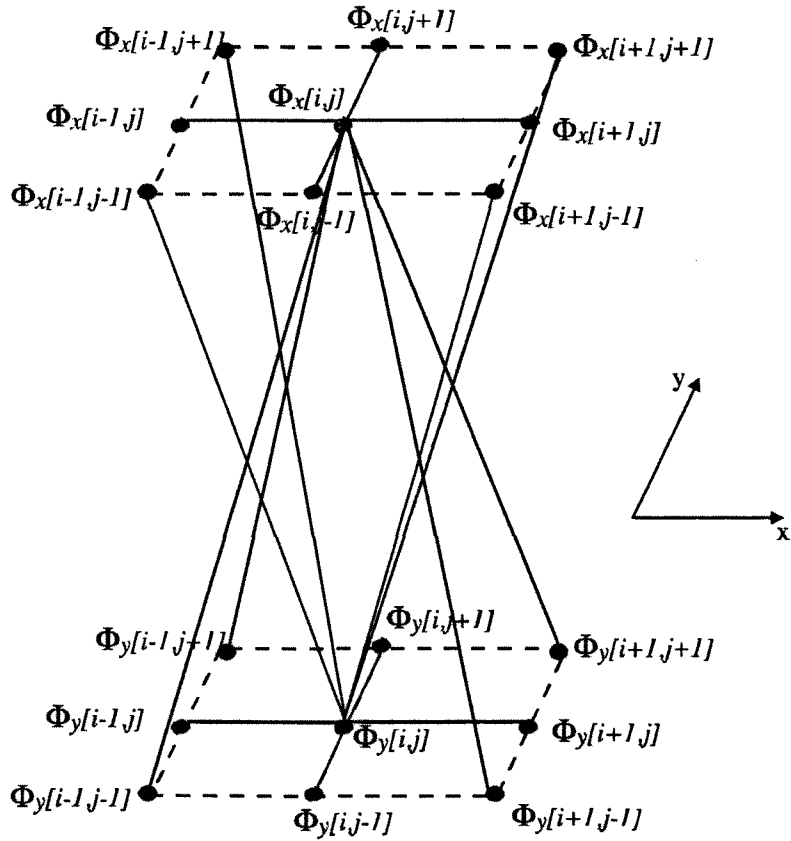
Figure 3.4c Combined connectivity of the Φ_x and Φ_y meshes

Similarly, each node in the Φ_y mesh has four transmission lines each connecting with a neighbouring node in the Φ_y mesh, four transmission lines each connecting with its diagonal spacial neighbouring node in the Φ_x mesh. Again, a stub transmission line is included. Each transmission line is scaled to incorporate the relevant coefficient of the spacial derivative.

3.3 State space analysis of the proposed nodal structure

Analysis of the nodal structure proposed for modelling elastic deformation by the TLM-state space analogy, provides validation of the discrete representation of the

structure. Since the analysis must consider nodes in both meshes, and each node has associated with it nine transmission lines, the analysis requires manipulation of 18 × 18 matrices. In order to simplify the resulting matrices, the spacial derivative coefficient h_2 can be incorporated into the remaining coefficients such that the coefficient is effectively removed. This is achieved in the elastic deformation equations by dividing each side of the equations in (3.1) by G, resulting in the equations shown below.

$$\frac{\rho}{G}\frac{\partial^2 u}{\partial t^2} = \left(2+\frac{\lambda}{G}\right)\frac{\partial^2 u}{\partial x^2} + \frac{\partial^2 u}{\partial y^2} + \left(1+\frac{\lambda}{G}\right)\frac{\partial^2 v}{\partial x \partial y}$$

$$(3.9)$$

$$\frac{\rho}{G}\frac{\partial^2 v}{\partial t^2} = \frac{\partial^2 v}{\partial x^2} + \left(2+\frac{\lambda}{G}\right)\frac{\partial^2 v}{\partial y^2} + \left(1+\frac{\lambda}{G}\right)\frac{\partial^2 u}{\partial x \partial y}$$

The notation used for identification of the link lines in the nodal structure is illustrated in figure 3.5. Stub transmission lines are labelled 1 and 10, the transmission lines which implement the cross derivatives are labelled 6, 7, 8, 9, 15, 16, 17 and 18, and the standard transmission lines are labelled 2, 3, 4, 5, 11, 12, 13 and 14.
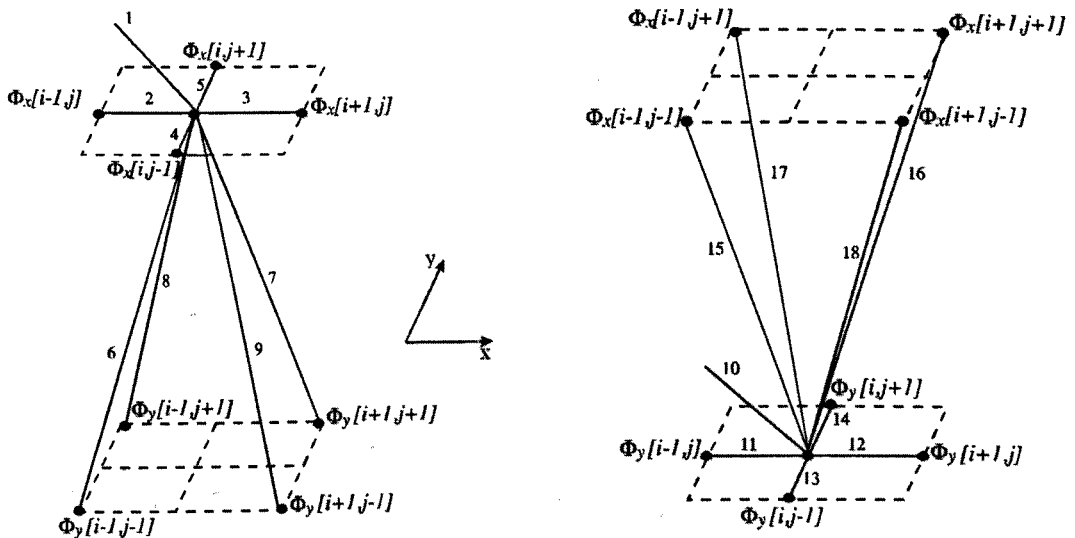
Figure 3.5 Notation used for identification of the transmission lines

It is apparent from (3.9) that, due to the scaled spacial derivatives, link lines in the Φ_x mesh which run parallel to the x axis need to be scaled by the value $h_1 = (2 + \lambda/G)$. No scaling is required on the link lines which run parallel to the y axis in this mesh ($h_2 = 1$). Similarly, link lines in the Φ_y mesh which run parallel to the y axis require scaling by the value $h_1 = (2 + \lambda/G)$, and no scaling is required on the link lines which run parallel to the x axis. All cross derivative link lines require scaling by $h = (1 + \lambda/G)$. This results in the following link line impedance values

$$Z_2 = Z_3 = Z_{13} = Z_{14} = Z/h_1$$

$$Z_4 = Z_5 = Z_{11} = Z_{12} = Z/h_2$$

$$Z_6 = Z_7 = Z_{15} = Z_{16} = (4Z)/h$$

$$Z_8 = Z_9 = Z_{17} = Z_{18} = -(4Z)/h$$

Further,

$$Z_1 = Z_{10} = Z_s$$

defines the stub impedance.

The 18 × 1 partitioned incident pulse vector, consisting of two column vectors of pulses incident on nodes in the meshes, Φ_x and Φ_y is defined as,

$$_k\mathbf{V}^i_{i,j} = \begin{bmatrix} \left[\mathbf{V}^i_{x,i,j}\right] \\ \left[\mathbf{V}^i_{y,i,j}\right] \end{bmatrix}_k = \begin{bmatrix} \begin{bmatrix} V^i_{i,j,1} \\ \vdots \\ V^i_{i,j,9} \end{bmatrix} \\ \begin{bmatrix} V^i_{i,j,10} \\ \vdots \\ V^i_{i,j,18} \end{bmatrix} \end{bmatrix}_k \qquad (3.10)$$

72

and extending the TLM matrix notation outlined in section 1.3.3.3, the nodal potentials of the two meshes may be determined by use of the following expressions,

$$_k\Phi_{x,i,j} = \mathbf{q}_x \ _k\mathbf{V}^i_{x,i,j} \tag{3.11}$$

$$_k\Phi_{y,i,j} = \mathbf{q}_y \ _k\mathbf{V}^i_{y,i,j} \tag{3.12}$$

The entries of $\mathbf{q}_x$ and $\mathbf{q}_y$ may be determined from the nodal potential equation specified in equation (1.1). Since the nodal structure is resistance free, application of equation (1.1) yields

$$_k\Phi_{x,i,j} = \frac{2}{Y_x}\left[\sum_{l=1}^{9}\frac{_kV^i_{i,j,l}}{Z_l}\right] \quad \text{where } Y_x = \sum_{l=1}^{9}\frac{1}{Z_l} \tag{3.13}$$

and

$$_k\Phi_{y,i,j} = \frac{2}{Y_y}\left[\sum_{l=10}^{18}\frac{_kV^i_{i,j,l}}{Z_l}\right] \quad \text{where } Y_y = \sum_{l=10}^{18}\frac{1}{Z_l} \tag{3.14}$$

If the nominal link line impedance, Z, is set equal to unity before scaling, as is generally the case in TLM wave models, (3.13) and (3.14) expressed in matrix form may be written

73

$$_k\Phi_{x,i,j} = \left(\frac{2}{Y_x}\right)\left[\frac{1}{Z_s} \quad h_1 \quad h_1 \quad 1 \quad 1 \quad \frac{h}{4} \quad \frac{h}{4} \quad -\frac{h}{4} \quad -\frac{h}{4}\right]\begin{bmatrix} V^i{}_1 \\ V^i{}_2 \\ V^i{}_3 \\ V^i{}_4 \\ V^i{}_5 \\ V^i{}_6 \\ V^i{}_7 \\ V^i{}_8 \\ {}_k V^i{}_9 \end{bmatrix}_{i,j}$$

$$(3.15)$$

$$_k\Phi_{y,i,j} = \left(\frac{2}{Y_y}\right)\left[\frac{1}{Z_s} \quad 1 \quad 1 \quad h_1 \quad h_1 \quad \frac{h}{4} \quad \frac{h}{4} \quad -\frac{h}{4} \quad -\frac{h}{4}\right]\begin{bmatrix} V^i{}_{10} \\ V^i{}_{11} \\ V^i{}_{12} \\ V^i{}_{13} \\ V^i{}_{14} \\ V^i{}_{15} \\ V^i{}_{16} \\ V^i{}_{17} \\ {}_k V^i{}_{18} \end{bmatrix}_{i,j}$$

$$(3.16)$$

74

from which $\mathbf{q}_x$ and $\mathbf{q}_y$ can be identified as

$$\mathbf{q}_x = \frac{2}{Y}\left[\frac{1}{Z_s} \quad h_1 \quad h_1 \quad 1 \quad 1 \quad \frac{h}{4} \quad \frac{h}{4} \quad -\frac{h}{4} \quad -\frac{h}{4}\right] \qquad (3.17)$$

$$\mathbf{q}_y = \frac{2}{Y}\left[\frac{1}{Z_s} \quad 1 \quad 1 \quad h_1 \quad h_1 \quad \frac{h}{4} \quad \frac{h}{4} \quad -\frac{h}{4} \quad -\frac{h}{4}\right] \qquad (3.18)$$

where $Y = Y_x = Y_y = \dfrac{1}{Z_s} + 2h_1 + 2$

To find the scattering matrix $\mathbf{S}$, matrices $\mathbf{p}$ and $\mathbf{r}$ must be determined (see expressions (1.45) and (1.46)). Using (1.44) the reflected pulse equation for each mesh becomes

$$_k\mathbf{V}^r_{x,i,j} = \left(\mathbf{p}_x\right)_k \Phi_{x,i,j} + \left(\mathbf{r}_x\right)_k \mathbf{V}^i_{x,i,j} \qquad (3.19)$$

and

$$_k\mathbf{V}^r_{y,i,j} = \left(\mathbf{p}_y\right)_k \Phi_{y,i,j} + \left(\mathbf{r}_y\right)_k \mathbf{V}^i_{y,i,j} \qquad (3.20)$$

The elements of $\mathbf{p}_x$, $\mathbf{p}_y$, $\mathbf{r}_x$ and $\mathbf{r}_y$ can be determined by use of the reflected pulse equation, equation (1.2), which for the proposed nodal structure simplifies to,

$$_kV^r_{x,i,j,l} = {}_k\Phi_{x,i,j} - {}_kV^i_{x,i,j,l} \qquad l = 1 \text{ to } 9 \qquad (3.21)$$

and

$$_kV^r_{y,i,j,l} = {}_k\Phi_{y,i,j} - {}_kV^i_{y,i,j,l} \qquad l = 10 \text{ to } 18 \qquad (3.22)$$

75

or in matrix form

$$
\begin{bmatrix} V^r{}_1 \\ V^r{}_2 \\ V^r{}_3 \\ V^r{}_4 \\ V^r{}_5 \\ V^r{}_6 \\ V^r{}_7 \\ V^r{}_8 \\ V^r{}_9 \end{bmatrix}_{k\ i,j} = \begin{bmatrix} 1 \\ 1 \\ 1 \\ 1 \\ 1 \\ 1 \\ 1 \\ 1 \\ 1 \end{bmatrix}_k \Phi_{x,i,j} - \begin{bmatrix} 1 & 0 & 0 & 0 & 0 & 0 & 0 & 0 & 0 \\ 0 & 1 & 0 & 0 & 0 & 0 & 0 & 0 & 0 \\ 0 & 0 & 1 & 0 & 0 & 0 & 0 & 0 & 0 \\ 0 & 0 & 0 & 1 & 0 & 0 & 0 & 0 & 0 \\ 0 & 0 & 0 & 0 & 1 & 0 & 0 & 0 & 0 \\ 0 & 0 & 0 & 0 & 0 & 1 & 0 & 0 & 0 \\ 0 & 0 & 0 & 0 & 0 & 0 & 1 & 0 & 0 \\ 0 & 0 & 0 & 0 & 0 & 0 & 0 & 1 & 0 \\ 0 & 0 & 0 & 0 & 0 & 0 & 0 & 0 & 1 \end{bmatrix} \begin{bmatrix} V^i{}_1 \\ V^i{}_2 \\ V^i{}_3 \\ V^i{}_4 \\ V^i{}_5 \\ V^i{}_6 \\ V^i{}_7 \\ V^i{}_8 \\ V^i{}_9 \end{bmatrix}_{k\ i,j}
$$

(3.23)

$$
\begin{bmatrix} V^r{}_{10} \\ V^r{}_{11} \\ V^r{}_{12} \\ V^r{}_{13} \\ V^r{}_{14} \\ V^r{}_{15} \\ V^r{}_{16} \\ V^r{}_{17} \\ V^r{}_{18} \end{bmatrix}_{k\ i,j} = \begin{bmatrix} 1 \\ 1 \\ 1 \\ 1 \\ 1 \\ 1 \\ 1 \\ 1 \\ 1 \end{bmatrix}_k \Phi_{y,i,j} - \begin{bmatrix} 1 & 0 & 0 & 0 & 0 & 0 & 0 & 0 & 0 \\ 0 & 1 & 0 & 0 & 0 & 0 & 0 & 0 & 0 \\ 0 & 0 & 1 & 0 & 0 & 0 & 0 & 0 & 0 \\ 0 & 0 & 0 & 1 & 0 & 0 & 0 & 0 & 0 \\ 0 & 0 & 0 & 0 & 1 & 0 & 0 & 0 & 0 \\ 0 & 0 & 0 & 0 & 0 & 1 & 0 & 0 & 0 \\ 0 & 0 & 0 & 0 & 0 & 0 & 1 & 0 & 0 \\ 0 & 0 & 0 & 0 & 0 & 0 & 0 & 1 & 0 \\ 0 & 0 & 0 & 0 & 0 & 0 & 0 & 0 & 1 \end{bmatrix} \begin{bmatrix} V^i{}_{10} \\ V^i{}_{11} \\ V^i{}_{12} \\ V^i{}_{13} \\ V^i{}_{14} \\ V^i{}_{15} \\ V^i{}_{16} \\ V^i{}_{17} \\ V^i{}_{18} \end{bmatrix}_{k\ i,j}
$$

(3.24)

from which it is apparent that $\mathbf{p}_x$ and $\mathbf{p}_y$ are unit column vectors, and $\mathbf{r}_x$ and $\mathbf{r}_y$ are negative unit matrices.

Given that $\mathbf{S} = \mathbf{pq} + \mathbf{r}$, the scattering matrix can be defined as

$$\mathbf{S} = \begin{bmatrix} [\mathbf{p}_x\mathbf{q}_x] & [0] \\ [0] & [\mathbf{p}_y\mathbf{q}_y] \end{bmatrix} + \begin{bmatrix} [\mathbf{r}_x] & [0] \\ [0] & [\mathbf{r}_y] \end{bmatrix} \tag{3.25}$$

Substituting into this values for $\mathbf{p}_x$, $\mathbf{p}_y$, $\mathbf{q}_x$, $\mathbf{q}_y$, $\mathbf{r}_x$ and $\mathbf{r}_y$ gives

$$\mathbf{S} = \frac{1}{Y}\begin{bmatrix} \mathbf{A} & [0] \\ [0] & \mathbf{B} \end{bmatrix}$$

where

$$\mathbf{A} = \begin{bmatrix}
\frac{2}{Z_s}-Y & 2h_1 & 2h_1 & 2 & 2 & \frac{h}{2} & \frac{h}{2} & -\frac{h}{2} & -\frac{h}{2} \\
\frac{2}{Z_s} & 2h_1-Y & 2h_1 & 2 & 2 & \frac{h}{2} & \frac{h}{2} & -\frac{h}{2} & -\frac{h}{2} \\
\frac{2}{Z_s} & 2h_1 & 2h_1-Y & 2 & 2 & \frac{h}{2} & \frac{h}{2} & -\frac{h}{2} & -\frac{h}{2} \\
\frac{2}{Z_s} & 2h_1 & 2h_1 & 2-Y & 2 & \frac{h}{2} & \frac{h}{2} & -\frac{h}{2} & -\frac{h}{2} \\
\frac{2}{Z_s} & 2h_1 & 2h_1 & 2 & 2-Y & \frac{h}{2} & \frac{h}{2} & -\frac{h}{2} & -\frac{h}{2} \\
\frac{2}{Z_s} & 2h_1 & 2h_1 & 2 & 2 & \frac{h}{2}-Y & \frac{h}{2} & -\frac{h}{2} & -\frac{h}{2} \\
\frac{2}{Z_s} & 2h_1 & 2h_1 & 2 & 2 & \frac{h}{2} & \frac{h}{2}-Y & -\frac{h}{2} & -\frac{h}{2} \\
\frac{2}{Z_s} & 2h_1 & 2h_1 & 2 & 2 & \frac{h}{2} & \frac{h}{2} & -\frac{h}{2}-Y & -\frac{h}{2} \\
\frac{2}{Z_s} & 2h_1 & 2h_1 & 2 & 2 & \frac{h}{2} & \frac{h}{2} & -\frac{h}{2} & -\frac{h}{2}-Y
\end{bmatrix}$$

$$\mathbf{B} = \begin{bmatrix}
\frac{2}{Z_s}-Y & 2 & 2 & 2h_1 & 2h_1 & \frac{h}{2} & \frac{h}{2} & -\frac{h}{2} & -\frac{h}{2} \\
\frac{2}{Z_s} & 2-Y & 2 & 2h_1 & 2h_1 & \frac{h}{2} & \frac{h}{2} & -\frac{h}{2} & -\frac{h}{2} \\
\frac{2}{Z_s} & 2 & 2-Y & 2h_1 & 2h_1 & \frac{h}{2} & \frac{h}{2} & -\frac{h}{2} & -\frac{h}{2} \\
\frac{2}{Z_s} & 2 & 2 & 2h_1-Y & 2h_1 & \frac{h}{2} & \frac{h}{2} & -\frac{h}{2} & -\frac{h}{2} \\
\frac{2}{Z_s} & 2 & 2 & 2h_1 & 2h_1-Y & \frac{h}{2} & \frac{h}{2} & -\frac{h}{2} & -\frac{h}{2} \\
\frac{2}{Z_s} & 2 & 2 & 2h_1 & 2h_1 & \frac{h}{2}-Y & \frac{h}{2} & -\frac{h}{2} & -\frac{h}{2} \\
\frac{2}{Z_s} & 2 & 2 & 2h_1 & 2h_1 & \frac{h}{2} & \frac{h}{2}-Y & -\frac{h}{2} & -\frac{h}{2} \\
\frac{2}{Z_s} & 2 & 2 & 2h_1 & 2h_1 & \frac{h}{2} & \frac{h}{2} & -\frac{h}{2}-Y & -\frac{h}{2} \\
\frac{2}{Z_s} & 2 & 2 & 2h_1 & 2h_1 & \frac{h}{2} & \frac{h}{2} & -\frac{h}{2} & -\frac{h}{2}-Y
\end{bmatrix}$$

$$\tag{3.26}$$

and the scattering equation, (1.46), can be written

$$
\begin{bmatrix} V^r_{i,j,1} \\ V^r_{i,j,2} \\ V^r_{i,j,3} \\ V^r_{i,j,4} \\ V^r_{i,j,5} \\ V^r_{i,j,6} \\ V^r_{i,j,7} \\ V^r_{i,j,8} \\ V^r_{i,j,9} \\ V^r_{i,j,10} \\ V^r_{i,j,11} \\ V^r_{i,j,12} \\ V^r_{i,j,13} \\ V^r_{i,j,14} \\ V^r_{i,j,15} \\ V^r_{i,j,16} \\ V^r_{i,j,17} \\ V^r_{i,j,18} \end{bmatrix}
= \frac{1}{Y}
\left[\begin{array}{c|c} A & [0] \\ \hline [0] & B \end{array} \right]
\begin{bmatrix} V^i_{i,j,1} \\ V^i_{i,j,2} \\ V^i_{i,j,3} \\ V^i_{i,j,4} \\ V^i_{i,j,5} \\ V^i_{i,j,6} \\ V^i_{i,j,7} \\ V^i_{i,j,8} \\ V^i_{i,j,9} \\ V^i_{i,j,10} \\ V^i_{i,j,11} \\ V^i_{i,j,12} \\ V^i_{i,j,13} \\ V^i_{i,j,14} \\ V^i_{i,j,15} \\ V^i_{i,j,16} \\ V^i_{i,j,17} \\ V^i_{i,j,18} \end{bmatrix}
$$

where

$$
A = \begin{bmatrix}
\frac{2}{Z_e}-Y & 2h_1 & 2h_1 & 2 & 2 & \frac{h}{2} & \frac{h}{2} & -\frac{h}{2} & -\frac{h}{2} \\
\frac{2}{Z_e} & 2h_1-Y & 2h_1 & 2 & 2 & \frac{h}{2} & \frac{h}{2} & -\frac{h}{2} & -\frac{h}{2} \\
\frac{2}{Z_e} & 2h_1 & 2h_1-Y & 2 & 2 & \frac{h}{2} & \frac{h}{2} & -\frac{h}{2} & -\frac{h}{2} \\
\frac{2}{Z_e} & 2h_1 & 2h_1 & 2-Y & 2 & \frac{h}{2} & \frac{h}{2} & -\frac{h}{2} & -\frac{h}{2} \\
\frac{2}{Z_e} & 2h_1 & 2h_1 & 2 & 2-Y & \frac{h}{2} & \frac{h}{2} & -\frac{h}{2} & -\frac{h}{2} \\
\frac{2}{Z_e} & 2h_1 & 2h_1 & 2 & 2 & \frac{h}{2}-Y & \frac{h}{2} & -\frac{h}{2} & -\frac{h}{2} \\
\frac{2}{Z_e} & 2h_1 & 2h_1 & 2 & 2 & \frac{h}{2} & \frac{h}{2}-Y & -\frac{h}{2} & -\frac{h}{2} \\
\frac{2}{Z_e} & 2h_1 & 2h_1 & 2 & 2 & \frac{h}{2} & \frac{h}{2} & -\frac{h}{2}-Y & -\frac{h}{2} \\
\frac{2}{Z_e} & 2h_1 & 2h_1 & 2 & 2 & \frac{h}{2} & \frac{h}{2} & -\frac{h}{2} & -\frac{h}{2}-Y
\end{bmatrix}
$$

$$
B = \begin{bmatrix}
\frac{2}{Z_e}-Y & 2 & 2 & 2h_1 & 2h_1 & \frac{h}{2} & \frac{h}{2} & -\frac{h}{2} & -\frac{h}{2} \\
\frac{2}{Z_e} & 2-Y & 2 & 2h_1 & 2h_1 & \frac{h}{2} & \frac{h}{2} & -\frac{h}{2} & -\frac{h}{2} \\
\frac{2}{Z_e} & 2 & 2-Y & 2h_1 & 2h_1 & \frac{h}{2} & \frac{h}{2} & -\frac{h}{2} & -\frac{h}{2} \\
\frac{2}{Z_e} & 2 & 2 & 2h_1-Y & 2h_1 & \frac{h}{2} & \frac{h}{2} & -\frac{h}{2} & -\frac{h}{2} \\
\frac{2}{Z_e} & 2 & 2 & 2h_1 & 2h_1-Y & \frac{h}{2} & \frac{h}{2} & -\frac{h}{2} & -\frac{h}{2} \\
\frac{2}{Z_e} & 2 & 2 & 2h_1 & 2h_1 & \frac{h}{2}-Y & \frac{h}{2} & -\frac{h}{2} & -\frac{h}{2} \\
\frac{2}{Z_e} & 2 & 2 & 2h_1 & 2h_1 & \frac{h}{2} & \frac{h}{2}-Y & -\frac{h}{2} & -\frac{h}{2} \\
\frac{2}{Z_e} & 2 & 2 & 2h_1 & 2h_1 & \frac{h}{2} & \frac{h}{2} & -\frac{h}{2}-Y & -\frac{h}{2} \\
\frac{2}{Z_e} & 2 & 2 & 2h_1 & 2h_1 & \frac{h}{2} & \frac{h}{2} & -\frac{h}{2} & -\frac{h}{2}-Y
\end{bmatrix}
$$

(3.27)

To determine the modified scattering matrix **S'**, and the time and space shift matrix **T**, it is necessary to consider the scattering notation.

The notation used to describe the connection of pulses is

$$
\begin{bmatrix}
V^i_{i,j,1} \\
V^i_{i-1,j,3} \\
V^i_{i+1,j,2} \\
V^i_{i,j-1,5} \\
V^i_{i,j+1,4} \\
V^i_{i-1,j-1,16} \\
V^i_{i+1,j+1,15} \\
V^i_{i-1,j+1,18} \\
V^i_{i+1,j-1,17} \\
V^i_{i,j,10} \\
V^i_{i-1,j,12} \\
V^i_{i+1,j,11} \\
V^i_{i,j-1,14} \\
V^i_{i,j+1,13} \\
V^i_{i-1,j-1,7} \\
V^i_{i+1,j+1,6} \\
V^i_{i-1,j+1,9} \\
V^i_{i+1,j-1,8}
\end{bmatrix}_{k+1}
=
\begin{bmatrix}
V^r_{i,j,1} \\
V^r_{i,j,2} \\
V^r_{i,j,3} \\
V^r_{i,j,4} \\
V^r_{i,j,5} \\
V^r_{i,j,6} \\
V^r_{i,j,7} \\
V^r_{i,j,8} \\
V^r_{i,j,9} \\
V^r_{i,j,10} \\
V^r_{i,j,11} \\
V^r_{i,j,12} \\
V^r_{i,j,13} \\
V^r_{i,j,14} \\
V^r_{i,j,15} \\
V^r_{i,j,16} \\
V^r_{i,j,17} \\
V^r_{i,j,18}
\end{bmatrix}_{k}
$$

(3.28)

which, when substituted into expressing (3.27), gives

$$
\begin{bmatrix}
V^i{}_{i,j,1}\\
V^i{}_{i-1,j,3}\\
V^i{}_{i+1,j,2}\\
V^i{}_{i,j-1,5}\\
V^i{}_{i,j+1,4}\\
V^i{}_{i-1,j-1,16}\\
V^i{}_{i+1,j-1,15}\\
V^i{}_{i-1,j+1,18}\\
V^i{}_{i+1,j+1,17}\\
V^i{}_{i,j,10}\\
V^i{}_{i-1,j,12}\\
V^i{}_{i+1,j,11}\\
V^i{}_{i,j-1,14}\\
V^i{}_{i,j+1,13}\\
V^i{}_{i-1,j-1,17}\\
V^i{}_{i+1,j+1,16}\\
V^i{}_{i-1,j+1,19}\\
V^i{}_{i+1,j-1,18}
\end{bmatrix}_{k+1}
= \frac{1}{Y}
\begin{bmatrix}
\mathbf{A} & [0] \\
[0] & \mathbf{B}
\end{bmatrix}
\begin{bmatrix}
V^i{}_{i,j,1}\\
V^i{}_{i,j,2}\\
V^i{}_{i,j,3}\\
V^i{}_{i,j,4}\\
V^i{}_{i,j,5}\\
V^i{}_{i,j,6}\\
V^i{}_{i,j,7}\\
V^i{}_{i,j,8}\\
V^i{}_{i,j,9}\\
V^i{}_{i,j,10}\\
V^i{}_{i,j,11}\\
V^i{}_{i,j,12}\\
V^i{}_{i,j,13}\\
V^i{}_{i,j,14}\\
V^i{}_{i,j,15}\\
V^i{}_{i,j,16}\\
V^i{}_{i,j,17}\\
V^i{}_{i,j,18}
\end{bmatrix}
$$

where

$$
\mathbf{A}=
\begin{bmatrix}
\frac{2}{Z_e}-Y & 2h_1 & 2h_1 & 2 & 2 & \frac{h}{2} & \frac{h}{2} & -\frac{h}{2} & -\frac{h}{2}\\
\frac{2}{Z_e} & 2h_1-Y & 2h_1 & 2 & 2 & \frac{h}{2} & \frac{h}{2} & -\frac{h}{2} & -\frac{h}{2}\\
\frac{2}{Z_e} & 2h_1 & 2h_1-Y & 2 & 2 & \frac{h}{2} & \frac{h}{2} & -\frac{h}{2} & -\frac{h}{2}\\
\frac{2}{Z_e} & 2h_1 & 2h_1 & 2-Y & 2 & \frac{h}{2} & \frac{h}{2} & -\frac{h}{2} & -\frac{h}{2}\\
\frac{2}{Z_e} & 2h_1 & 2h_1 & 2 & 2-Y & \frac{h}{2} & \frac{h}{2} & -\frac{h}{2} & -\frac{h}{2}\\
\frac{2}{Z_e} & 2h_1 & 2h_1 & 2 & 2 & \frac{h}{2}-Y & \frac{h}{2} & -\frac{h}{2} & -\frac{h}{2}\\
\frac{2}{Z_e} & 2h_1 & 2h_1 & 2 & 2 & \frac{h}{2} & \frac{h}{2}-Y & -\frac{h}{2} & -\frac{h}{2}\\
\frac{2}{Z_e} & 2h_1 & 2h_1 & 2 & 2 & \frac{h}{2} & \frac{h}{2} & -\frac{h}{2}-Y & -\frac{h}{2}\\
\frac{2}{Z_e} & 2h_1 & 2h_1 & 2 & 2 & \frac{h}{2} & \frac{h}{2} & -\frac{h}{2} & -\frac{h}{2}-Y
\end{bmatrix}
$$

$$
\mathbf{B}=
\begin{bmatrix}
\frac{2}{Z_e}-Y & 2 & 2 & 2h_1 & 2h_1 & \frac{h}{2} & \frac{h}{2} & -\frac{h}{2} & -\frac{h}{2}\\
\frac{2}{Z_e} & 2-Y & 2 & 2h_1 & 2h_1 & \frac{h}{2} & \frac{h}{2} & -\frac{h}{2} & -\frac{h}{2}\\
\frac{2}{Z_e} & 2 & 2-Y & 2h_1 & 2h_1 & \frac{h}{2} & \frac{h}{2} & -\frac{h}{2} & -\frac{h}{2}\\
\frac{2}{Z_e} & 2 & 2 & 2h_1-Y & 2h_1 & \frac{h}{2} & \frac{h}{2} & -\frac{h}{2} & -\frac{h}{2}\\
\frac{2}{Z_e} & 2 & 2 & 2h_1 & 2h_1-Y & \frac{h}{2} & \frac{h}{2} & -\frac{h}{2} & -\frac{h}{2}\\
\frac{2}{Z_e} & 2 & 2 & 2h_1 & 2h_1 & \frac{h}{2}-Y & \frac{h}{2} & -\frac{h}{2} & -\frac{h}{2}\\
\frac{2}{Z_e} & 2 & 2 & 2h_1 & 2h_1 & \frac{h}{2} & \frac{h}{2}-Y & -\frac{h}{2} & -\frac{h}{2}\\
\frac{2}{Z_e} & 2 & 2 & 2h_1 & 2h_1 & \frac{h}{2} & \frac{h}{2} & -\frac{h}{2}-Y & -\frac{h}{2}\\
\frac{2}{Z_e} & 2 & 2 & 2h_1 & 2h_1 & \frac{h}{2} & \frac{h}{2} & -\frac{h}{2} & -\frac{h}{2}-Y
\end{bmatrix}
$$

$$(3.29)$$

Rearranging, such that link line incident pulse indices match on both sides of the equation, gives

$$
\begin{bmatrix} V^i_{i,j,1} \\ V^i_{i+1,j,2} \\ V^i_{i-1,j,3} \\ V^i_{i,j+1,4} \\ V^i_{i,j-1,5} \\ V^i_{i+1,j+1,6} \\ V^i_{i-1,j-1,7} \\ V^i_{i+1,j-1,8} \\ V^i_{i-1,j+1,9} \\ V^i_{i,j,10} \\ V^i_{i+1,j,11} \\ V^i_{i-1,j,12} \\ V^i_{i,j+1,13} \\ V^i_{i,j-1,14} \\ V^i_{i+1,j+1,15} \\ V^i_{i-1,j-1,16} \\ V^i_{i+1,j-1,17} \\ V^i_{i-1,j+1,18} \end{bmatrix}_{k+1}
= \frac{1}{Y}
\begin{bmatrix}
\frac{2}{Z_s}-Y & 2rt & 2rt & 2 & 2 & \frac{h}{2} & \frac{h}{2} & -\frac{h}{2} & -\frac{h}{2} & 0 & 0 & 0 & 0 & 0 & 0 & 0 & 0 & 0 \\
\frac{2}{Z_s} & 2rt & 2rt-Y & 2 & 2 & \frac{h}{2} & \frac{h}{2} & -\frac{h}{2} & -\frac{h}{2} & 0 & 0 & 0 & 0 & 0 & 0 & 0 & 0 & 0 \\
\frac{2}{Z_s} & 2rt-Y & 2rt & 2 & 2 & \frac{h}{2} & \frac{h}{2} & -\frac{h}{2} & -\frac{h}{2} & 0 & 0 & 0 & 0 & 0 & 0 & 0 & 0 & 0 \\
\frac{2}{Z_s} & 2rt & 2rt & 2 & 2-Y & \frac{h}{2} & \frac{h}{2} & -\frac{h}{2} & -\frac{h}{2} & 0 & 0 & 0 & 0 & 0 & 0 & 0 & 0 & 0 \\
\frac{2}{Z_s} & 2rt & 2rt & 2-Y & 2 & \frac{h}{2} & \frac{h}{2} & -\frac{h}{2} & -\frac{h}{2} & 0 & 0 & 0 & 0 & 0 & 0 & 0 & 0 & 0 \\
0 & 0 & 0 & 0 & 0 & 0 & 0 & 0 & 0 & \frac{2}{Z_s} & 2 & 2 & 2rt & 2rt & \frac{h}{2} & \frac{h}{2}-Y & -\frac{h}{2} & -\frac{h}{2} \\
0 & 0 & 0 & 0 & 0 & 0 & 0 & 0 & 0 & \frac{2}{Z_s} & 2 & 2 & 2rt & 2rt & \frac{h}{2}-Y & \frac{h}{2} & -\frac{h}{2} & -\frac{h}{2} \\
0 & 0 & 0 & 0 & 0 & 0 & 0 & 0 & 0 & \frac{2}{Z_s} & 2 & 2 & 2rt & 2rt & \frac{h}{2} & \frac{h}{2} & -\frac{h}{2} & -\frac{h}{2}-Y \\
0 & 0 & 0 & 0 & 0 & 0 & 0 & 0 & 0 & \frac{2}{Z_s} & 2 & 2 & 2rt & 2rt & \frac{h}{2} & \frac{h}{2} & -\frac{h}{2}-Y & -\frac{h}{2} \\
0 & 0 & 0 & 0 & 0 & 0 & 0 & 0 & 0 & \frac{2}{Z_s}-Y & 2 & 2 & 2rt & 2rt & \frac{h}{2} & \frac{h}{2} & -\frac{h}{2} & -\frac{h}{2} \\
0 & 0 & 0 & 0 & 0 & 0 & 0 & 0 & 0 & \frac{2}{Z_s} & 2 & 2-Y & 2rt & 2rt & \frac{h}{2} & \frac{h}{2} & -\frac{h}{2} & -\frac{h}{2} \\
0 & 0 & 0 & 0 & 0 & 0 & 0 & 0 & 0 & \frac{2}{Z_s} & 2-Y & 2 & 2rt & 2rt & \frac{h}{2} & \frac{h}{2} & -\frac{h}{2} & -\frac{h}{2} \\
0 & 0 & 0 & 0 & 0 & 0 & 0 & 0 & 0 & \frac{2}{Z_s} & 2 & 2 & 2rt & 2rt-Y & \frac{h}{2} & \frac{h}{2} & -\frac{h}{2} & -\frac{h}{2} \\
0 & 0 & 0 & 0 & 0 & 0 & 0 & 0 & 0 & \frac{2}{Z_s} & 2 & 2 & 2rt-Y & 2rt & \frac{h}{2} & \frac{h}{2} & -\frac{h}{2} & -\frac{h}{2} \\
\frac{2}{Z_s} & 2rt & 2rt & 2 & 2 & \frac{h}{2} & \frac{h}{2}-Y & -\frac{h}{2} & -\frac{h}{2} & 0 & 0 & 0 & 0 & 0 & 0 & 0 & 0 & 0 \\
\frac{2}{Z_s} & 2rt & 2rt & 2 & 2 & \frac{h}{2}-Y & \frac{h}{2} & -\frac{h}{2} & -\frac{h}{2} & 0 & 0 & 0 & 0 & 0 & 0 & 0 & 0 & 0 \\
\frac{2}{Z_s} & 2rt & 2rt & 2 & 2 & \frac{h}{2} & \frac{h}{2} & -\frac{h}{2} & -\frac{h}{2}-Y & 0 & 0 & 0 & 0 & 0 & 0 & 0 & 0 & 0 \\
\frac{2}{Z_s} & 2rt & 2rt & 2 & 2 & \frac{h}{2} & \frac{h}{2} & -\frac{h}{2}-Y & -\frac{h}{2} & 0 & 0 & 0 & 0 & 0 & 0 & 0 & 0 & 0
\end{bmatrix}
\begin{bmatrix} V^i_{i,j,1} \\ V^i_{i,j,2} \\ V^i_{i,j,3} \\ V^i_{i,j,4} \\ V^i_{i,j,5} \\ V^i_{i,j,6} \\ V^i_{i,j,7} \\ V^i_{i,j,8} \\ V^i_{i,j,9} \\ V^i_{i,j,10} \\ V^i_{i,j,11} \\ V^i_{i,j,12} \\ V^i_{i,j,13} \\ V^i_{i,j,14} \\ V^i_{i,j,15} \\ V^i_{i,j,16} \\ V^i_{i,j,17} \\ V^i_{i,j,18} \end{bmatrix}_{k}
$$

(3.30)

from which the modified scattering matrix, **S'**, can be identified as

$$
\mathbf{S'} = \frac{1}{Y}
\begin{bmatrix}
\frac{2}{Z_s}-Y & 2rt & 2rt & 2 & 2 & \frac{h}{2} & \frac{h}{2} & -\frac{h}{2} & -\frac{h}{2} & 0 & 0 & 0 & 0 & 0 & 0 & 0 & 0 & 0 \\
\frac{2}{Z_s} & 2rt & 2rt-Y & 2 & 2 & \frac{h}{2} & \frac{h}{2} & -\frac{h}{2} & -\frac{h}{2} & 0 & 0 & 0 & 0 & 0 & 0 & 0 & 0 & 0 \\
\frac{2}{Z_s} & 2rt-Y & 2rt & 2 & 2 & \frac{h}{2} & \frac{h}{2} & -\frac{h}{2} & -\frac{h}{2} & 0 & 0 & 0 & 0 & 0 & 0 & 0 & 0 & 0 \\
\frac{2}{Z_s} & 2rt & 2rt & 2 & 2-Y & \frac{h}{2} & \frac{h}{2} & -\frac{h}{2} & -\frac{h}{2} & 0 & 0 & 0 & 0 & 0 & 0 & 0 & 0 & 0 \\
\frac{2}{Z_s} & 2rt & 2rt & 2-Y & 2 & \frac{h}{2} & \frac{h}{2} & -\frac{h}{2} & -\frac{h}{2} & 0 & 0 & 0 & 0 & 0 & 0 & 0 & 0 & 0 \\
0 & 0 & 0 & 0 & 0 & 0 & 0 & 0 & 0 & \frac{2}{Z_s} & 2 & 2 & 2rt & 2rt & \frac{h}{2} & \frac{h}{2}-Y & -\frac{h}{2} & -\frac{h}{2} \\
0 & 0 & 0 & 0 & 0 & 0 & 0 & 0 & 0 & \frac{2}{Z_s} & 2 & 2 & 2rt & 2rt & \frac{h}{2}-Y & \frac{h}{2} & -\frac{h}{2} & -\frac{h}{2} \\
0 & 0 & 0 & 0 & 0 & 0 & 0 & 0 & 0 & \frac{2}{Z_s} & 2 & 2 & 2rt & 2rt & \frac{h}{2} & \frac{h}{2} & -\frac{h}{2} & -\frac{h}{2}-Y \\
0 & 0 & 0 & 0 & 0 & 0 & 0 & 0 & 0 & \frac{2}{Z_s} & 2 & 2 & 2rt & 2rt & \frac{h}{2} & \frac{h}{2} & -\frac{h}{2}-Y & -\frac{h}{2} \\
0 & 0 & 0 & 0 & 0 & 0 & 0 & 0 & 0 & \frac{2}{Z_s}-Y & 2 & 2 & 2rt & 2rt & \frac{h}{2} & \frac{h}{2} & -\frac{h}{2} & -\frac{h}{2} \\
0 & 0 & 0 & 0 & 0 & 0 & 0 & 0 & 0 & \frac{2}{Z_s} & 2 & 2-Y & 2rt & 2rt & \frac{h}{2} & \frac{h}{2} & -\frac{h}{2} & -\frac{h}{2} \\
0 & 0 & 0 & 0 & 0 & 0 & 0 & 0 & 0 & \frac{2}{Z_s} & 2-Y & 2 & 2rt & 2rt & \frac{h}{2} & \frac{h}{2} & -\frac{h}{2} & -\frac{h}{2} \\
0 & 0 & 0 & 0 & 0 & 0 & 0 & 0 & 0 & \frac{2}{Z_s} & 2 & 2 & 2rt & 2rt-Y & \frac{h}{2} & \frac{h}{2} & -\frac{h}{2} & -\frac{h}{2} \\
0 & 0 & 0 & 0 & 0 & 0 & 0 & 0 & 0 & \frac{2}{Z_s} & 2 & 2 & 2rt-Y & 2rt & \frac{h}{2} & \frac{h}{2} & -\frac{h}{2} & -\frac{h}{2} \\
\frac{2}{Z_s} & 2rt & 2rt & 2 & 2 & \frac{h}{2} & \frac{h}{2}-Y & -\frac{h}{2} & -\frac{h}{2} & 0 & 0 & 0 & 0 & 0 & 0 & 0 & 0 & 0 \\
\frac{2}{Z_s} & 2rt & 2rt & 2 & 2 & \frac{h}{2}-Y & \frac{h}{2} & -\frac{h}{2} & -\frac{h}{2} & 0 & 0 & 0 & 0 & 0 & 0 & 0 & 0 & 0 \\
\frac{2}{Z_s} & 2rt & 2rt & 2 & 2 & \frac{h}{2} & \frac{h}{2} & -\frac{h}{2} & -\frac{h}{2}-Y & 0 & 0 & 0 & 0 & 0 & 0 & 0 & 0 & 0 \\
\frac{2}{Z_s} & 2rt & 2rt & 2 & 2 & \frac{h}{2} & \frac{h}{2} & -\frac{h}{2}-Y & -\frac{h}{2} & 0 & 0 & 0 & 0 & 0 & 0 & 0 & 0 & 0 \\
\end{bmatrix}
$$

$$(3.31)$$

82

The pulses incident on adjacent nodes at iteration $k + 1$, can be related to the incident pulses on node i, j at iteration k by the expression

$$
\begin{bmatrix} V^i_{i,j,1} \\ V^i_{i+1,j,2} \\ V^i_{i-1,j,3} \\ V^i_{i,j+1,4} \\ V^i_{i,j-1,5} \\ V^i_{i+1,j+1,6} \\ V^i_{i-1,j-1,7} \\ V^i_{i+1,j-1,8} \\ V^i_{i-1,j+1,9} \\ V^i_{i,j,10} \\ V^i_{i+1,j,11} \\ V^i_{i-1,j,12} \\ V^i_{i,j+1,13} \\ V^i_{i,j-1,14} \\ V^i_{i+1,j+1,15} \\ V^i_{i-1,j-1,16} \\ V^i_{i+1,j-1,17} \\ V^i_{i-1,j+1,18} \end{bmatrix}_{k+1}
= Q
\begin{bmatrix}
1 & 0 & 0 & 0 & 0 & 0 & 0 & 0 & 0 & 0 & 0 & 0 & 0 & 0 & 0 & 0 & 0 & 0 \\
0 & I & 0 & 0 & 0 & 0 & 0 & 0 & 0 & 0 & 0 & 0 & 0 & 0 & 0 & 0 & 0 & 0 \\
0 & 0 & I^{-1} & 0 & 0 & 0 & 0 & 0 & 0 & 0 & 0 & 0 & 0 & 0 & 0 & 0 & 0 & 0 \\
0 & 0 & 0 & J & 0 & 0 & 0 & 0 & 0 & 0 & 0 & 0 & 0 & 0 & 0 & 0 & 0 & 0 \\
0 & 0 & 0 & 0 & J^{-1} & 0 & 0 & 0 & 0 & 0 & 0 & 0 & 0 & 0 & 0 & 0 & 0 & 0 \\
0 & 0 & 0 & 0 & 0 & IJ & 0 & 0 & 0 & 0 & 0 & 0 & 0 & 0 & 0 & 0 & 0 & 0 \\
0 & 0 & 0 & 0 & 0 & 0 & I^{-1}J^{-1} & 0 & 0 & 0 & 0 & 0 & 0 & 0 & 0 & 0 & 0 & 0 \\
0 & 0 & 0 & 0 & 0 & 0 & 0 & IJ^{-1} & 0 & 0 & 0 & 0 & 0 & 0 & 0 & 0 & 0 & 0 \\
0 & 0 & 0 & 0 & 0 & 0 & 0 & 0 & I^{-1}J & 0 & 0 & 0 & 0 & 0 & 0 & 0 & 0 & 0 \\
0 & 0 & 0 & 0 & 0 & 0 & 0 & 0 & 0 & 1 & 0 & 0 & 0 & 0 & 0 & 0 & 0 & 0 \\
0 & 0 & 0 & 0 & 0 & 0 & 0 & 0 & 0 & 0 & I & 0 & 0 & 0 & 0 & 0 & 0 & 0 \\
0 & 0 & 0 & 0 & 0 & 0 & 0 & 0 & 0 & 0 & 0 & I^{-1} & 0 & 0 & 0 & 0 & 0 & 0 \\
0 & 0 & 0 & 0 & 0 & 0 & 0 & 0 & 0 & 0 & 0 & 0 & J & 0 & 0 & 0 & 0 & 0 \\
0 & 0 & 0 & 0 & 0 & 0 & 0 & 0 & 0 & 0 & 0 & 0 & 0 & J^{-1} & 0 & 0 & 0 & 0 \\
0 & 0 & 0 & 0 & 0 & 0 & 0 & 0 & 0 & 0 & 0 & 0 & 0 & 0 & IJ & 0 & 0 & 0 \\
0 & 0 & 0 & 0 & 0 & 0 & 0 & 0 & 0 & 0 & 0 & 0 & 0 & 0 & 0 & I^{-1}J^{-1} & 0 & 0 \\
0 & 0 & 0 & 0 & 0 & 0 & 0 & 0 & 0 & 0 & 0 & 0 & 0 & 0 & 0 & 0 & IJ^{-1} & 0 \\
0 & 0 & 0 & 0 & 0 & 0 & 0 & 0 & 0 & 0 & 0 & 0 & 0 & 0 & 0 & 0 & 0 & I^{-1}J
\end{bmatrix}_{k}
\begin{bmatrix} V^i_{i,j,1} \\ V^i_{i,j,2} \\ V^i_{i,j,3} \\ V^i_{i,j,4} \\ V^i_{i,j,5} \\ V^i_{i,j,6} \\ V^i_{i,j,7} \\ V^i_{i,j,8} \\ V^i_{i,j,9} \\ V^i_{i,j,10} \\ V^i_{i,j,11} \\ V^i_{i,j,12} \\ V^i_{i,j,13} \\ V^i_{i,j,14} \\ V^i_{i,j,15} \\ V^i_{i,j,16} \\ V^i_{i,j,17} \\ V^i_{i,j,18} \end{bmatrix}_{k}
$$

(3.32)

so that the matrix $\mathbf{T}$ can be identified as

$$
\mathbf{T} = \operatorname{diag} Q \begin{bmatrix} 1 & I & I^{-1} & J & J^{-1} & IJ & I^{-1}J^{-1} & IJ^{-1} & I^{-1}J & 1 & I & I^{-1} & J & J^{-1} & IJ & I^{-1}J^{-1} & IJ^{-1} & I^{-1}J \end{bmatrix}
$$

(3.33)

83

Substituting into (1.58), the matrices **T** and **S'**, gives

$$\frac{1}{Y}\begin{vmatrix}
Y(Q+1)-\frac{2}{Z_s} & -2rt & -2rt & -2 & -2 & \frac{h}{2} & \frac{h}{2} & \frac{h}{2} & \frac{h}{2} & 0 & 0 & 0 & 0 & 0 & 0 & 0 & 0 & 0 \\
-\frac{2}{Z_s} & YQI-2rt & Y-2rt & -2 & -2 & \frac{h}{2} & \frac{h}{2} & \frac{h}{2} & \frac{h}{2} & 0 & 0 & 0 & 0 & 0 & 0 & 0 & 0 & 0 \\
-\frac{2}{Z_s} & Y-2rt & YQ\Gamma^{-1}-2rt & -2 & -2 & \frac{h}{2} & \frac{h}{2} & \frac{h}{2} & \frac{h}{2} & 0 & 0 & 0 & 0 & 0 & 0 & 0 & 0 & 0 \\
-\frac{2}{Z_s} & -2rt & -2rt & YQJ-2 & Y-2 & -\frac{h}{2} & -\frac{h}{2} & \frac{h}{2} & \frac{h}{2} & 0 & 0 & 0 & 0 & 0 & 0 & 0 & 0 & 0 \\
-\frac{2}{Z_s} & -2rt & -2rt & Y-2 & YQ\Gamma^{-1}-2 & -\frac{h}{2} & -\frac{h}{2} & \frac{h}{2} & \frac{h}{2} & 0 & 0 & 0 & 0 & 0 & 0 & 0 & 0 & 0 \\
0 & 0 & 0 & 0 & 0 & YQU & 0 & 0 & 0 & -\frac{2}{Z_s} & -2 & -2 & -2rt & -2rt & \frac{h}{2} & Y-\frac{h}{2} & \frac{h}{2} & \frac{h}{2} \\
0 & 0 & 0 & 0 & 0 & 0 & YQ\Gamma^{-1}J^{-1} & 0 & 0 & -\frac{2}{Z_s} & -2 & -2 & -2rt & -2rt & Y-\frac{h}{2} & -\frac{h}{2} & \frac{h}{2} & \frac{h}{2} \\
0 & 0 & 0 & 0 & 0 & 0 & 0 & YQU^{-1} & 0 & -\frac{2}{Z_s} & -2 & -2 & -2rt & -2rt & \frac{h}{2} & -\frac{h}{2} & \frac{h}{2} & Y+\frac{h}{2} \\
0 & 0 & 0 & 0 & 0 & 0 & 0 & 0 & YQ\Gamma^{-1}J & -\frac{2}{Z_s} & -2 & -2 & -2rt & -2rt & \frac{h}{2} & \frac{h}{2} & Y+\frac{h}{2} & \frac{h}{2} \\
0 & 0 & 0 & 0 & 0 & 0 & 0 & 0 & 0 & Y(Q+1)-\frac{2}{Z_s} & -2 & -2 & -2rt & -2rt & \frac{h}{2} & \frac{h}{2} & \frac{h}{2} & \frac{h}{2} \\
0 & 0 & 0 & 0 & 0 & 0 & 0 & 0 & 0 & -\frac{2}{Z_s} & YQI-2 & Y-2 & -2rt & -2rt & \frac{h}{2} & -\frac{h}{2} & \frac{h}{2} & \frac{h}{2} \\
0 & 0 & 0 & 0 & 0 & 0 & 0 & 0 & 0 & -\frac{2}{Z_s} & Y-2 & YQ\Gamma^{-1}-2 & -2rt & -2rt & \frac{h}{2} & \frac{h}{2} & \frac{h}{2} & \frac{h}{2} \\
0 & 0 & 0 & 0 & 0 & 0 & 0 & 0 & 0 & -\frac{2}{Z_s} & -2 & -2 & YQJ-2rt & Y-2rt & \frac{h}{2} & -\frac{h}{2} & \frac{h}{2} & \frac{h}{2} \\
0 & 0 & 0 & 0 & 0 & 0 & 0 & 0 & 0 & -\frac{2}{Z_s} & -2 & -2 & Y-2rt & YQ\Gamma^{-1}-2rt & -\frac{h}{2} & -\frac{h}{2} & \frac{h}{2} & \frac{h}{2} \\
-\frac{2}{Z_s} & -2rt & -2rt & -2 & -2 & -\frac{h}{2} & Y-\frac{h}{2} & \frac{h}{2} & \frac{h}{2} & 0 & 0 & 0 & 0 & 0 & YQU & 0 & 0 & 0 \\
-\frac{2}{Z_s} & -2rt & -2rt & -2 & -2 & Y-\frac{h}{2} & -\frac{h}{2} & \frac{h}{2} & \frac{h}{2} & 0 & 0 & 0 & 0 & 0 & 0 & YQ\Gamma^{-1}J^{-1} & 0 & 0 \\
-\frac{2}{Z_s} & -2rt & -2rt & -2 & -2 & \frac{h}{2} & \frac{h}{2} & +\frac{h}{2} & Y+\frac{h}{2} & 0 & 0 & 0 & 0 & 0 & 0 & 0 & YQU^{-1} & 0 \\
-\frac{2}{Z_s} & -2rt & -2rt & -2 & -2 & \frac{h}{2} & \frac{h}{2} & Y+\frac{h}{2} & \frac{h}{2} & 0 & 0 & 0 & 0 & 0 & 0 & 0 & 0 & YQ\Gamma^{-1}J
\end{vmatrix}=0$$

(3.34)

from which the characteristic equation can be determined.

Manipulation of (3.34) using symbolic mathematics software Maple, yields the characteristic equation

$$AB + CA + CB = 0 \qquad (3.35)$$

where

$$A = \frac{\frac{1}{z_s} + 2h_1 + 2}{2}\left(Q - 2 + Q^{-1}\right) - h_1\left(I - 2 + I^{-1}\right) - \left(J - 2 + J^{-1}\right)$$
$$- \frac{h}{4}\left(IJ - I^{-1}J^{-1} - IJ^{-1} + I^{-1}J\right)$$

$$B = \frac{\frac{1}{z_s} + 2h_1 + 2}{2}\left(Q - 2 + Q^{-1}\right) - \left(I - 2 + I^{-1}\right) - h_1\left(J - 2 + J^{-1}\right)$$
$$- \frac{h}{4}\left(IJ - I^{-1}J^{-1} - IJ^{-1} + I^{-1}J\right)$$

$$C = \frac{h}{4}\left(IJ - I^{-1}J^{-1} - IJ^{-1} + I^{-1}J\right)$$

or, using equivalent continuous time representations,

$$A = \frac{\left(\frac{1}{z_s} + 2h_1 + 2\right)}{2}\frac{(\Delta t)^2}{(\Delta l)^2}\frac{\partial^2}{\partial t^2} - h_1\frac{\partial^2}{\partial x^2} - \frac{\partial^2}{\partial y^2} - h\frac{\partial^2}{\partial x\partial y}$$

$$B = \frac{\left(\frac{1}{z_s} + 2h_1 + 2\right)}{2}\frac{(\Delta t)^2}{(\Delta l)^2}\frac{\partial^2}{\partial t^2} - \frac{\partial^2}{\partial x^2} - h_1\frac{\partial^2}{\partial y^2} - h\frac{\partial^2}{\partial x\partial y} \qquad (3.36)$$

$$C = h\frac{\partial^2}{\partial x\partial y}$$

A number of "spurious solutions" similar to those of previous analyses are obtained in addition to (3.35).

To satisfy (3.35), either

$$A = B = C = 0 \qquad (3.37)$$

$$A = C = 0 \qquad (3.38)$$

$$B = C = 0 \qquad (3.39)$$

or

$$A = B = 0 \qquad (3.40)$$

Taking these solutions in turn and using the continuous time representations the following solutions are obtained.

From (3.37),

$$\frac{\left(\frac{1}{Z_s} + 2h_1 + 2\right)}{2} \frac{(\Delta t)^2}{(\Delta l)^2} \frac{\partial^2 \Phi_x}{\partial t^2} = h_1 \frac{\partial^2 \Phi_x}{\partial x^2} + \frac{\partial^2 \Phi_x}{\partial y^2}$$

$$\frac{\left(\frac{1}{Z_s} + 2h_1 + 2\right)}{2} \frac{(\Delta t)^2}{(\Delta l)^2} \frac{\partial^2 \Phi_y}{\partial t^2} = \frac{\partial^2 \Phi_y}{\partial x^2} + h_1 \frac{\partial^2 \Phi_y}{\partial y^2}$$

$$(3.41)$$

which represents waves propagating in two independent meshes, and corresponding to wave propagation in Φ_x and Φ_y meshes.

From (3.38),

$$\frac{\left(\frac{1}{Z_s} + 2h_1 + 2\right)}{2} \frac{(\Delta t)^2}{(\Delta l)^2} \frac{\partial^2 \Phi_x}{\partial t^2} = h_1 \frac{\partial^2 \Phi_x}{\partial x^2} + \frac{\partial^2 \Phi_x}{\partial y^2} \qquad (3.42)$$

86

which represents waves propagating in Φ_x mesh.

From (3.39),

$$\frac{\left(\frac{1}{Z_s}+2h_1+2\right)}{2}\frac{(\Delta t)^2}{(\Delta l)^2}\frac{\partial^2\Phi_y}{\partial t^2}=\frac{\partial^2\Phi_y}{\partial x^2}+h_1\frac{\partial^2\Phi_y}{\partial y^2} \qquad (3.43)$$

which represents waves propagating in the Φ_y mesh.

From (3.40),

$$\frac{\left(\frac{1}{Z_s}+2h_1+2\right)}{2}\frac{(\Delta t)^2}{(\Delta l)^2}\frac{\partial^2\Phi_x}{\partial t^2}=h_1\frac{\partial^2\Phi_x}{\partial x^2}+\frac{\partial^2\Phi_x}{\partial y^2}+h\frac{\partial^2\Phi_y}{\partial x\partial y}$$

$$\frac{\left(\frac{1}{Z_s}+2h_1+2\right)}{2}\frac{(\Delta t)^2}{(\Delta l)^2}\frac{\partial^2\Phi_y}{\partial t^2}=\frac{\partial^2\Phi_y}{\partial x^2}+h_1\frac{\partial^2\Phi_y}{\partial y^2}+h\frac{\partial^2\Phi_x}{\partial x\partial y} \qquad (3.44)$$

which represents waves propagating in two interdependent meshes, and corresponds to the desired solution for the elastic deformation model.

The stub impedance, Z_s, is determined by equating the wave velocity of the elastic deformation equations, (3.9), with the wave velocity of the TLM-state space derived equations, (3.44), giving

$$\sqrt{\frac{G}{\rho}}=\frac{\Delta l}{\Delta t}\sqrt{\frac{2}{\frac{1}{Z_s}+2h_1+2}} \qquad (3.45)$$

from which

$$Z_s = \frac{1}{2\left(\dfrac{\rho}{G}\dfrac{\Delta l^2}{\Delta t^2} - \left(1 + h_1\right)\right)}$$ (3.46)

The space step Δl is chosen to be sufficiently small to represent the smallest wavelength of interest, the time step Δt is chosen to ensure a positive stub impedance.

Noting that,

$$h = \left(1 + \frac{\lambda}{G}\right)$$

$$h_1 = \left(2 + \frac{\lambda}{G}\right)$$ (3.47)

and substituting into (3.44), expressions for h, h_1 and Z_s, gives

$$\frac{\rho}{G}\frac{\partial^2 u}{\partial t^2} = \left(2 + \frac{\lambda}{G}\right)\frac{\partial^2 u}{\partial x^2} + \frac{\partial^2 u}{\partial y^2} + \left(1 + \frac{\lambda}{G}\right)\frac{\partial^2 v}{\partial x \partial y}$$

$$\frac{\rho}{G}\frac{\partial^2 v}{\partial t^2} = \frac{\partial^2 v}{\partial x^2} + \left(2 + \frac{\lambda}{G}\right)\frac{\partial^2 v}{\partial y^2} + \left(1 + \frac{\lambda}{G}\right)\frac{\partial^2 u}{\partial x \partial y}$$ (3.48)

which are the elastic wave equations as presented in expression (3.9).

In the preceding analysis, the equations of elasticity were divided through by G at the outset, resulting in equations containing only one spacial derivative coefficient, h_1. This was done only to simplify the analysis, the nodal structure is equally effective with two spacial derivative coefficients, h_1 and h_2, which would result in the following model parameters,

$$h = G + \lambda$$
$$h_1 = 2G + \lambda$$
$$h_2 = G$$
$$Z_s = \frac{1}{2\left(\rho\frac{\Delta l^2}{\Delta t^2} - (h_1 + h_2)\right)}$$

(3.49)

The model would then solve the elastic wave equations as specified in (3.1). Chapter 5 presents several applications of the nodal structure analysed in this section for the solution of various two-dimensional isotropic elastic deformation problems.

3.4 Extension to anisotropic elastic deformation

Many elastic problems inviting analysis cannot be assumed to be isotropic. For example, consider the analysis of a wooden or composite material, subjected to applied forces. Such a problem would require analysis by techniques capable of solving anisotropic elastic equations. Therefore the extension of the two-dimensional, isotropic, TLM elastic deformation model to anisotropic materials should provide an extremely useful analysis tool, and provide an alternative to other numerical techniques. A publication shows the extension of the finite difference method to anisotropic elastic modelling in the area of seismic analysis [Faria E L,

Stoffa P L, 1994]. This section extends the two-dimensional isotropic elastic wave model, as described in previous sections, to the case of anisotropic, hyperelastic material.

The equations which describe anisotropic elastic deformation are presented in chapter two of this thesis. The equations of motion for a two-dimensional anisotropic, hyperelastic ($c_{ij} = c_{ji}$) material may be extracted from (2.18) giving

$$\rho \frac{\partial^2 u}{\partial t^2} = c_{11} \frac{\partial^2 u}{\partial x^2} + c_{66} \frac{\partial^2 u}{\partial y^2} + 2c_{16} \frac{\partial^2 u}{\partial x \partial y} + c_{16} \frac{\partial^2 v}{\partial x^2} + c_{26} \frac{\partial^2 v}{\partial y^2} + \left(c_{12} + c_{66}\right) \frac{\partial^2 v}{\partial x \partial y}$$

$$\rho \frac{\partial^2 v}{\partial t^2} = c_{66} \frac{\partial^2 v}{\partial x^2} + c_{22} \frac{\partial^2 v}{\partial y^2} + 2c_{26} \frac{\partial^2 v}{\partial x \partial y} + c_{16} \frac{\partial^2 u}{\partial x^2} + c_{26} \frac{\partial^2 u}{\partial y^2} + \left(c_{12} + c_{66}\right) \frac{\partial^2 u}{\partial x \partial y}$$

$$(3.50)$$

Comparing these with the equations for isotropic deformation, repeated below in (3.51), the extensions required of the isotropic model in order to model anisotropic, hyperelastic deformation can be seen.

$$\rho \frac{\partial^2 u}{\partial t^2} = (2G + \lambda) \frac{\partial^2 u}{\partial x^2} + G \frac{\partial^2 u}{\partial y^2} + (G + \lambda) \frac{\partial^2 v}{\partial x \partial y}$$

$$(3.51)$$

$$\rho \frac{\partial^2 v}{\partial t^2} = (2G + \lambda) \frac{\partial^2 v}{\partial y^2} + G \frac{\partial^2 v}{\partial x^2} + (G + \lambda) \frac{\partial^2 u}{\partial x \partial y}$$

Considering only the equations which describe deformation in the x direction, it is seen that the anisotropic, hyperelastic equation contains the additional spacial derivatives

$$2c_{16} \frac{\partial^2 u}{\partial x \partial y} \qquad\qquad (3.52)$$

$$c_{16} \frac{\partial^2 v}{\partial x^2} \qquad\qquad (3.53)$$

and

$$c_{26} \frac{\partial^2 v}{\partial y^2} \qquad\qquad (3.54)$$

Section 3.2.1 demonstrates how cross derivatives of the form (3.52) can be incorporated into TLM models by use of the nodal structure reported by Witwit *et al*, illustrated in figure 3.2. Additional scaled transmission lines, centred on nodal position (i, j), connect diagonally to nodes within the same mesh at positions $(i - 1, j + 1)$, $(i + 1, j + 1)$, $(i + 1, j - 1)$, and $(i - 1, j - 1)$. For the case of anisotropic, hyperelastic material, these transmission lines should have impedance scaling values of magnitude

$$\frac{4}{\left(2c_{16}\right)} \qquad\qquad (3.55)$$

Considering implementation of the remaining derivative terms in the anisotropic, hyperelastic equations, (3.53) and (3.54), intuitively, one might expect that since the nodal structure illustrated in figure 3.6a implements the spacial derivatives

$$\frac{\partial^2 \Phi_x}{\partial x^2} + \frac{\partial^2 \Phi_x}{\partial y^2} \qquad\qquad (3.56)$$

91

the nodal structure illustrated in figure 3.6b would implement the spacial derivatives

$$\frac{\partial^2 \Phi_y}{\partial x^2} + \frac{\partial^2 \Phi_y}{\partial y^2} \qquad (3.57)$$

In figure 3.6b, transmission lines centred on nodal position (i, j) in the Φ_x mesh connect to nodal positions $(i, j + 1)$, $(i, j - 1)$, $(i + 1, j)$, and $(i - 1, j)$ in the Φ_y mesh. To ensure correct coefficients for these spacial derivatives, the transmission line impedances, connecting $\Phi_x[i, j]$ to $\Phi_y[i - 1, j]$ and $\Phi_y[i + 1, j]$, are scaled by

$$\frac{1}{c_{16}} \qquad (3.58)$$

and those connecting $\Phi_x[i, j]$ to $\Phi_y[i, j - 1]$ and $\Phi_y[i, j + 1]$ are scaled by

$$\frac{1}{c_{26}} \qquad (3.59)$$

a

b
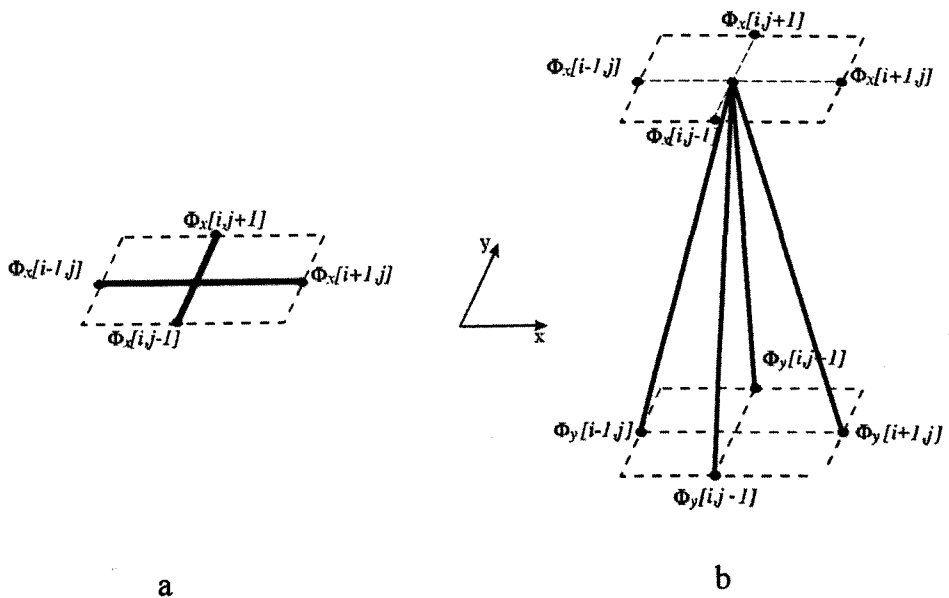
Figure 3.6 Nodal structures for implementation of spacial derivatives in the Φx mesh

(a) with respect to Φx and (b) with respect to Φy

The proposed nodal structure, for solution of displacement in the x direction, will therefore consist of the nodal structure used for the isotropic case, with an additional eight appropriately scaled transmission lines, for implementation of the extra spacial derivatives which feature in the anisotropic, hyperelastic equations. The full node is illustrated in figure 3.7, in which transmission lines have been omitted for clarity.
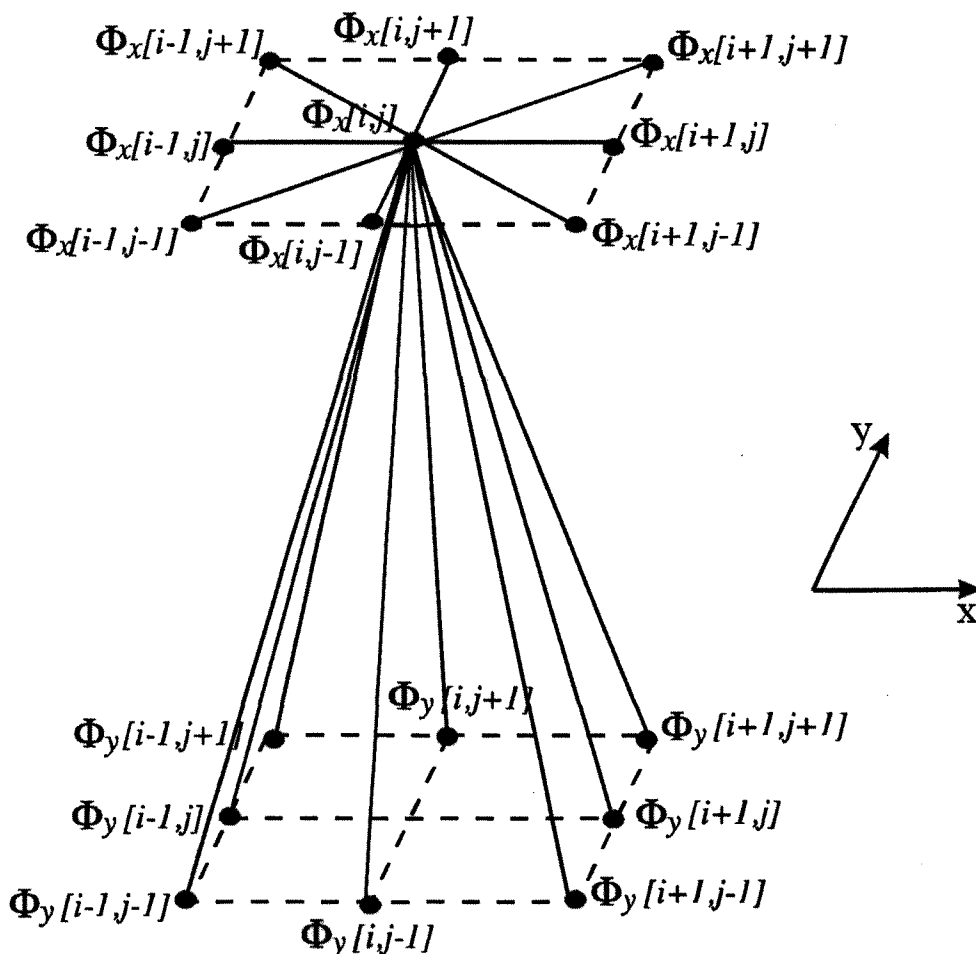
Figure 3.7 Proposed nodal structure for Φ_x mesh for solution of

anisotropic, hyperelastic waves

The nodal structure for the Φ_y mesh, consists of that of the isotropic elastic model, with eight additional transmission lines. Four of which implement the spacial cross derivative

$$2c_{26}\frac{\partial^2 v}{\partial x \partial y} \qquad\qquad (3.60)$$

These transmission lines, centred on nodal position (i, j) in the Φ_y, mesh, connect diagonally to nodes within the same mesh at positions $(i - 1, j + 1)$, $(i + 1, j + 1)$, $(i + 1, j - 1)$, and $(i - 1, j - 1)$, with scaled impedance of magnitude $(4Z/(2c_{26})$. The four remaining transmission lines implement the spacial derivatives

$$c_{16}\frac{\partial^2 u}{\partial x^2} \qquad\qquad (3.61)$$

and

$$c_{26}\frac{\partial^2 u}{\partial y^2} \qquad\qquad (3.62)$$

These transmission lines, centred on nodal position (i, j) in the Φ_y mesh connect to nodal positions $(i, j + 1)$, $(i, j - 1)$, $(i + 1, j)$, and $(i - 1, j)$ in the Φ_x mesh. The transmission lines connecting $\Phi_y[i, j]$ to $\Phi_x[i - 1, j]$ and $\Phi_x[i + 1, j]$ have impedance scaling of

$$\frac{1}{c_{16}} \qquad\qquad (3.63)$$

and those connecting $\Phi_y[i, j]$ to $\Phi_x[i, j - 1]$ and $\Phi_x[i, j + 1]$ have impedance scaling of

$$\frac{1}{c_{26}} \qquad\qquad (3.64)$$

Analysis of the nodal structure proposed for TLM modelling of two-dimensional, anisotropic, hyperelastic elastic deformation proves beyond the capability of the symbolic software available, due to the size of the scattering and associated matrices. However, the proposed nodal structure is used to model several cases of anisotropic elastic waves, the results of which are presented in chapter 5, and provides validation of the nodal structure.

3.5 Summary

Extensions to the standard TLM wave model nodal structure, required for modelling isotropic and anisotropic, hyperelastic elastic deformation in the bulk of the material have been proposed. Building on the work of Witwit *et al*, which describes the formulation of an eight port network from which scaled spacial cross derivatives can be incorporated into single mesh TLM models, methods of incorporating derivatives from a second mesh have been introduced. These methods appear readily extendible to any number of meshes. Scaling of spacial derivatives in TLM has also been described. The analysis of the resulting TLM nodal structure suitable for modelling the equations of isotropic elasticity, based on the TLM-state space analogy, has been described and provides validation of the nodal structure in terms of discrete representation of the elastic deformation equations. Extension of the isotropic nodal structure has been presented which should enable anisotropic, hyperelastic materials to be modelled.

Elastic analyses are generally concerned with finite bodies and interfaces of elastic bodies to externally applied loads and restraints. The following chapter describes the implementation of the boundary equations in the TLM elastic deformation model.

4

Boundary treatment

4.1 Introduction

Various types of boundary condition are applicable to elastic problems. The boundary conditions describe the interface of a body to its immediate surroundings. A generally applicable model should have the ability to model all practical boundary conditions. To this end it is necessary for the TLM elastic deformation model to implement displacement loaded, force loaded, free, restrained and frictional boundary conditions. The following section takes each of these boundary conditions in turn and describes their implementation using a nodal structure which is common to all of these boundary types. The examples of models of elastic bodies contained in this thesis are rectangular in shape, hence consideration is given to the treatment of boundaries at corners.

4.2 Boundary nodal structure

Irrespective of which boundary conditions are to be applied to a boundary, the TLM mesh must be terminated at boundaries. Generally, this is achieved by a skin of external nodes which surround the body, such that the boundary of the body lies half way between the internal or bulk nodes and the external or boundary nodes, as described in section 1.4.4. Figure 4.1 illustrates this concept, as applied to a two-dimensional, rectangular elastic body.
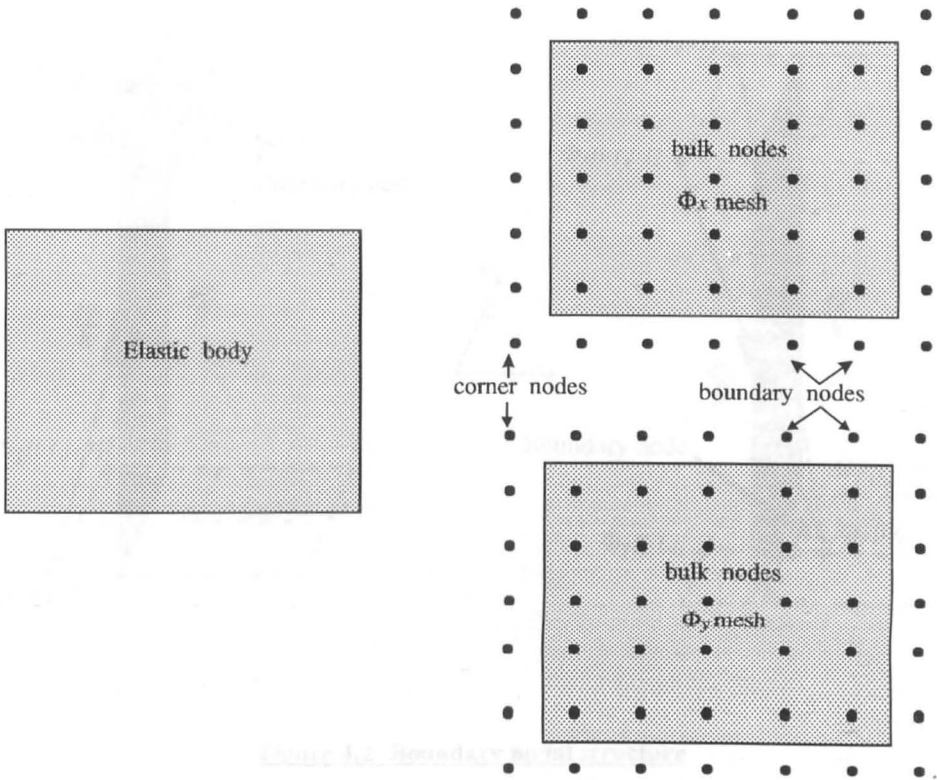
Figure 4.1 A two-dimensional rectangular elastic body and its discretised TLM model identifying bulk, boundary and corner nodes

The nodal structure of boundary nodes differs from that of internal nodes since the boundary nodes do not have adjacent nodes on all sides, and so require fewer transmission lines. Hence, the eight port nodal structure of the isotropic elastic bulk node must be modified if it is to be applied to the boundaries. The proposed nodal structure, for implementation of boundary nodes in the TLM isotropic elastic model, is illustrated in figure 4.2. Figure 4.2 illustrates the nodal structure for a node on a boundary which lies parallel to the y axis, the bulk of the elastic body lying to the left of the boundary. The structure consists of a single transmission line connecting the boundary node at position (i,j) to its immediate bulk node neighbour in the same mesh at position $(i - 1,j)$, and a further two transmission lines connecting the boundary node to diagonal neighbouring nodes, $(i - 1,j - 1)$ and $(i - 1,j + 1)$, in the other mesh. Similar structures terminate meshes along the remaining boundaries.

$\Phi_{x[i,j+1]}$

$\Phi_{x[i-1,j]}$ $\Phi_{x[i,j]}$

$\dfrac{Z}{h_1}$

$\Phi_{x[i,j-1]}$

Boundary node

$\dfrac{4Z}{h}$ $-\dfrac{4Z}{h}$

$\Phi_{y[i-1,j+1]}$

$\Phi_{y[i-1,j-1]}$

$\Phi_{x[i-1,j+1]}$

$\Phi_{x[i-1,j-1]}$

y

x

$-\dfrac{4Z}{h}$

$\dfrac{4Z}{h}$

Boundary node

$\Phi_{y[i,j+1]}$

$\Phi_{y[i-1,j]}$ $\Phi_{y[i,j]}$

$\dfrac{Z}{h_2}$

$\Phi_{y[i,j-1]}$
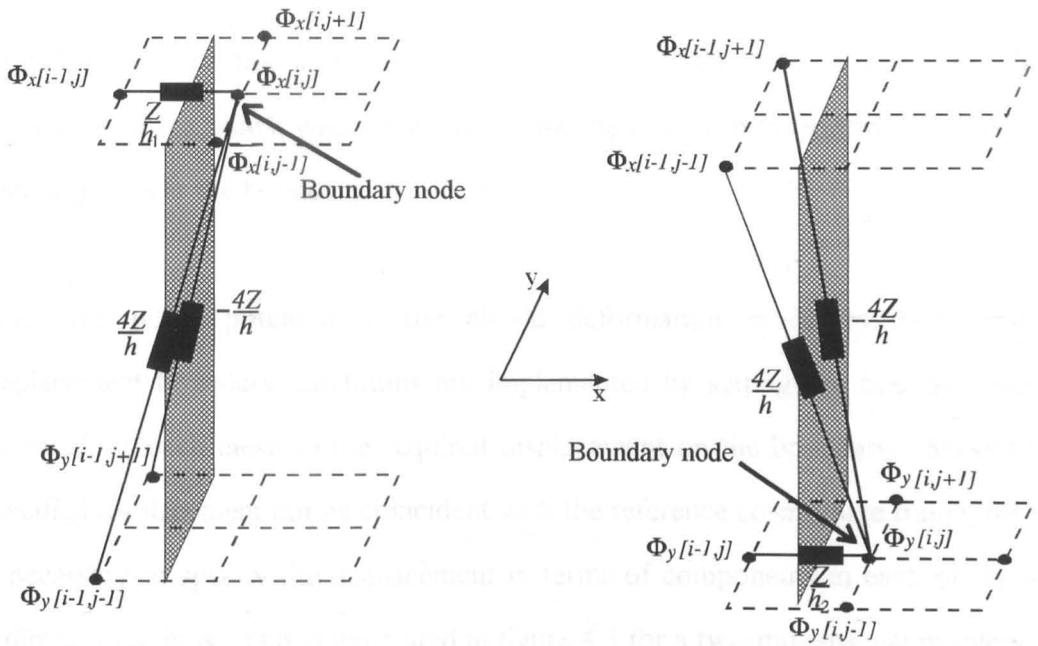
Figure 4.2 Boundary nodal structure

The potential of boundary nodes is calculated not in terms of incident pulses, as is the case for bulk nodes, but externally, in order to effect the correct boundary condition. Irrespective of which boundary condition is to be applied at a node, the boundary node potentials, $\Phi_x[i,j]$ and $\Phi_y[i,j]$, must be specified. This is in common with boundary conditions applied to other TLM models [Johns P B, Pulko S H, 1986]. The following sections describe the determination of boundary nodal potentials for various boundary conditions.

4.3 Displacement and restrained boundaries

Many elastic problems have boundary conditions which are specified in terms of displacements and restraints. For example, consider an elastic body with a clamped boundary so that movement is restricted in all co-ordinate directions. The displacement on such a boundary is zero in all co-ordinate directions. Also, consider

99

a rigid punch impacting an elastic body at a specified velocity or acceleration. The movement of the punch when in contact with the body can be specified in terms of displacements at the boundary.

Since the nodal potential in the elastic deformation model is displacement, displacement boundary conditions are implemented by setting the boundary nodal potentials in each mesh to the required displacement on the boundary. Should the specified displacement not lie coincident with the reference co-ordinate frame, then it is necessary to specify the displacement in terms of components in each of the co-ordinate directions. This is illustrated in figure 4.3 for a two-dimensional problem.
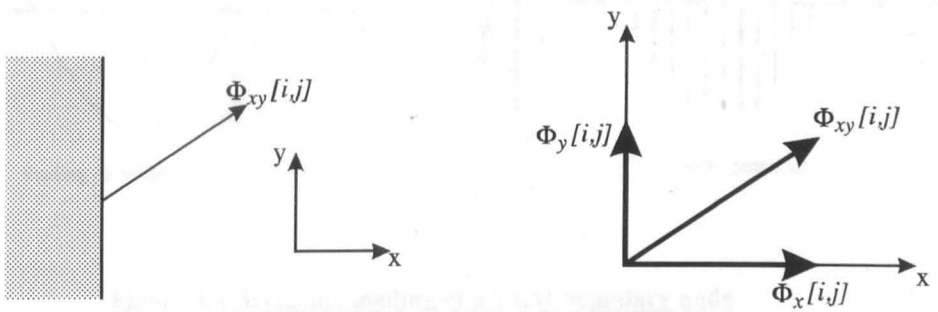
a.   Displacement specified on the boundary   b.   Reducing to component parts
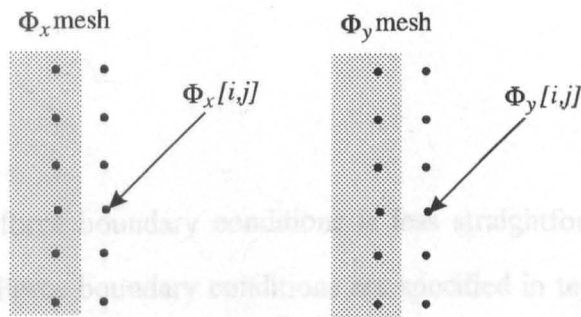
c.   Applying boundary conditions to the model

Figure 4.3 Stages in applying displacement boundary conditions to a TLM model

Dynamic displacement loading allows the specification of boundary velocities and accelerations. For a given acceleration or velocity, the displacement applied to the node is obtained by integration of the load with respect to time. As an iterative routine, dynamic loading of displacement boundary conditions is implemented simply by applying a new nodal displacement value at each iteration. This requires the time step to be small compared with dynamics of the loading. Figure 4.4 shows a continuous time sinusoidal loading function and the dynamic loading applied to the TLM boundary node to effect this loading.
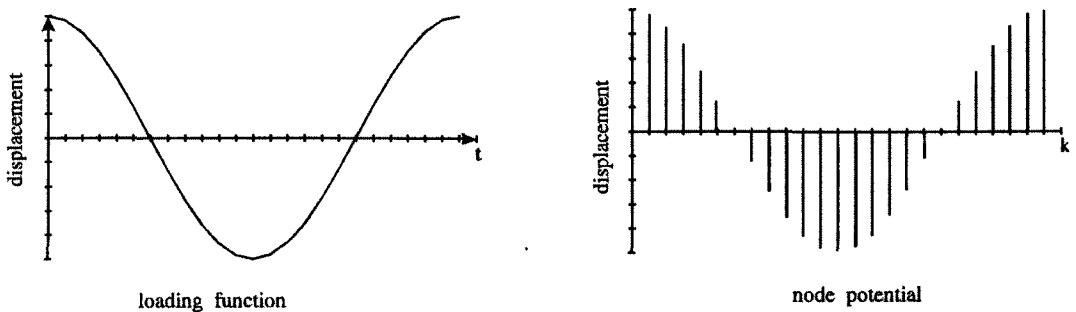
Figure 4.4 Dynamic loading of a TLM boundary node

4.4 Force boundaries

The implementation of force boundary conditions is less straightforward than the case of displacements. Force boundary conditions are specified in terms of stresses and surface forces as described in section 2.7. Expression (2.20) relates the applied surface forces to the internal stress state at the boundary of an elastic material. For two-dimensions this reduces to

$$\overline{X} = l\sigma_x + m\tau_{xy}$$

$$\overline{Y} = l\tau_{xy} + m\sigma_y$$

<div align="right">(4.1)</div>

where l and m are the direction cosines of the normal to the surface as defined in equation (2.21). Free boundaries have zero surface forces, consequently $\overline{X} = \overline{Y} = 0$.

The proposed TLM boundary nodal structure requires nodal potentials, corresponding to displacements, to be specified at the boundary. Recalling Hooke's law (2.12), which relates the stress state of a body to the strain, the equations in (4.1) may be written in terms of strains as

$$\overline{X} = l\left((2G+\lambda)\varepsilon_x + \lambda\varepsilon_y\right) + m\left(G\gamma_{xy}\right)$$

<div align="right">(4.2)</div>

and

$$\overline{Y} = l\left(G\gamma_{xy}\right) + m\left(\lambda\varepsilon_x + (2G+\lambda)\varepsilon_y\right)$$

<div align="right">(4.3)</div>

Substituting into these the small strain differential equations specified in (2.6) and (2.7) gives

$$\overline{X} = l\left((2G+\lambda)\frac{\partial u}{\partial x} + \lambda\frac{\partial v}{\partial y}\right) + m\left(G\left(\frac{\partial v}{\partial x} + \frac{\partial u}{\partial y}\right)\right)$$

<div align="right">(4.4)</div>

$$\overline{Y} = l\left(G\left(\frac{\partial v}{\partial x} + \frac{\partial u}{\partial y}\right)\right) + m\left(\lambda\frac{\partial u}{\partial x} + (2G+\lambda)\frac{\partial v}{\partial y}\right)$$

In these equations the surface forces are related to the displacements on the boundary, but, due to the spacial derivatives, it is not possible to specify boundary nodal potentials directly from these equations. The derivatives may be expressed as difference equations to yield a direct relationship between the surface forces and boundary displacements. Replacing the derivatives in (4.4) with the difference equations (Appendix 1)

$$\frac{\Phi_x(i+1,j)-\Phi_x(i-1,j)}{2\Delta l} \cong \frac{\partial u}{\partial x}$$

$$\frac{\Phi_y(i,j+1)-\Phi_y(i,j-1)}{2\Delta l} \cong \frac{\partial v}{\partial y}$$

$$\frac{\Phi_y(i+1,j)-\Phi_y(i-1,j)}{2\Delta l} \cong \frac{\partial v}{\partial x}$$

$$\frac{\Phi_x(i,j+1)-\Phi_x(i,j-1)}{2\Delta l} \cong \frac{\partial u}{\partial y}$$

$$(4.5)$$

gives

$$\overline{X} = l\left((2G+\lambda)\left(\frac{\Phi_x(i+1,j)-\Phi_x(i-1,j)}{2\Delta l}\right)+\lambda\left(\frac{\Phi_y(i,j+1)-\Phi_y(i,j-1)}{2\Delta l}\right)\right) \\ +m\left(G\left(\left(\frac{\Phi_y(i+1,j)-\Phi_y(i-1,j)}{2\Delta l}\right)+\left(\frac{\Phi_x(i,j+1)-\Phi_x(i,j-1)}{2\Delta l}\right)\right)\right)$$

$$(4.6)$$

and

$$\overline{Y} = l\left(G\left(\left(\frac{\Phi_y(i+1,j)-\Phi_y(i-1,j)}{2\Delta l}\right)+\left(\frac{\Phi_x(i,j+1)-\Phi_x(i,j-1)}{2\Delta l}\right)\right)\right) \\ +m\left(\lambda\left(\frac{\Phi_x(i+1,j)-\Phi_x(i-1,j)}{2\Delta l}\right)+(2G+\lambda)\left(\frac{\Phi_y(i,j+1)-\Phi_y(i,j-1)}{2\Delta l}\right)\right)$$

$$(4.7)$$

Of the nodal potentials in these equations, some are within the bulk, and have potentials specified in terms of incident pulses, the remaining are boundary potentials for which the equations must be solved.

As an example, consider figure 4.5 which illustrates part of an elastic body with an applied point force, F_y, on its lower surface.
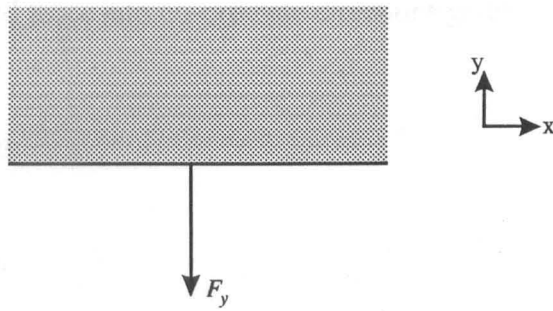
Figure 4.5 Boundary of an elastic body with applied point force

The boundary region of the TLM meshes are illustrated below.
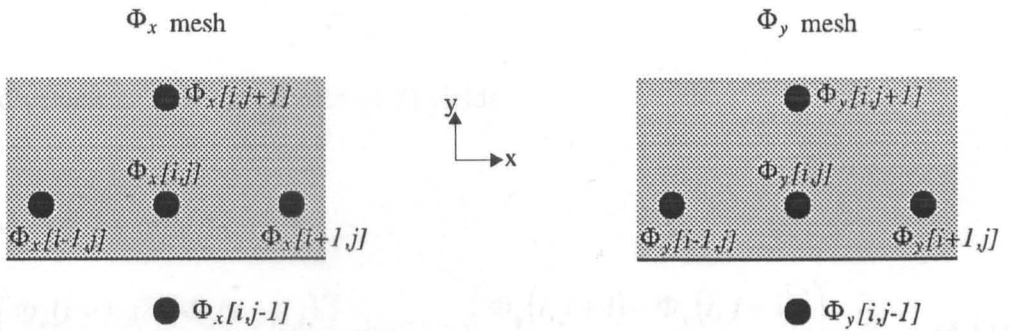
Figure 4.6 Template for forming the boundary difference equations

Since the boundary of the body lies parallel with the x axis of the reference co-ordinate frame, the direction cosines are calculated, using (2.21), to be

$$l = cos(90^0) = 0$$

$$m = cos(0^0) = 1$$

(4.8)

Resolving the applied force into co-ordinate directions gives

$$\overline{X} = 0$$

$$\overline{Y} = F_y$$

(4.9)

Substituting values for l, m and $\overline{X}$ into (4.6) yields

$$G\left(\left(\frac{\Phi_y(i+1,j) - \Phi_y(i-1,j)}{2\Delta l}\right) + \left(\frac{\Phi_x(i,j+1) - \Phi_x(i,j-1)}{2\Delta l}\right)\right) = 0 \qquad (4.10)$$

and values for l, m and $\overline{Y}$ into (4.7) yields

$$\left(\lambda\left(\frac{\Phi_x(i+1,j) - \Phi_x(i-1,j)}{2\Delta l}\right) + (2G + \lambda)\left(\frac{\Phi_y(i,j+1) - \Phi_y(i,j-1)}{2\Delta l}\right)\right) = F_y \qquad (4.11)$$

Solving the above equations for the nodal potentials, $\Phi_x[i,j-1]$ and $\Phi_y[i,j-1]$, which are boundary potentials, yields

$$\Phi_x(i,j-1) = \Phi_x(i,j+1) + \Phi_y(i+1,j) - \Phi_y(i-1,j)$$

$$\Phi_y(i,j-1) = \Phi_y(i,j+1) - \left(\frac{2\Delta l F_y - \lambda\left(\Phi_x(i+1,j) - \Phi_x(i-1,j)\right)}{2G+\lambda} \right)$$

(4.12)

This method of boundary treatment, which is based on the centred approximation of the derivative equations in (4.4), is identical to that used in some finite difference models of elastic deformation [Shibuya T, Nakahara I, Koizumi T, Kaibara K, 1975]. Investigations into the implementation of force boundary conditions using this approximation, by researchers of finite difference methods, have indicated the method to be unstable given certain elastic parameters [Ilan A, Loewenthal D, 1976]. As a result, modified implementations of the boundary equations based on the method outlined above have been introduced. These include the one-sided approximation and composed approximation [Ilan A, Loewenthal D, 1976], and new composed approximation [Ilan A, 1978].

In forming the difference equations of the continuous time boundary equations (4.4), the one-sided approximation uses the central difference approximation parallel to the boundary, and the one-sided difference approximation perpendicular to the boundary. This results in the boundary templates shown in figure 4.7.

106
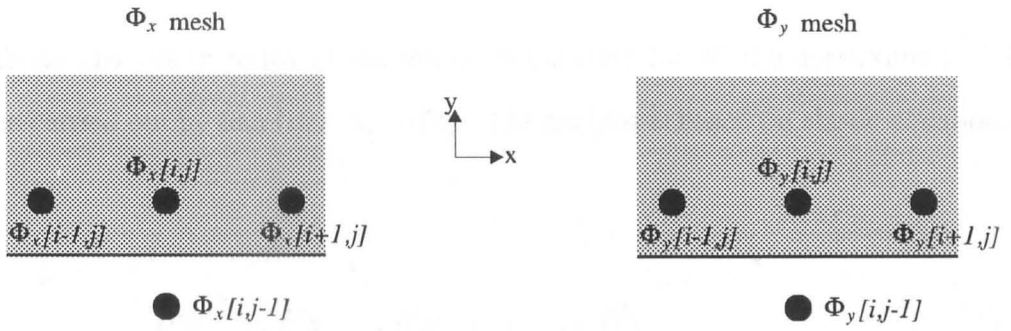
Figure 4.7 Template for forming the boundary difference equations using the one-sided approximation

The corresponding boundary equations expressed as difference equations are

$$\Phi_x(i, j-1) = \Phi_x(i, j) + 0.5\big(\Phi_y(i+1, j) - \Phi_y(i-1, j)\big)$$

(4.13)

$$\Phi_y(i, j-1) = \Phi_y(i, j) - 0.5\left(\frac{2\Delta l F_y - \lambda\big(\Phi_x(i+1, j) - \Phi_x(i-1, j)\big)}{2G+\lambda}\right)$$

Derivations of the centred and one-sided difference approximations are presented in Appendix 1.

The composed and new composed approximations result in equations that are not one step since the equations at iteration k are dependent upon values at iteration k-1 and k-2. One of the advantages of TLM is that it is a one step routine and since implementation of these approximations in TLM models would violate this they are not considered suitable.

Stability analysis in terms of the elastic parameters for all the approximations has been carried out by Ilan [Ilan A, 1978]. The analysis is based on elastic equations of the form

$$\frac{\partial^2 u}{\partial t^2} = \alpha^2 \frac{\partial^2 u}{\partial x^2} + \beta^2 \frac{\partial^2 u}{\partial y^2} + \left(\alpha^2 - \beta^2\right)\frac{\partial^2 v}{\partial x \partial y}$$

$$\frac{\partial^2 v}{\partial t^2} = \beta^2 \frac{\partial^2 v}{\partial x^2} + \alpha^2 \frac{\partial^2 v}{\partial y^2} + \left(\alpha^2 - \beta^2\right)\frac{\partial^2 u}{\partial x \partial y}$$

(4.14)

and Ilan determines the values of the ratio β/α for which the various difference approximations are stable. The results of the analysis are presented below.

Approximation	Range of Stability
Centred	$\frac{\beta}{\alpha} > 0.300$
One-sided	$\frac{\beta}{\alpha} > 0.350$
Composed	$\frac{\beta}{\alpha} > 0.575$
New composed	$\frac{\beta}{\alpha} > 0.000$

Table 4.1 Stability range for various finite difference boundary approximations [Ilan A, 1978]

Applying the analysis to the isotropic elastic deformation equations the corresponding parameters, β and α, are

$$\alpha^2 = \frac{2G + \lambda}{\rho}$$

(4.15)

$$\beta^2 = \frac{G}{\rho} \qquad (4.16)$$

and the ratio β/α may be expressed as

$$\frac{\beta}{\alpha} = \sqrt{\frac{G}{2G + \lambda}} \qquad (4.17)$$

Recalling from chapter two that G and λ may be expressed in terms of Young's modulus and Poisson's ratio, equations (2.13) and (2.14), the above expression may be written

$$\frac{\beta}{\alpha} = \sqrt{\frac{1 - 2v}{2(1 - v)}} \qquad (4.18)$$

With reference to the stability ranges presented in table 4.1, the corresponding limits for values of Poisson's ratio for each approximation may be determined.

The value $\beta/\alpha = 0.3$, the stability limit for the centred difference approximation, corresponds to Poisson's ratio equal to 0.45. Similarly, the value $\beta/\alpha = 0.35$, corresponds to Poisson's ratio equal to 0.43. Hence, the centred approximation becomes unstable in the finite difference model for Poisson's ratio greater that 0.45 and the one-sided approximation becomes unstable for Poisson's ratio greater than 0.43. Given that the implementation of the boundary using centred and one-sided

approximations can give rise to instability in the finite difference models, even when the stability criterion for the bulk (von Neumann) is satisfied, it can be expected that similar behaviour will be present in the TLM models given the same boundary implementation. This is investigated in chapter five where use is made of both central and one-sided approximations.

The similarity of the proposed boundary treatment to the methods used in other applications of TLM, for example, thermal diffusion, is discussed in section 4.2. However, in the elastic boundary formulation a feedback path exists since the external nodal potentials are determined not only from the applied external force, but also from the stress state within the body. The consequences of using this type of boundary formulation on the stability of the TLM routine have not been fully investigated and present an opportunity for future valuable research.

4.5 Frictional boundary

Friction presents itself in many engineering problems and is a consequence of the roughness and adhesion of materials resisting movement in contact regions between bodies [Bowden F P, Tabor D, 1956]. The modelling of frictional contact problems provides a useful analysis tool, and has been incorporated into several other numerical techniques [Olukoko O A, Becker A A, Fenner R T, 1993]. Friction occurring between bodies in contact may be described by Coulomb's law of friction [Bowden F P, Tabor D, 1956]. When surfaces are in contact, one of two regimes may exist. If there is no relative movement between adjacent points on the contacting surfaces then the points are in the "stick" regime. Alternatively, if relative movement between adjacent points on the contacting surfaces exists, then the points are in the "slip" regime. Coulomb's law of friction defines which of the

aforementioned regimes is appropriate for a point of contact, depending on the coefficient of friction and the forces acting in the region of the point. If the tangential force at the point of contact is less than the product of the coefficient of friction and the normal force, then the contact point will stick. Otherwise the point of contact will slip and the value of the tangential force is equal to the product of the coefficient of friction and the normal force, or more concisely

$$\text{stick:} \quad |\tau_t| < \mu\tau_n$$

$$\text{slip:} \quad |\tau_t| = \mu\tau_n$$

(4.19)

where

$$-\mu\tau_n \leq \tau_t \leq \mu\tau_n$$

and

τ_t is the tangential force at the surface point of contact

τ_n is the normal force at the surface point of contact

μ is the coefficient of friction.

The notation is illustrated in figure 4.8.

If at the outset the bodies are not in contact, then the problem of determining at which point the bodies come into contact presents itself. Consider the case of two elastic bodies some distance apart but travelling towards each other as illustrated in figure 4.9.
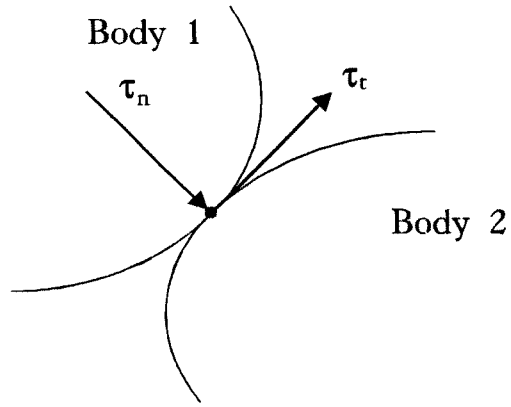
Figure 4.8 Normal and tangential forces at a contacting boundary point

In this state the boundary conditions are those for free boundaries as described in section 4.4. As the bodies approach each other, a contact condition may be identified by monitoring the co-ordinate points of nodes on the surfaces of the bodies. If the co-ordinates of a surface node in one of the bodies coincide with the
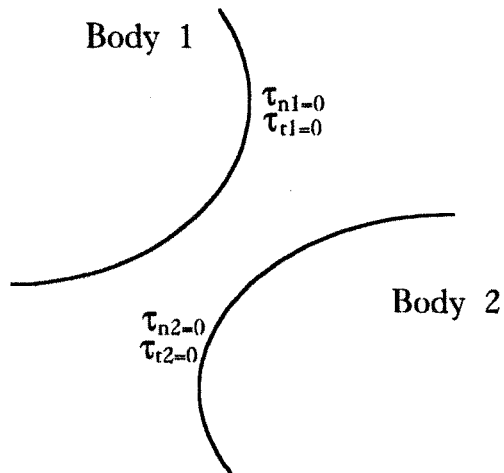
Figure 4.9 Two non-contacting bodies

surface or the bulk of the second body then the bodies are defined as being in contact. For the case of a surface node entering the bulk of the second body, as shown in figure 4.10, then an overlap condition has occurred and correction to the surface node must be applied.

Body 1

Body 2
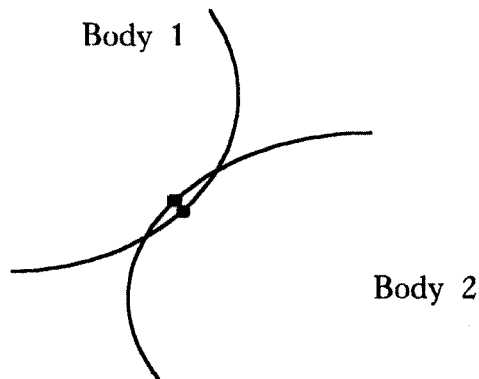
Figure 4.10 Overlap condition

Upon contact, normal and tangential forces are generated at each of the contact points. The force generated by one body loads the body with which it is in contact, and vice versa. The normal and tangential forces at the boundary are generated when the two boundaries overlap and correction is made to the boundary nodal positions to ensure that the boundaries are compatible, as illustrated in figure 4.11. This is in common with other numerical techniques [Olukoko O A, Becker A A, Fenner R T, 1993]

For the case of contact between two bodies with an infinite coefficient of friction the normal force and the normal displacement across the boundaries are continuous. Similarly a continuous tangential force and displacement exists across the boundary, since no relative tangential displacement between the two body surfaces is possible.
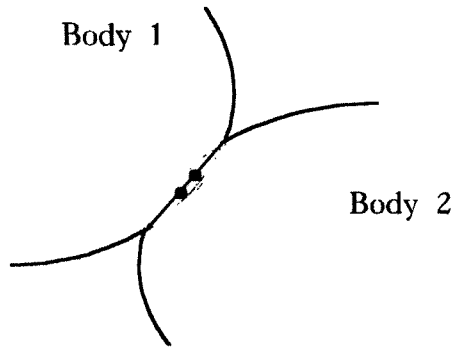
Figure 4.11 Correction of boundary node positions

Therefore

$$\tau_{n1} = \tau_{n2}$$

$$\tau_{t1} = \tau_{t2}$$

(4.20)

where subscript n denotes normal force, subscript t denotes tangential force, and 1 and 2 identify the individual bodies.

In the case of contact between two bodies of finite coefficient of friction, the normal force and displacement remain continuous across the boundary but the tangential force and displacement will be continuous only up to the friction threshold, specified by

$$|\tau_t| = \mu\tau_n$$

(4.21)

Once this threshold is reached, tangential forces and displacements are no longer continuous across the surface and slipping occurs. Then the slip condition of equation (4.19) determines the behaviour of the boundary.

To demonstrate how frictional contact can be applied to the boundaries of a TLM model, consider the case of an elastic body brought into contact with a rigid base as shown in figure 4.12.
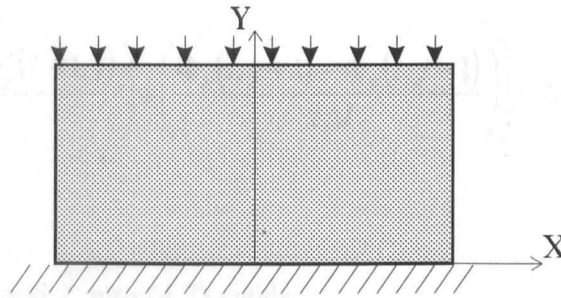
Figure 4.12 An elastic body in contact with a rigid base

Considering the contacting surface only, the nodal template used for forming the boundary equations is as illustrated in figure 4.6. It is not necessary to discretise the base since it is rigid and no displacement can occur. When there is no contact between the elastic body and the rigid base, then the lower surface of the body is free and the forces on this surface are

$$\overline{X} = \overline{Y} = 0 \qquad (4.22)$$

Considering equation (4.1), the direction cosines, as defined in (2.21) are

$$l = cos(90^0) = 0$$

$$(4.23)$$

$$m = cos(0^0) = 1$$

Substituting values for l, m and $\overline{X}$ into (4.6) yields

$$G\left(\left(\frac{\Phi_y(i+1,j) - \Phi_y(i-1,j)}{2\Delta l}\right) + \left(\frac{\Phi_x(i,j+1) - \Phi_x(i,j-1)}{2\Delta l}\right)\right) = 0 \qquad (4.24)$$

and values for l, m and $\overline{Y}$ into (4.7) yields

$$\left(\lambda\left(\frac{\Phi_x(i+1,j) - \Phi_x(i-1,j)}{2\Delta l}\right) + (2G+\lambda)\left(\frac{\Phi_y(i,j+1) - \Phi_y(i,j-1)}{2\Delta l}\right)\right) = 0 \qquad (4.25)$$

Solving (4.24) and (4.25) for the boundary nodal potentials, $\Phi_x[i,j-1]$ and $\Phi_y[i,j-1]$, yields

$$\Phi_x(i,j-1) = \Phi_x(i,j+1) + \Phi_y(i+1,j) - \Phi_y(i-1,j)$$

$$(4.26)$$

$$\Phi_y(i,j-1) = \Phi_y(i,j+1) + \left(\frac{\lambda(\Phi_x(i+1,j) + \Phi_x(i-1,j))}{2G+\lambda}\right)$$

Upon contact, there can be no further displacement of the contacting boundary in the y direction. Consequently, the boundary nodal potential in the Φ_y mesh is set equal to zero, giving

$$\Phi_y(i,j-1) = 0 \qquad (4.27)$$

Initially, the contact region assumes the stick condition so that the boundary nodal potential in the Φ_x mesh is set equal to zero, thus

$$\Phi_x(i,j-1) = 0 \qquad (4.28)$$

This is reasonable since the boundary must generate normal forces before the slip condition can occur. Over subsequent iterations, the normal force on the contacting boundary may increase, and zero potential is maintained on the Φ_x mesh. If the Coulomb threshold is reached, the tangential surface force is given by the slip condition of (4.19), which can be expressed as

$$\overline{X} = \mu F_y \qquad (4.29)$$

where F_y is the normal stress generated due to contact with the rigid base.

Substituting (4.29) and (4.23) into (4.6), gives

$$\mu F_y = G\left(\left(\frac{\Phi_y(i+1,j) - \Phi_y(i-1,j)}{2\Delta l}\right) + \left(\frac{\Phi_x(i,j+1) - \Phi_x(i,j-1)}{2\Delta l}\right)\right) \qquad (4.30)$$

117

Displacement in the x direction due to slipping is determined by solving this equation for $\Phi_x(i, j - 1)$, giving

$$\Phi_x(i, j-1) = \Phi_y(i+1, j) - \Phi_y(i-1, j) + \Phi_x(i, j+1) - \frac{2\Delta l \mu F_y}{G} \qquad (4.31)$$

F_y can be determined from stress measures taken at the contacting boundary. The normal force on the boundary is given by

$$F_y = \sigma_y \qquad (4.32)$$

From Hooke's law, (2.12), σ_y can be expressed in terms of strain components as

$$\sigma_y = \lambda \varepsilon_x + (2G + \lambda)\varepsilon_y \qquad (4.33)$$

Expressing the strain components as derivatives, from (2.6), gives

$$\sigma_y = \lambda \frac{\partial u}{\partial x} + (2G + \lambda)\frac{\partial v}{\partial y} \qquad (4.34)$$

Replacing the displacement derivatives with difference approximations as specified in (4.5) yields

$$\sigma_y = \lambda \left(\frac{\Phi_x(i+1, j) - \Phi_x(i-1, j)}{2\Delta l} \right) + (2G + \lambda)\left(\frac{\Phi_y(i, j+1) - \Phi_y(i, j-1)}{2\Delta l} \right) \qquad (4.35)$$

which provides a measure of the normal force acting on the contacting boundary.

Chapter five presents the results from a TLM elastic deformation model of an elastic body in contact with a rigid base.

4.6 Corners

Corners require special attention with regard to nodal structure and the boundary conditions applied at the corner region. Frequently, corners are the interface between different boundary conditions on different faces of the body, consequently the boundary conditions at corners are not well defined. Figure 4.13 shows the corner region of an elastic body and the associated region of the TLM meshes.
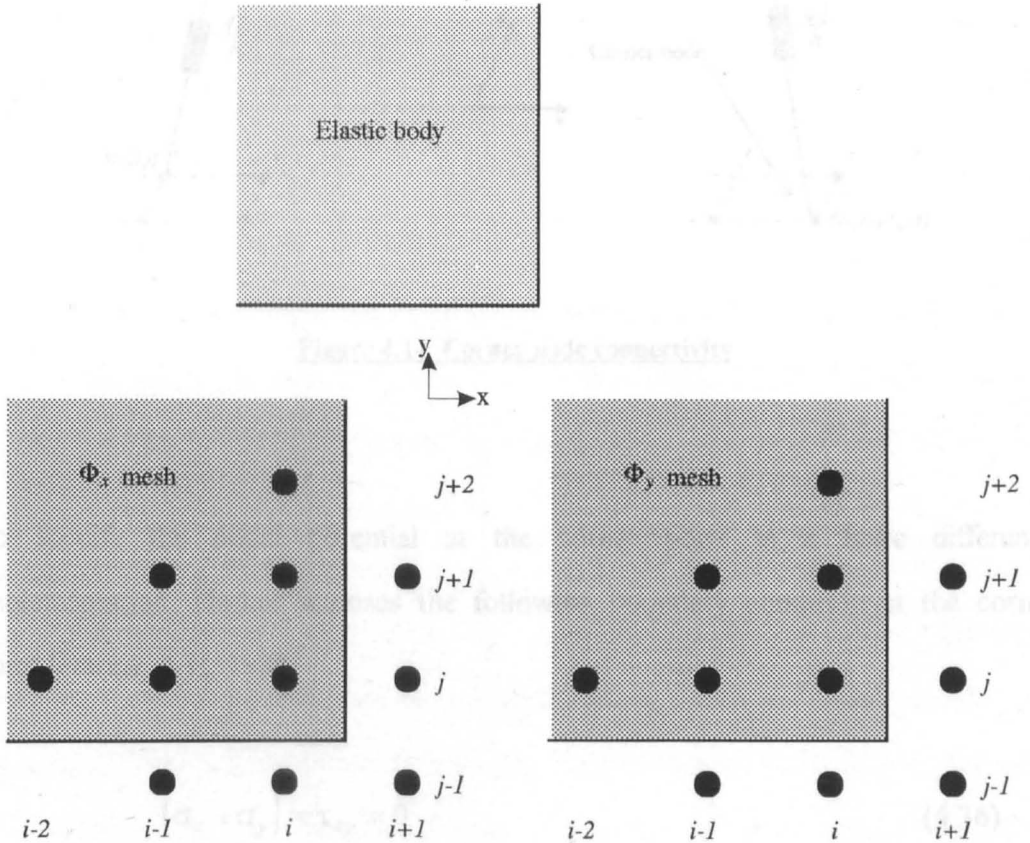
Figure 4.13 Corner region of the body and model

Applying the central or one-sided templates for force or free boundaries to the nodes at positions $(i,j-1)$ and $(i+1,j)$, requires simultaneous solution of the two boundary conditions on each face [Harker A H, 1988]. With regard to specifying the nodal potentials at position $(i+1,j-1)$, the TLM elastic deformation model requires the specification of the nodal potential at this point, since termination of the TLM mesh requires a transmission line connection between the corner node in one mesh, and its diagonal neighbour in the other mesh, as illustrated below.
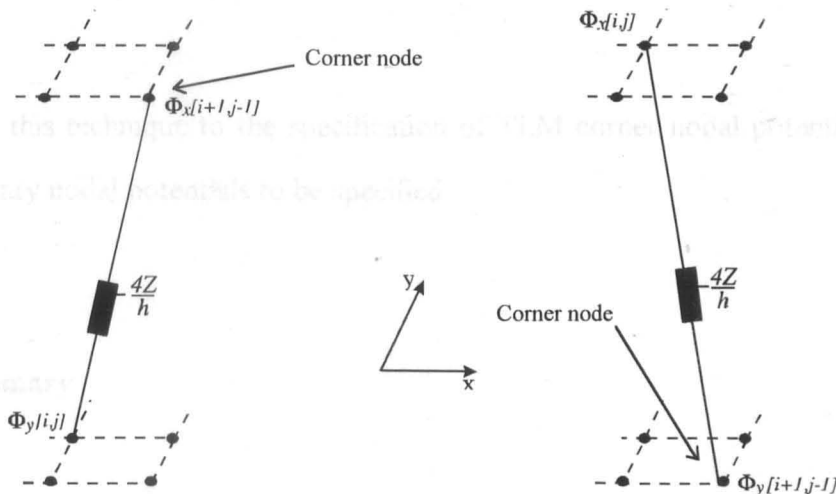
Figure 4.14 Corner node connectivity

To specify the nodal potential at the corner point in a finite difference implementation, Harker imposes the following boundary condition at the corner point [Harker A H, 1988]

$$\left(\sigma_x + \sigma_y\right) = \tau_{xy} = 0 \qquad (4.36)$$

In implementing the boundary conditions as difference equations, the reference co-ordinate axes are rotated by 45° so that the boundary equations, in difference form, for the corner illustrated in figure 4.14 may be expressed as

$$\Phi_x(i+1, j-1) = \Phi_x(i-1, j+1) + \Phi_y(i-1, j+1) - \Phi_y(i+1, j+1)$$

$$(4.37)$$

$$\Phi_y(i+1, j-1) = \Phi_y(i-1, j+1) + \Phi_x(i-1, j-1) - \Phi_x(i+1, j+1)$$

Applying this technique to the specification of TLM corner nodal potentials allows all boundary nodal potentials to be specified.

4.7 Summary

The boundary treatment for the TLM elastic deformation model has been presented. Boundaries are implemented by a skin of surface nodes which surround the bulk nodes. The boundary nodal potentials may be calculated to effect displacement, force and frictional boundary conditions. Due to the equivalence of displacement and nodal potential, displacement boundary conditions simply require the appropriate nodal potential to be set equal to the required displacement. Force boundary conditions require the discretisation of the boundary equations by use of difference equations. The implementation of force boundary conditions is the same as that used by the finite difference method of elastic modelling. The stability limits of the various differencing schemes, determined by Ilan, have been presented [Ilan A, 1978]. Calculation of boundary nodal potentials, adjacent to corners, requires the

simultaneous solution of boundary condition equations. The application of boundary equations to corner points has been considered also and is equivalent to the method used in some finite difference elastic models.

5

Numerical Implementations

5.1 Introduction

The preceding chapters describe the TLM modelling method and develop nodal structures suitable for two-dimensional, isotropic and anisotropic elastic deformation modelling. Methods are developed for applying a wide variety of boundary conditions. This chapter applies the TLM elastic deformation model to several elastic problems, the results of which are used to validate the technique and demonstrate its capability. The various models presented in this chapter are validated against results using analytical or numerical methods as published by various authors.

5.2 Two-dimensional isotropic models

5.2.1 Semi-infinite plate

The case of a two-dimensional, semi-infinite plate subjected to an applied force is useful as an initial model, since the modelled region contains no corners and only one boundary. Analytical and finite difference solutions have been reported [Shibuya T, Nakahara I, Koizumi T, Kaibara K, 1975]. The elastic problem requires the calculation of transient and steady state stress values at several points in the bulk and on the surface of an elastic half plane resulting from loading applied along part of the surface. Figure 5.1 illustrates the problem. The predictions from the TLM model,

for direct stresses, σ_x and σ_y, and the shear stress, τ_{xy}, at the positions indicated in figure 5.1, are to be compared with those for the finite difference model, reported by Shibuya *et al.*
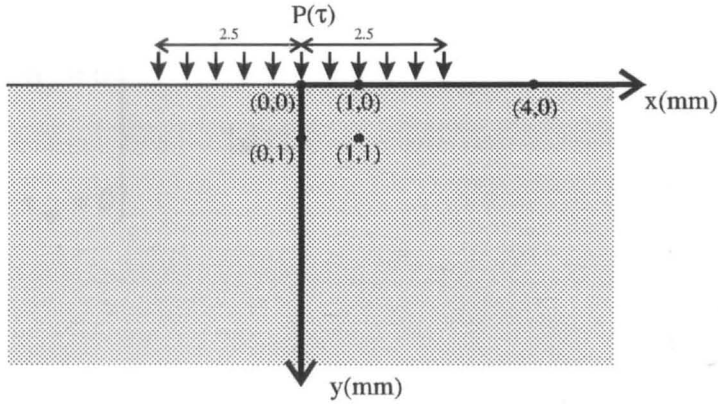
Figure 5.1 Semi-infinite plate subjected to excitation P(τ) over part of its surface - co-ordinates refer to points on a 1mm grid

The applied excitation $P(\tau)$ is of the form shown in figure 5.2. τ represents the scaled time variable such that $\tau = t\sqrt{(2G+\lambda)/\rho}$, where t signifies time in seconds.
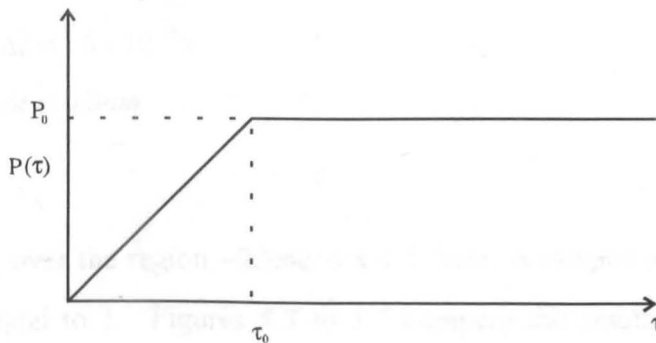
Figure 5.2 Load applied to the semi-infinite plate

The appropriate boundary descriptions are

$$\left. \begin{array}{l} \sigma_y = P(\tau) \\ \\ \tau_{xy} = 0 \end{array} \right\} \quad |x| \leq 2.5$$

$$\left. \begin{array}{l} \sigma_y = 0 \\ \\ \tau_{xy} = 0 \end{array} \right\} \quad |x| \rangle 2.5$$

and the material properties of the plate are those of mild steel, given by

$$E = 2.1 \times 10^{10} \, \text{N/m}^2$$

$$\rho = 7860 \, \text{kg/m}^3$$

$$v = 0.3$$

The TLM model operates with the following time and space steps for consistency with the finite difference model

$$\Delta t = 1.6 \times 10^{-5} s$$

$$\Delta l = 0.1mm$$

The excitation, over the region $-2.5mm \leq x \leq 2.5mm$, is ramped according to figure 5.2, with τ_0 equal to 1. Figures 5.3 to 5.7 compare the results produced by the TLM elastic deformation model with those reported by Shibuya *et al*, for the finite difference model [Shibuya T *et al*, 1975]. The solid curves represent the results for

125

the TLM model, and the broken curves represent the results for the finite difference model. In all cases the level of agreement between the two methods is excellent.
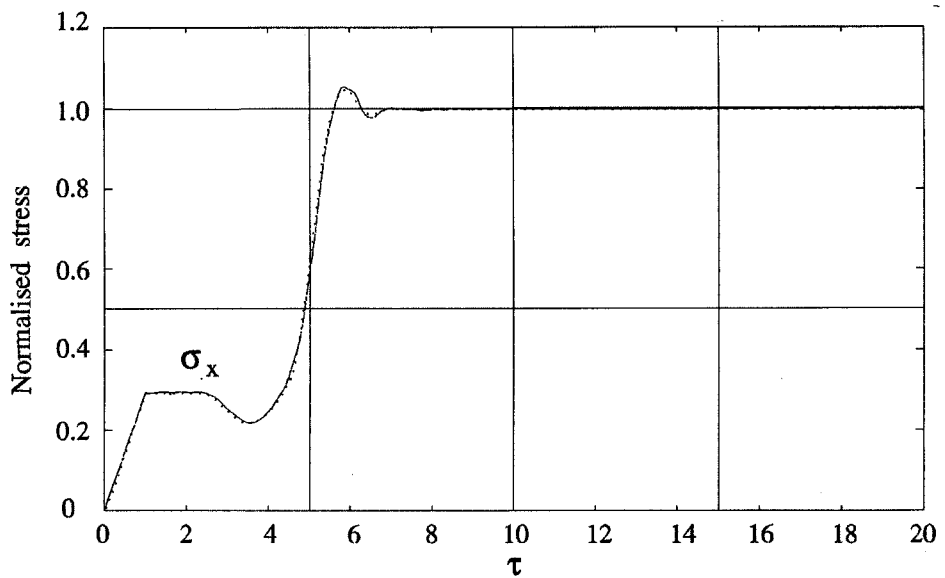
Figure 5.3 Stress at the point (0,0)
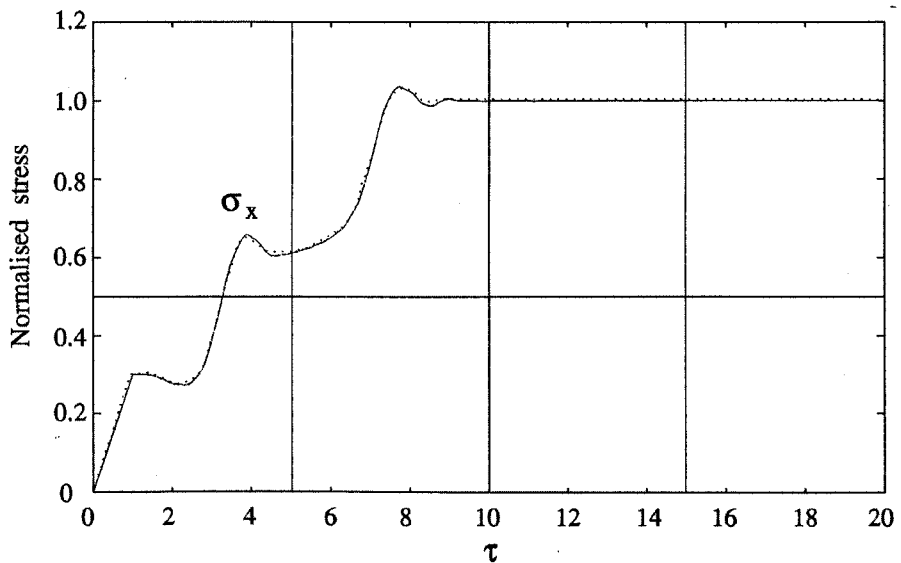
Figure 5.4 Stress at the point (1,0)
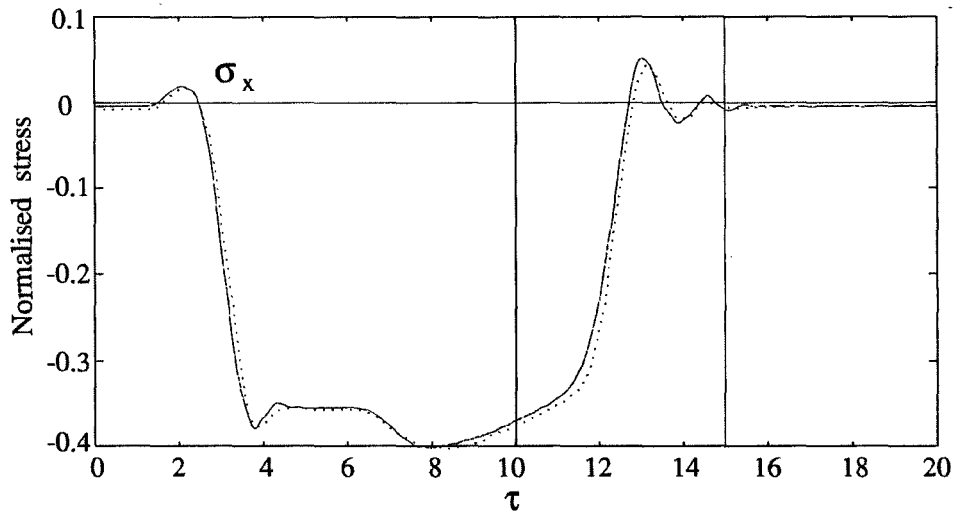
Figure 5.5 Stress at the point (4,0)
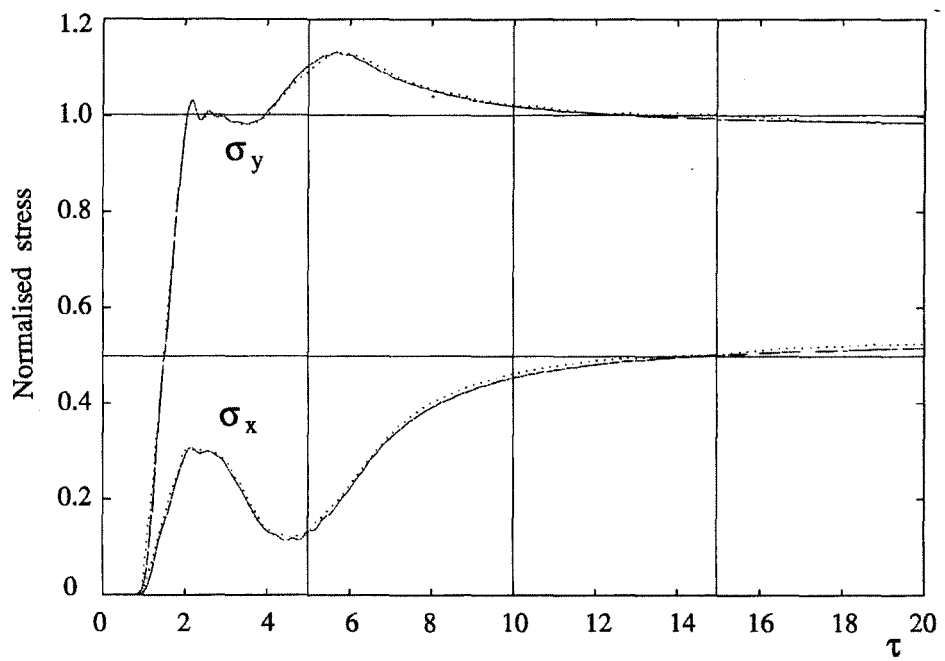
Figure 5.6 Stresses at the point (0,1)

127
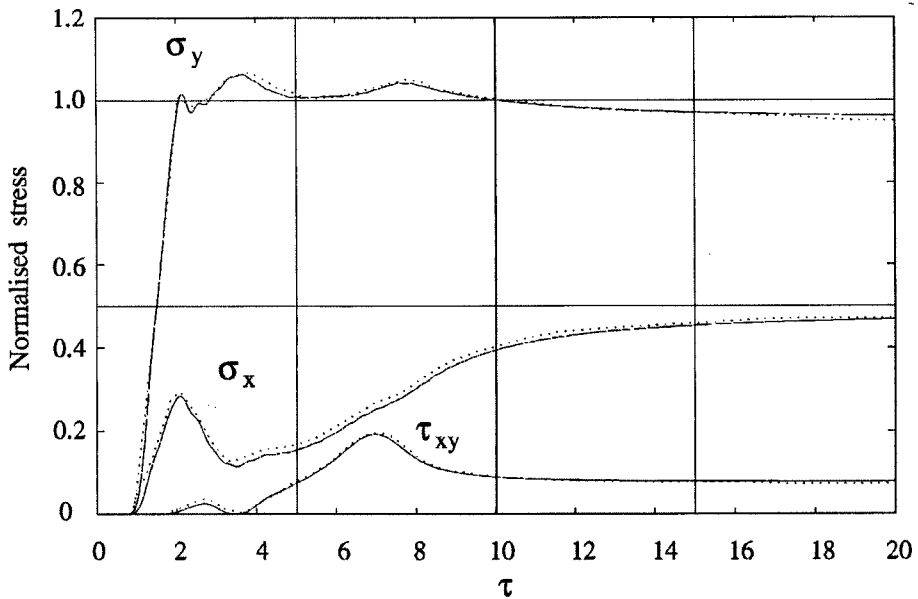
Figure 5.7 Stresses at the point (1,1)

In chapter four, the range of stability of the various differencing schemes for implemention of the boundary equations in finite difference models is presented. It is found that the finite difference boundary schemes are unstable for certain values of Poisson's ratio [Ilan A, 1978]. In order to establish whether the same stability range is applicable to the TLM models, when using finite difference derived boundary potentials, tests are performed on the TLM semi-infinite plate model with appropriate values of Poisson's ratio. Using the central approximation to discretise the boundary equations, Poisson's ratios of 0.45 (the limit of the stability range) and 0.46 (outside of the stability range) are chosen. Figure 5.8 shows the results of such a test. It is clear that, for Poisson's ratio of 0.45, the displacement monitored at the point (1,0), provides stable results. However, for Poission's ratio of 0.46 the displacement diverges and the finite difference boundary implementation renders the model unstable.

128
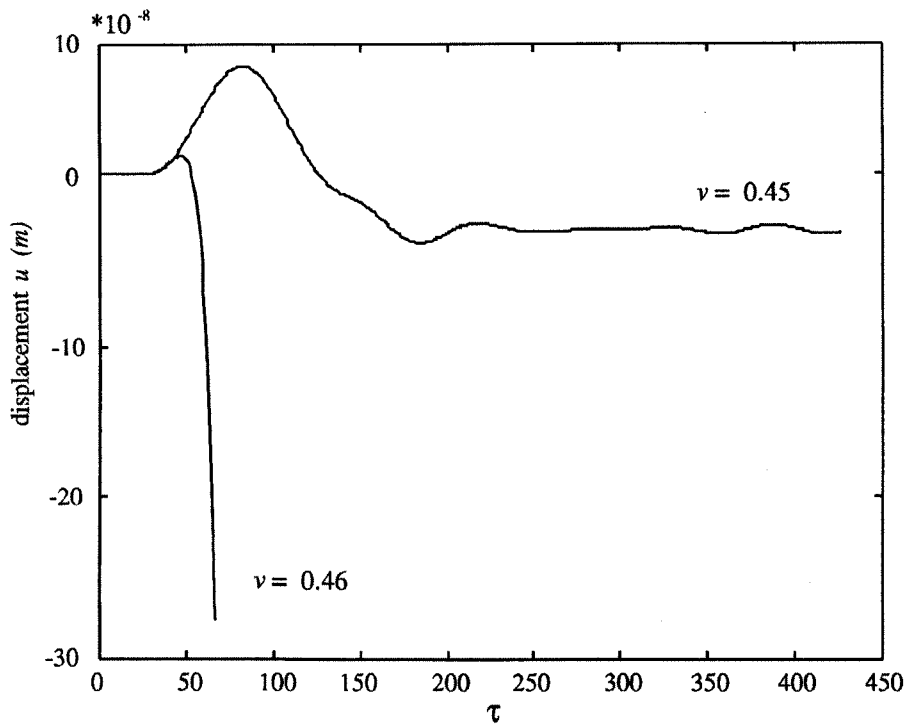
Figure 5.8 Stability test for central difference boundary condition - *u* displacement at position (1,0) in the semi-infinite plate model

5.2.2 Bridge structure

The following example, that of a bridge structure, demonstrates the application of the TLM model to a slightly more complex geometry. The geometry contains a number of corners, and the boundaries include fixed, force loaded and free conditions.

The bridge structure is illustrated in figure 5.9. The structure is clamped to a rigid base and force loading is applied to one side of the structure.
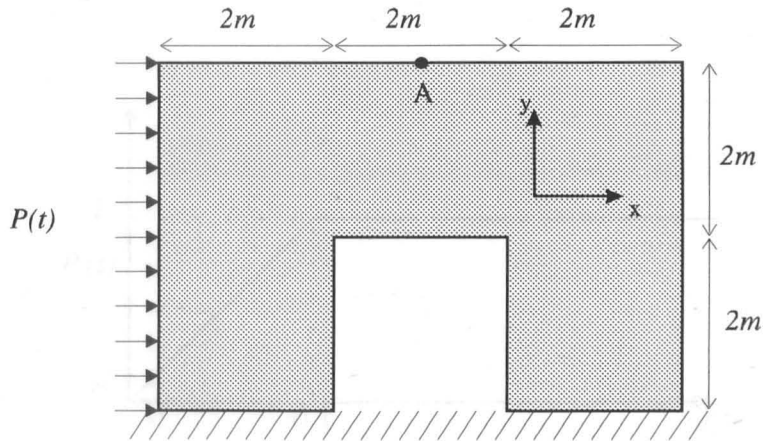
Figure 5.9 Dimensions of the bridge structure

The boundary conditions for the structure are:

$$
\left.
\begin{array}{l}
\sigma_x = P(t) \\
\tau_{xy} = 0
\end{array}
\right\} \text{ loaded surface}
$$

$$
\left.
\begin{array}{l}
\sigma_y = 0 \\
\tau_{xy} = 0
\end{array}
\right\} \text{ free surfaces parallel to } x
$$

$$
\left.
\begin{array}{l}
\sigma_x = 0 \\
\tau_{xy} = 0
\end{array}
\right\} \text{ free surfaces parallel to } y
$$

$$
\left.
\begin{array}{l}
u = 0 \\
v = 0
\end{array}
\right\} \text{ clamped surface}
$$

The elastic problem is to investigate the horizontal displacement at the central position marked A in figure 5.9, due to the loading function *P(t)*. The dynamics of the force load are illustrated below.
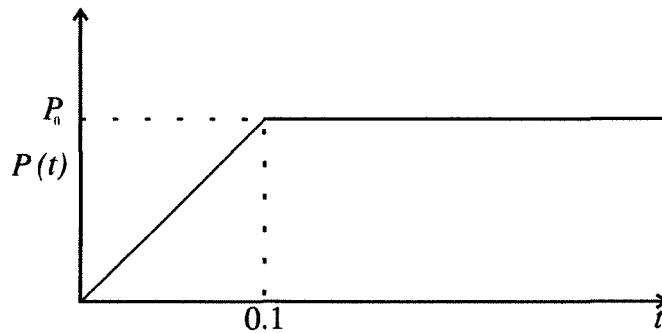
Figure 5.10 Load applied to the bridge structure

The material properties of the structure are

$$E = 1 \times 10^4 \, N / m^2$$
$$\rho = 1 Kg / m^3$$
$$\nu = 0.2$$

and the structure is discretised by a square mesh with an internodal spacing of 0.2m and a time step of 800µs is used in the simulation , giving

$$\Delta t = 8 \times 10^{-4} \, s$$
$$\Delta l = 0.2m$$

The TLM elastic deformation model predictions are compared with those reported by Brebbia using a boundary element formulation [Brebbia C A, 1984] in figure 5.11.
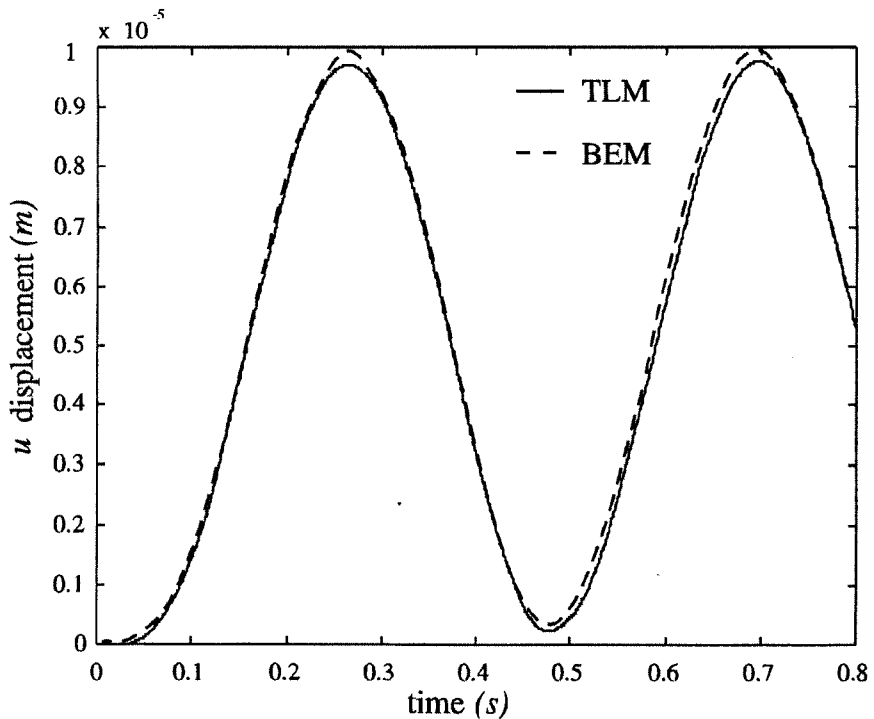
Figure 5.11 Displacement at point A of the bridge structure

The predictions, which are in close agreement, indicate that the structure oscillates about a mean displacement. The results would imply that the treatment of corners in the TLM model is satisfactory, since it would be expected that any errors in the treatment of boundaries at corners would propagate through the model resulting in an erroneous solution in the remainder of the model.

5.2.3 Frictional contact model

Section 4.5 describes the TLM boundary implementation for the case of frictional contact between bodies. Considering the case of an elastic body in contact with a rigid base, as illustrated in figure 5.12, Lee reports finite element predictions of the steady state normal and tangential forces at the interface of the contacting surfaces [Lee S, 1994].
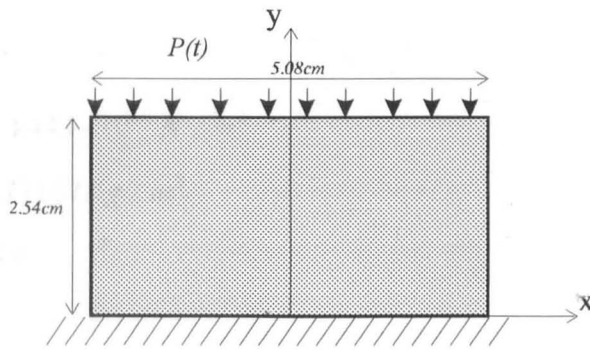
Figure 5.12 An elastic body in contact with a rigid base

The boundary conditions for the elastic body can be defined as

$$
\left.\begin{array}{l}
\sigma_y = P(t) \\[2mm]
\tau_{xy} = 0
\end{array}\right\} \text{ loaded surface}
$$

$$
\left.\begin{array}{l}
\sigma_x = 0 \\[2mm]
\tau_{xy} = 0
\end{array}\right\} \text{ free surfaces}
$$

$$v = 0$$
$$\tau_{xy} = \mu\sigma_x$$

contacting surface in *slip*

$$v = 0$$
$$u = 0$$

contacting surface in *stick*

and the material properties of the body are

$$E = 1.443 \times 10^{10}\, N / m^2$$

$$\rho = 77107 Kg / m^3$$

$$\nu = 0.3$$

The pressure applied to the top surface of the elastic body, *P(t)*, is ramped over 2.2ms, from 0 to 275862069 N/m².

The results presented by Lee are for damped steady state distributions. The corresponding TLM simulation therefore requires the incorporation of damping. This is achieved by the introduction of resistance into the network transmission lines.

The TLM model operates with the following time and space steps:

$$\Delta t = 6 \times 10^{-7} s$$

$$\Delta l = 3.33 \times 10^{-4} m$$

chosen to correspond with those of Lee. Transmission line resistors are incorporated into the model, these having a nominal value of 0.01 Ω.

Comparisons of the TLM predictions with those obtained by Lee, for the tangential stress distribution along the contacting surface, with friction coefficients of 0.05 and 0.15, are shown in figure 5.13. Similarly, the predictions for the normal stress distribution are shown in figure 5.14.
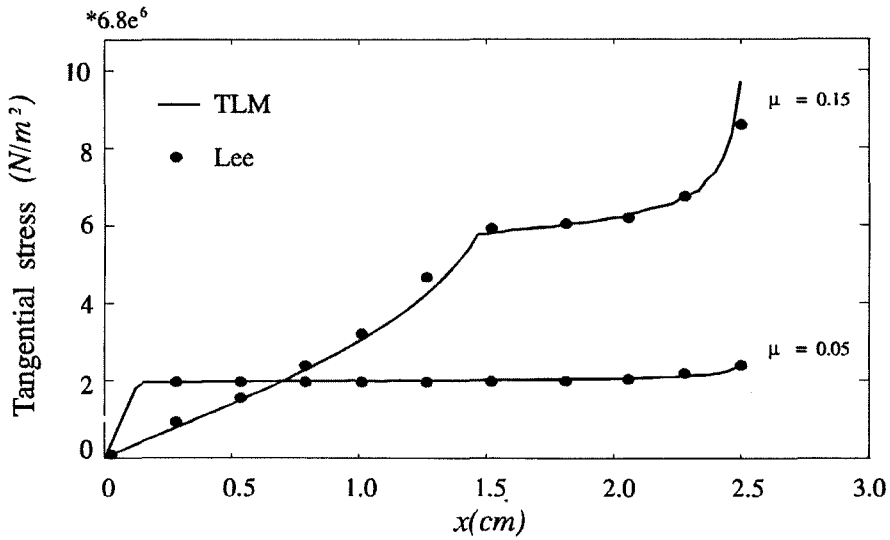
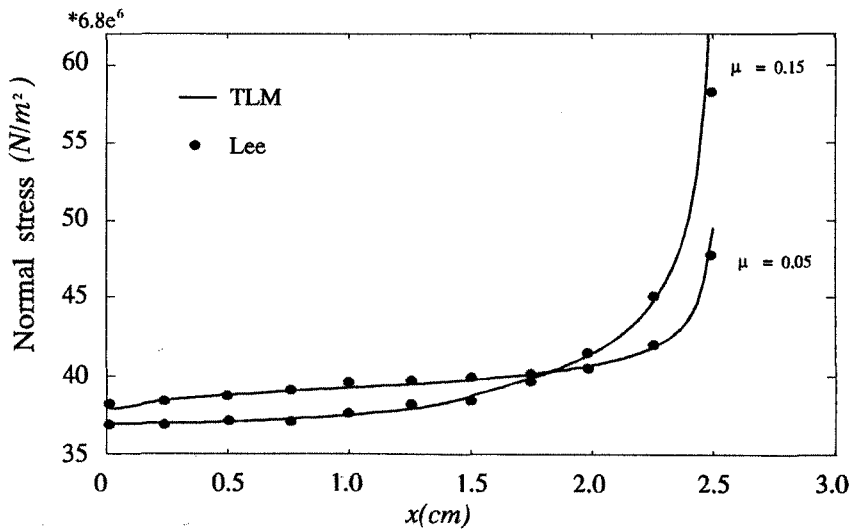**Figure 5.13 Tangential stress distribution along the contacting boundary**

Figure 5.14 Normal stress distribution along the contacting boundary

135

The level of agreement between the two methods is excellent. It is interesting to note the tangential stress distribution for $\mu = 0.15$ in figure 5.13, from which the slip and stick regions at the interface can be determined. Over the region $0 < x < 1.5$, the interface exhibits stick characteristics. This is a result of the tangential stress values over this region, which are less than the product of the friction coefficient and the normal stress. Over the region $1.5 < x < 2.54$, the interface exhibits slip characteristics, and the tangential stresses are equal to the product of the friction coefficient and the normal stresses, as specified by Coulombs friction law. For the case of $\mu = 0.05$ the whole interface is in the slip condition.

5.3 Anisotropic models

The formulation for anisotropic elastic modelling by TLM is set out in section 3.4. The example chosen to demonstrate the TLM anisotropic elasticity model, is that of an infinitely long orthotropic hyperelastic plate, of thickness $2H$, which is subjected to point loading, as illustrated in figure 5.15. Plates of ice, zinc, copper and beechwood are considered. This example was considered by Scott and Miklowitz, for which they present results of far field approximations of displacements at a point in the plate [Scott R A, Miklowitz J, 1967].
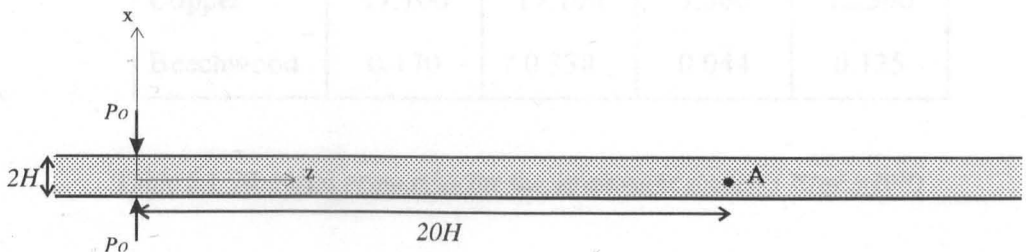

Figure 5.15 Infinitely long anisotropic plate subjected to point loading

The boundary conditions for the problem may be stated as:

$$\left.\begin{array}{l} \sigma_x = Po \\ \\ \tau_{xz} = 0 \end{array}\right\} z = 0, x = \pm H$$

$$\left.\begin{array}{l} \sigma_x = 0 \\ \\ \tau_{xz} = 0 \end{array}\right\} z \neq 0, x = \pm H$$

where Po is the value of step load applied at $t = 0$.

The materials under consideration and their material properties are presented in table 5.1.

Material	c_{11}	c_{33}	c_{55}	$c_{13} = c_{31}$
Ice	1.429	1.510	0.304	0.486
Zinc	16.368	6.347	3.879	5.030
Copper	17.100	17.100	7.560	12.390
Beechwood	0.170	0.338	0.044	0.135

Table 5.1 Material properties for the anisotropic models (N/m² ×10¹⁰)

The TLM predictions are compared with those reported by Scott and Miklowitz for far field analytical approximations in figures 5.16 and 5.17. The figures show horizontal displacements, normalised to loading Po.

τ is the scaled time variable, defined by Scott and Miklowitz as

$$\tau = \left(\frac{1}{H}\sqrt{\frac{c_{55}}{\rho}}\right)t - \sqrt{\frac{c_{55}}{\rho}}\frac{\xi}{c_p}$$

where $\xi = \dfrac{z}{H} = 20$ and $c_p = \sqrt{\dfrac{c_{11}c_{33} - c_{13}^2}{\rho c_{33}}}$

Comparing the predictions of the two methods, the TLM predicted displacement magnitudes are slightly larger and noisier than those of the far field approximation, and the TLM model predicts waveleng ths that are slightly longer than the far field approximation. Whether these anomalies are a result of the limitations of the far field approximation, or errors associated with the implementation of the TLM anisotropic model requires further investigation. However, the relative magnitude and frequency changes between the four materials show close agreement.

5.4 Summary

The TLM elastic deformation model has been applied to several classes of elastic problem in this chapter. The use of the TLM model has been demonstrated in modelling two-dimensional isotropic and anisotropic elastic bodies with frictional,
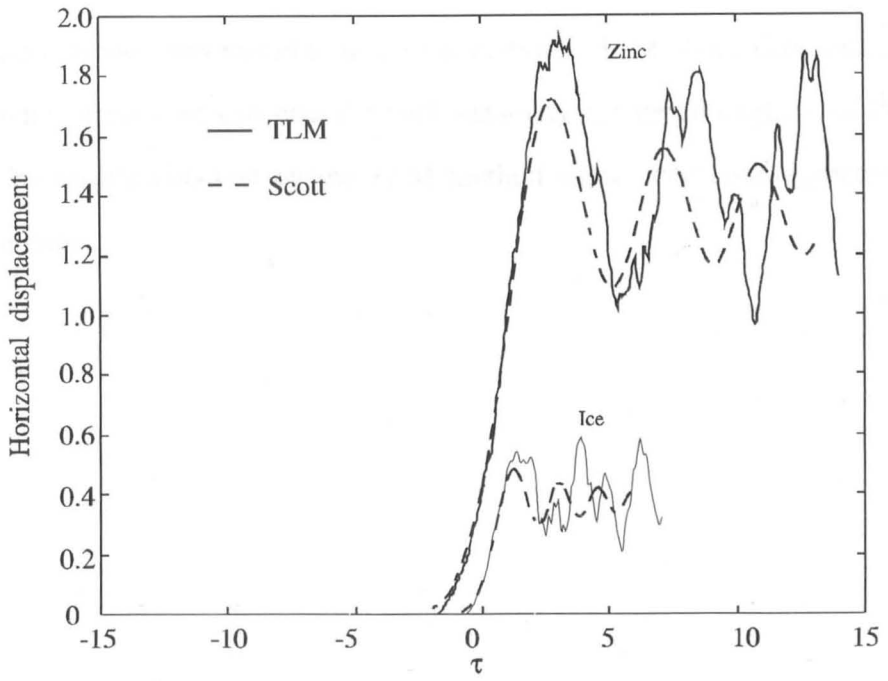
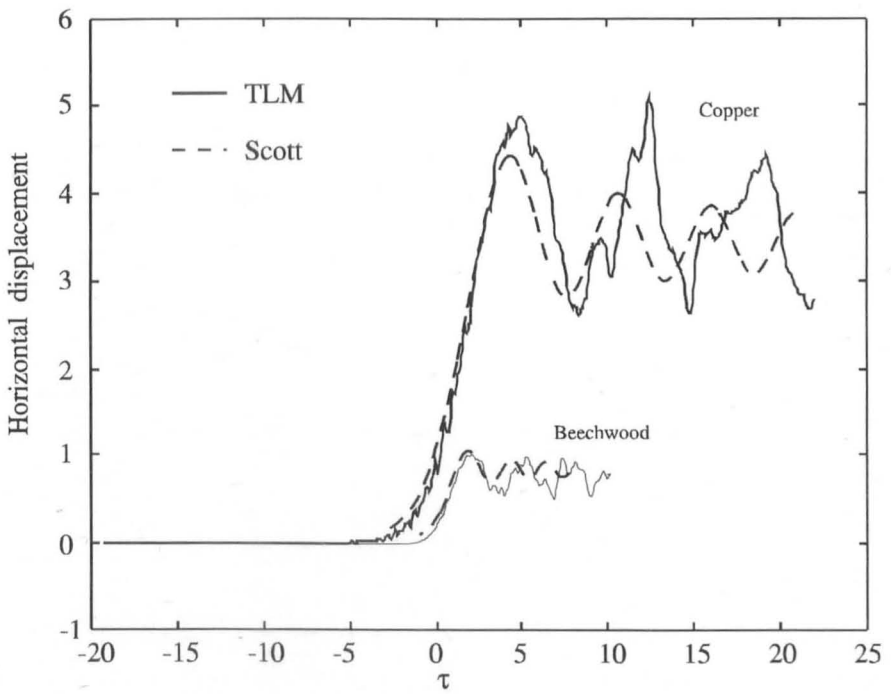**Figure 5.16 Predictions of horizontal displacements in Zinc and Ice**

Figure 5.17 Predictions of horizontal displacements in Copper and Beechwood

force, displacement, and mixed boundary conditions. It has been demonstrated that the boundary treatment can cause model instability for certain values of Poisson's ratio. The results obtained by the TLM method show very good agreement with other methods.

Extension to Three-Dimensions and General Anisotropy, Discussion and Further Work

6.1 Introduction

This chapter presents extensions to the two-dimensional elastic deformation model described in the previous chapters, for treatments of general anisotropy and three-dimensional isotropic elastic materials. The merits and limitations of the work described in this thesis are discussed, and suggestions for extension and improvement are presented.

6.2 Extension to general anisotropy

The TLM implementation of the hyperelastic anisotropic equations of motion is presented in section 3.4, and applied in section 5.3. The general equations for three-dimensional anisotropic elasticity are presented in expression (2.18), which, for two-dimensions, reduce to

$$\rho \frac{\partial^2 u}{\partial t^2} = c_{11} \frac{\partial^2 u}{\partial x^2} + c_{66} \frac{\partial^2 u}{\partial y^2} + \left(c_{16} + c_{61}\right) \frac{\partial^2 u}{\partial x \partial y} + c_{16} \frac{\partial^2 v}{\partial x^2} + c_{62} \frac{\partial^2 v}{\partial y^2} + \left(c_{12} + c_{66}\right) \frac{\partial^2 v}{\partial x \partial y}$$

and
$$\tag{6.1}$$

$$\rho \frac{\partial^2 v}{\partial t^2} = c_{66} \frac{\partial^2 v}{\partial x^2} + c_{22} \frac{\partial^2 v}{\partial y^2} + \left(c_{62} + c_{26}\right) \frac{\partial^2 v}{\partial x \partial y} + c_{61} \frac{\partial^2 u}{\partial x^2} + c_{26} \frac{\partial^2 u}{\partial y^2} + \left(c_{21} + c_{66}\right) \frac{\partial^2 u}{\partial x \partial y}$$

$$\tag{6.2}$$

For the convenient case of hyperelasticity, $c_{12} = c_{21}$. This equality ensures that the scaling of the cross derivative transmission lines, which form diagonal connections between the two meshes, is the same with respect to both Φ_x and Φ_y meshes. These transmission lines form common pulse paths between the two meshes. For the case of general anisotropic elastic materials, $c_{12} \neq c_{21}$, hence the scaling of the cross derivative transmission lines is different with respect to each mesh. This would require uni-directional cross derivative transmission lines, scaled appropriately for each mesh. This relatively trivial extension would facilitate the application to general anisotropic analysis.

6.3 Extension to three-dimensions

The equations of motion for a three-dimensional anisotropic material are presented in expression (2.18). Considering the case of an isotropic material, for which conditions (2.11) apply, the equations of motion reduce to

$$\rho\frac{\partial^2 u}{\partial t^2} = (2G + \lambda)\frac{\partial^2 u}{\partial x^2} + G\left(\frac{\partial^2 u}{\partial y^2} + \frac{\partial^2 u}{\partial z^2}\right) + (G + \lambda)\left(\frac{\partial^2 v}{\partial x \partial y} + \frac{\partial^2 w}{\partial x \partial z}\right)$$

$$\rho\frac{\partial^2 v}{\partial t^2} = (2G + \lambda)\frac{\partial^2 v}{\partial y^2} + G\left(\frac{\partial^2 v}{\partial x^2} + \frac{\partial^2 v}{\partial z^2}\right) + (G + \lambda)\left(\frac{\partial^2 u}{\partial x \partial y} + \frac{\partial^2 w}{\partial y \partial z}\right) \quad (6.3)$$

$$\rho\frac{\partial^2 w}{\partial t^2} = (2G + \lambda)\frac{\partial^2 w}{\partial z^2} + G\left(\frac{\partial^2 w}{\partial x^2} + \frac{\partial^2 w}{\partial y^2}\right) + (G + \lambda)\left(\frac{\partial^2 x}{\partial x \partial z} + \frac{\partial^2 v}{\partial y \partial z}\right)$$

The third dimension introduces the solution variable, w, which represents displacement in the z direction. It is apparent that to model the three-dimensional

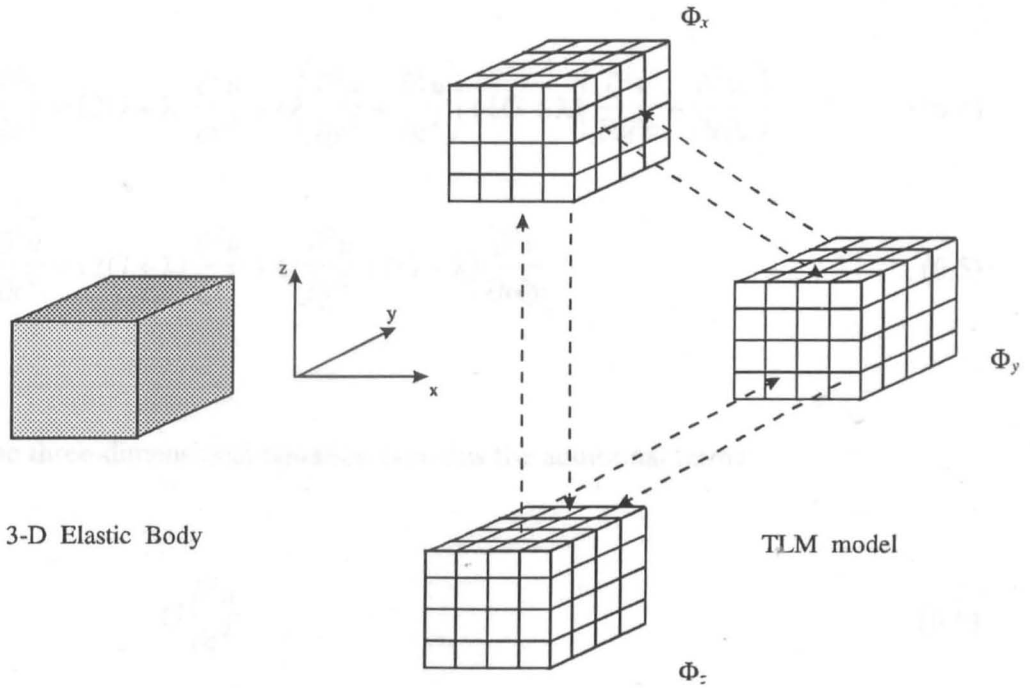equations, three TLM meshes will be required, as illustrated in the conceptual model of figure 6.1.

Figure 6.1 Conceptual model of three-dimensional TLM elastic deformation - three interdependent meshes representing deformation in each of the co-ordinate directions

Three three-dimensional meshes are required to hold the three displacement variables u, v and w in the x, y and z directions. Since the equation which describes displacement in the x direction contains cross derivatives of v (as in the case of the two-dimensional model) and w, the mesh describing displacement in the x direction, Φ_x, will have connections to both Φ_y and Φ_z as shown in figure 6.1. Similar connections are formed for the other meshes.

Comparing the three-dimensional description of deformation in the x direction, (6.4), with the equivalent two-dimensional equation, (6.5) the extensions required for the three-dimensional model are apparent.

$$\rho\frac{\partial^2 u}{\partial t^2} = (2G+\lambda)\frac{\partial^2 u}{\partial x^2} + G\left(\frac{\partial^2 u}{\partial y^2} + \frac{\partial^2 u}{\partial z^2}\right) + (G+\lambda)\left(\frac{\partial^2 v}{\partial x\partial y} + \frac{\partial^2 w}{\partial x\partial z}\right) \qquad (6.4)$$

$$\rho\frac{\partial^2 u}{\partial t^2} = (2G+\lambda)\frac{\partial^2 u}{\partial x^2} + G\frac{\partial^2 u}{\partial y^2} + (G+\lambda)\frac{\partial^2 v}{\partial x\partial y} \qquad (6.5)$$

The three-dimensional equation contains the additional terms

$$G\frac{\partial^2 u}{\partial z^2} \qquad (6.6)$$

and

$$(G+\lambda)\frac{\partial^2 w}{\partial x\partial z}. \qquad (6.7)$$

The first of these derivatives (6.6), may be incorporated by the addition of appropriately scaled transmission lines along the z direction. The second of these derivatives may be incorporated by the use of appropriately connected transmission lines to implement the cross derivative. The proposed nodal structure showing the connectivity for the Φ_x mesh is shown in figure 6.2a, from which impedances have been omitted for clarity. The nodal structures for modelling the deformation in the y and z directions are shown in figures 6.2b and 6.2c respectively.

144

The fifteen port nodal structure proposed for three-dimensional analysis, gives rise to a scattering matrix of size 45 × 45. Symbolic manipulation of the resulting characteristic determinant has proven to be beyond the capabilities of current PC based packages, consequently the analysis of the three-dimensional nodal structure by the TLM-state space analogy has not been possible. The development of the three-dimensional model is based on intuitive extensions to the two-dimensional model.
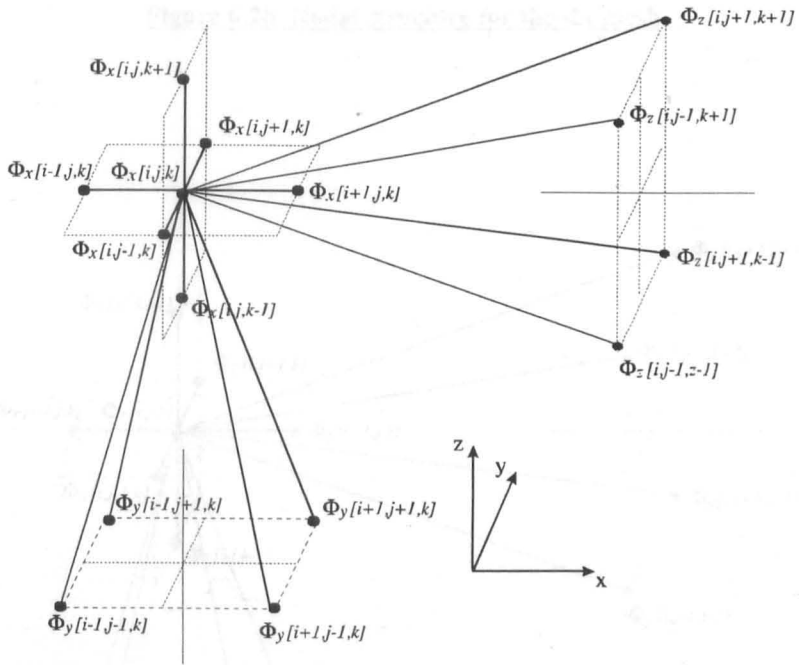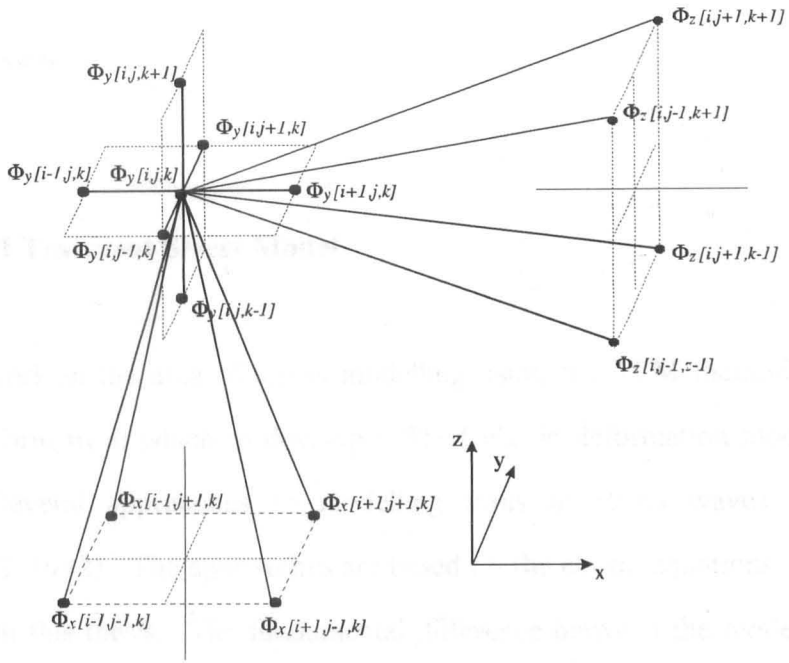

Figure 6.2a Nodal structure for the Φ_x mesh

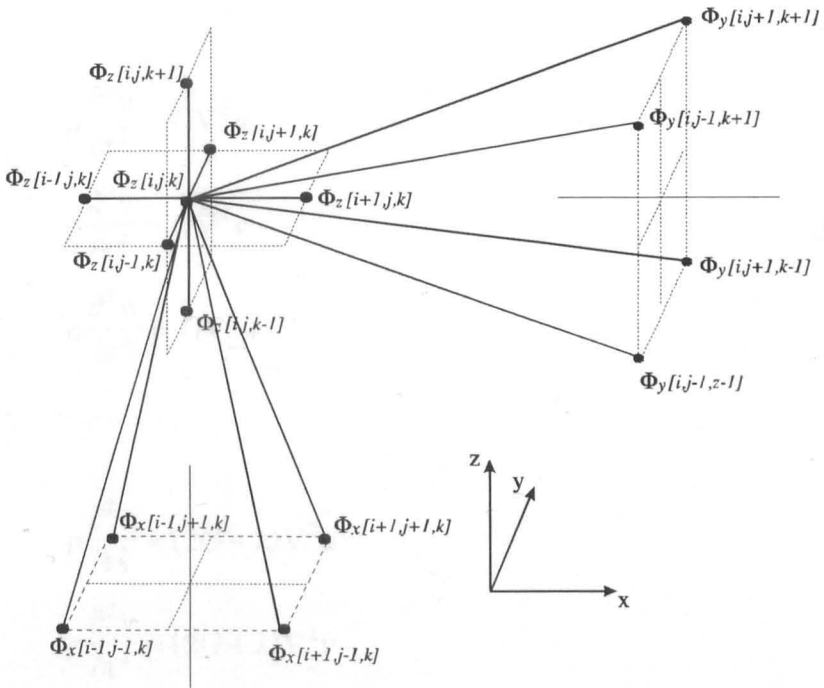**Figure 6.2b Nodal structure for the Φ_y mesh**

Figure 6.2c Nodal structure for the Φ_z mesh

6.4 Discussion

6.4.1 TLM Transient Stress Model

Previous work in the area of stress modelling using the TLM method provided a useful platform from which to develop a TLM elastic deformation model. Boston describes several approaches to modelling transient stress waves using TLM [Boston I E, 1992]. The approaches are based on the elastic equations of motion as presented in this thesis. The fundamental difference between the models proposed by Boston and those presented here is that Boston, following the lead of many texts, for example, Hudson [Hudson J A, 1980], chose to separate two different wave types, transverse and longitudinal, from the equations of motion. In his displacement approach, Boston expresses the equations of motion as sets of two independent wave equations

$$\rho \frac{\partial^2 u}{\partial t^2} = G\nabla^2 u$$

$$\rho \frac{\partial^2 v}{\partial t^2} = G\nabla^2 v \tag{6.8}$$

$$\rho \frac{\partial^2 w}{\partial t^2} = G\nabla^2 w$$

and

$$\rho \frac{\partial^2 u}{\partial t^2} = (2G + \lambda)\nabla^2 u$$

$$\rho \frac{\partial^2 v}{\partial t^2} = (2G + \lambda)\nabla^2 v \tag{6.9}$$

$$\rho \frac{\partial^2 w}{\partial t^2} = (2G + \lambda)\nabla^2 w$$

By representing the equations of motion in this form the cross derivatives in the equations of motion are neglected. Boston recognised the inadequacy of this approach when considering an implementation of such a model. He also recognised the need for information flow between each of the displacement networks,

"The second order terms in y and z (of the full system of equations) are links to the other networks representing the displacements v and w. The problem at this stage is understanding how these links operate and how exactly to implement them." [Boston I E, 1992].

The second part of this statement emphasises the value of the TLM-state space analogy as a tool for analysis of the nodal structures which was not available to Boston at the time of his work. The TLM elastic deformation model, as described in this thesis, models the full system of elastic equations of motion which is consistent with other numerical methods of elastic deformation modelling, for example, the finite difference method [Harker A H, 1988], the finite-element method [Fenner R T, 1975] and the boundary element method [Becker A A, 1992]. It seems that the cross derivatives account for the discrepancies observed between the implementations by Boston and the present work.

6.4.2 Bulk treatment

Chapter three presents the nodal structures suitable for modelling the two-dimensional elastic equations of motion. The TLM nodal potential is equivalent to displacement, consequently, two, two-dimensional meshes are required to model two-dimensional problems, one mesh representing displacement in one co-ordinate direction and one representing displacement in the other. In developing the nodal

structure for the TLM model, it has been necessary to incorporate scaled spacial derivatives. This is achieved by scaling the impedance of the transmission lines by values appropriate to the coefficients which scale the spacial derivatives in the elastic equations. Also, it has been necessary to incorporate scaled cross derivatives, this is achieved by additional transmission lines which form diagonal connections to and from each of the meshes. The work of Witwit *et al* proved valuable in making these extensions, and the TLM-state space analysis tool has been used to check the discrete representation of the nodal structure, and enabled analysis in terms of discrete components. This is consistent with the TLM algorithm which is discrete in all dimensions. The analysis leads to difference equations, from which the continuous time equivalent equations can be found. Analysis of the two-dimensional isotropic TLM elastic deformation nodal structure, by TLM-state space analysis, indicates that the structure models the discrete form of the elastic deformation equations. The analysis also reveals "spurious" solutions which result from the discretisation process, and are observed in the analyses of other numerical techniques [Schroeder W and Wolff I, 1994]. Use is made of stub transmission lines in the nodal structures. These allow flexibility in the choice of values for the space step and time step. The time and space steps are chosen to be small compared with the wave lengths of the process being modelled.

The nodal structure for the two-dimensional isotropic model is essentially an eight port network. Eight port networks have been reported by other workers [Simons N R S and Sebak A A, 1992] and [Witwit, A R M, Wilkinson A J, Pulko S H, 1995]. Simons and Sebak describe an eight port nodal structure, for the solution of two-dimensional Maxwell's equations, derived from a combination of two four port structures, one displaced by an angle of 45° for the other. Propagation on the mesh is controlled by variable intrinsic impedance of the transmission lines, such that waves can propagate across either the diagonally placed transmission lines (those rotated by 45°), across the non-rotated transmission lines, or across a combination

of the two structures [Simons N R S and Sebak A A, 1992]. The structure reported by Witwit *et al* is described in section 3.2.1, and allows the incorporation of cross derivatives into the system of equations. However, the link lines in these structures link nodes in the same mesh, unlike the structure for the elastic deformation model.

6.4.3 Boundary treatment

Since the nodal potential in the TLM model is displacement, implementation of boundary conditions requires that the boundaries be specified in terms of displacements. Displacement boundary conditions require the surface skin of boundary nodes to have nodal potentials which correspond to the appropriate displacement for a particular region on the boundary. Force and frictional boundaries require discretisation of the boundary equations which are specified in terms of applied forces and surface stresses. By specifying the boundary equations in difference form, the potential of the boundary skin of nodes can be calculated. The implementation of boundary equations by this method is exactly the same as the finite difference implementation of the boundary equations. Many researchers in the area of finite difference elastic analysis report on the instability of such boundary implementations at high Poisson's ratio, and propose modified schemes to overcome the instability [Ilan A, Loewenthal D, 1976], [Ilan A, 1978], [Dow J O *et al*, 1990], [Stacey R, 1994]. This instability has been shown to be present when applied to TLM boundary conditions for the same values of Poisson's ratio (section 5.1). The new composed approximation proposed by Ilan and Loewenthal is stable for the full range of Poisson's ratio yet it is a two step routine and as such violates the one step nature of TLM if it were to be applied to TLM models. Since the one step schemes, namely, centred approximation and one-sided approximation, are stable only within a given range of material properties, these schemes can be considered suitable only

within the range of stability. Operation of these schemes outside this range destroys the stability of the TLM model.

Implementation of a comprehensive set of boundary conditions has been described, including displacement, force, and frictional. Those not treated include infinite and symmetry boundary conditions for which it would be hoped that the existing treatments of these boundaries [Johns P B, Pulko S H, 1986] would be transferable to elastic boundaries, although special treatment for cross derivative transmission lines would be required.

6.5 Future work

The TLM elastic deformation model as described in this thesis provides an efficient numerical routine for the modelling of elastic problems. The treatment has been demonstrated to be effective in modelling two-dimensional isotropic and anisotropic hyperelastic elastic deformation, and the extensions to three-dimensional and general anisotropic models have been described. However, several issues require further investigation.

The introduction of new nodal structures not only opens up new areas of application for the TLM technique, but also new areas of research. The interconnection of TLM meshes by transmission lines, the incorporation of scaling, transmission lines with negative impedance values, are all novel ideas, and present questions in terms of the stability and dispersion with respect to the TLM algorithm which should be investigated. The introduction of interconnected meshes via transmission lines with negative impedances may introduce positive feedback paths which render such an implementation unstable. However, the only evidence of instability during the

course of this work is a result of the boundary implementation which is based on finite difference techniques. The dispersion characteristics of such a mesh are likely to differ from those of a standard TLM mesh as a result of the use of scaled transmission lines and additional pulse paths. Understanding needs to be gained in these areas.

A technique which uses a boundary treatment based on the finite difference approach which is unstable for high values of Poisson's ratio cannot be considered ideal. Investigations should be carried out into new methods of applying force boundary conditions. One possible solution would be the implementation of the boundary equations in terms of pulses reflected and absorbed at boundary walls rather than the calculation of boundary nodal potentials. This treatment would not require the discretisation of boundary equations by finite difference approximations and may lead to a boundary treatment which is consistent with the explicit, one step and unconditionally stable nature of the fundamental TLM routine without imposing limits on the material properties of the model.

Most of the models presented in chapter five of this thesis model transient elastic deformation, and excellent agreement with other methods is shown. However, the assumption, made in chapter two, that $\tau_{zy} = \tau_{yz}$, is based on equilibrium conditions of a small cube of elastic material. The question arises - is this assumption valid for transient analysis? Since this assumption is commonly used by other numerical and analytical techniques it is to be expected that good agreement between the methods is obtained. Further work into the validity of such an assumption for transient analysis could provide the answer.

A further assumption made in the development of the elastic deformation model is that the equations which allow the strains to be expressed in terms of displacements are based on the assumption that the strains are small [Timoshenko S, 1934]. This

152

may preclude the model from large strain analysis. However, it is possible that due to the iterative nature of TLM, if, at each iteration, the changes in strains are small, then the technique may be valid for large strains which develop over many iterations.

The development of the TLM elastic deformation model as it stands offers exciting possibilities in terms of coupled models. Coupling represents the modelling of two or more interacting phenomena. Coupled TLM models have been reported [Newton H R, Pulko S H, 1991] and coupled models may be implemented in terms of elastic deformation. For example, the coupling of a thermal model with the elastic deformation model so that thermal stress analysis may be undertaken for the prediction of residual thermal stresses.

Finite element analysis is the most widely used analysis tool in terms of elastic deformation modelling, although in certain areas other techniques find popularity. The main advantage of the finite element method is its ability to describe complex shapes. If the TLM elastic deformation model is to become a popular alternative to the finite element method in the field of elastic modelling, it will be necessary to develop methods which allow complex geometries to be modelled. Much work has already been done in the area of new meshing techniques for TLM which allow better boundary description of complex shapes applied to TLM diffusion [Austin J, Pulko S H, 1993] [Witwit A R M, 1995], electromagnetic wave [Meliani H, De Cogan D, Johns P B, 1988] and acoustic models [Jaycocks R, Pomeroy S C, 1996]. The extension of these techniques to elastic deformation modelling by TLM, in association with the benefits obtainable from parallel implementations of the algorithm [Parsons P J, Jaques S R, Pulko S H, Rabbi F A, 1996] and TLM specific hardware [Stothard D, Pomeroy S C, Sillitoe I P W, 1995], which are facilitated by the one step and explicit nature of the TLM algorithm, could ensure the competitive edge over other numerical techniques. Should the TLM technique offer the modelling of complex shapes to analysts and designers, then the advantages in terms

of run time and simplicity of the technique should help establish the technique in the area of elastic analysis, especially where transient analysis is required.

Conclusion

TLM nodal structures and models have been developed which model the deformation of elastic material. The model is based on the solution, by TLM, of the equations of motion of elastic material. Analysis of the nodal structure for the two-dimensional isotropic case by the TLM-state space analysis tool confirms that the structure models the two-dimensional isotropic equations of motion. The application of the model to various elastic problems has been implemented and the results obtained show excellent agreement with those obtained using other methods. The boundary conditions for the TLM model are based on a finite difference implementation, the stability of which is dependent upon the value of Poisson's ratio of the material being modelled. A model of two-dimensional anisotropic deformation has also been demonstrated and validated against analytic results. The extension to three-dimensional elastic modelling has also been described. The TLM elastic deformation model provides a simple, one step and explicit analysis tool applicable to a wide range of elastic problems.

Appendix 1

Derivation of the discrete difference equations from Taylor series expansions

The transformation from discrete difference to continuous differential is an approximation arrived at by consideration of Taylor series expansions of $f(x+h)$ and $f(x-h)$.

The expansions are defined as

$$f(x+h) = f(x) + \frac{h}{1!} f'(x) + \frac{h^2}{2!} f''(x) + O(h^3) \qquad \text{(A1)}$$

$$f(x-h) = f(x) - \frac{h}{1!} f'(x) + \frac{h^2}{2!} f''(x) - O(h^3) \qquad \text{(A2)}$$

where $f'(x)$ denotes $\frac{\partial}{\partial x} f(x)$ and $f''(x)$ denotes $\frac{\partial^2}{\partial x^2} f(x)$

Summing (A1) and (A2) gives

$$f(x+h) + f(x-h) = 2f(x) + h^2 f''(x) + O(h^4) \qquad \text{(A3)}$$

Neglecting terms greater than h^2 and solving for $f''(x)$, yields the approximation

$$f''(x) \approx \frac{f(x+h) - 2f(x) + f(x-h)}{h^2} \qquad \text{(A4)}$$

Subtracting (A2) from (A1) gives

$$f(x+h) - f(x-h) = 2hf'(x) + O(h^3)$$ (A5)

Neglecting terms greater than h^2 and solving for $f'(x)$, yields the approximation

$$f'(x) \approx \frac{f(x+h) - f(x-h)}{2h}$$ (A6)

The difference approximations expressed in (A4) and (A5) represent *centred difference* equations. *One sided difference* equations may be derived by considering equations (A1) and (A2) independently.

Restating (A1) and neglecting terms greater than h gives

$$f(x+h) \approx f(x) + \frac{h}{1!} f'(x)$$ (A7)

from which

$$f'(x) \approx \frac{f(x+h) - f(x)}{h}$$ (A8)

and represents the *forward difference* equation.

Restating (A2) and neglecting terms greater than h gives

$$f(x-h) \approx f(x) - \frac{h}{1!} f'(x) \qquad \text{(A9)}$$

from which

$$f'(x) \approx \frac{f(x) - f(x-h)}{h} \qquad \text{(A10)}$$

and represents the *backward difference* equation.

Summing the forward and backward difference equations, (A8) and (A10), gives

$$2f'(x) \approx \frac{f(x+h) - f(x-h)}{h} \qquad \text{(A11)}$$

For a function of two variables, x and y, the centred difference approximation becomes

$$\frac{\partial}{\partial x} f(x,y) \approx \frac{f(x+h,y) - f(x-h,y)}{2h} \qquad \text{(A12)}$$

and

$$\frac{\partial}{\partial y} f(x,y) \approx \frac{f(x,y+h) - f(x,y-h)}{2h} \qquad \text{(A13)}$$

The expression, $\dfrac{\partial^2}{\partial x \partial y} f(x,y)$ may be written

$$\frac{\partial}{\partial x}\left(\frac{\partial}{\partial y} f(x,y)\right) \tag{A14}$$

Substituting into this (A13)

$$\frac{\partial^2}{\partial x \partial y} f(x,y) \approx \frac{\partial}{\partial x}\left(\frac{f(x,y+h)-f(x,y-h)}{2h}\right) \tag{A15}$$

and applying (A12), yields

$$\frac{\partial^2}{\partial x \partial y} f(x,y) \approx \left(\frac{f(x+h,y+h)-f(x-h,y+h)-f(x+h,y-h)+f(x-h,y-h)}{4h^2}\right)$$

$$\tag{A16}$$

Introducing I and I^{-1}, the shift operators and defining as

$$I = f(x+h) \tag{A17}$$

and

$$I^{-1} = f(x-h) \tag{A18}$$

Substituting (A11) and (A12) into (A4) gives

$$f''(x) \approx \frac{I - 2 + I^{-1}}{h^2} \qquad (A19)$$

into (A6) gives

$$f'(x) \approx \frac{I - I^{-1}}{2h} \qquad (A20)$$

into (A8) gives

$$f'(x) \approx \frac{I - 1}{h} \qquad (A21)$$

into (A10) gives

$$f'(x) \approx \frac{1 - I^{-1}}{h} \qquad (A22)$$

into (A11) gives

$$2f'(x) \approx \frac{I - I^{-1}}{h} \qquad (A23)$$

Introducing J and J^{-1}, the shift operators for y

$$J = f(y + h) \qquad (A24)$$

and

$$J^{-1} = f(y - h) \qquad \qquad \text{(A25)}$$

and (A16) can be expressed as

$$\frac{\partial^2}{\partial x \partial y} f(x,y) \approx \left(\frac{IJ - I^{-1}J - IJ^{-1} + I^{-1}J^{-1}}{4h^2} \right) \qquad \qquad \text{(A26)}$$

References

Akhtarzad S and Johns P B (1974), *Solution of 6-component electromagnetic fields in three space dimensions and time by the T.L.M. method*, Electron. Lett., vol. 10, 1974.

Al-Mukhtar D A and Sitch J E (1981), *Transmission-line matrix method with irregularly graded space*, IEE Proc., part H : Microwaves, Opt., Antennas, vol. 128, 1981.

Austin J D and Pulko S H (1993), *General curvilinear orthogonal meshes for TLM diffusion applications*, Numerical Heat Transfer, part B, vol. 24, 1993.

Becker A A (1992), *The boundary element method in engineering*, McGraw-Hill, 1992.

Boston I E (1992), *Transient stress analysis by the transmission line matrix method*, Ph.D. thesis, University of Hull, England, 1992.

Bowden F P and Tabor D (1956), *Friction and Lubrication*, Methuen and Co., London, 1956.

Brebbia C A (1984), Boundary element techniques in computer-aided engineering, NATO ASI series, Martinus Nijhoff, 1984.

Butler G and Johns P B (1979), *The solution of moving boundary heat problems using the TLM method of numerical analysis*, Numerical Methods in Thermal Problems, Pineridge Press, Swansea, 1979.

Cadzow J A and Martens H R (1970), *Discrete-time and computer control systems*, Ed Kuo F F, Prentice-Hall, 1970.

Chen Z, Ney M M and Hoefer W J R (1991), A new boundary description in two-dimensional TLM models of microwave circuits, IEEE Trans. Microwave Theory Tech., vol. 39, no. 3, March 1991.

Christopoulos C (1995), *Transmission-line modeling method: TLM*, New York, IEEE/OUP series on electromagnetic wave theory, 1995.

de Cogan D and Henini M (1987), *TLM modelling of the thermal behaviour of conducting films on insulating substrates*, J. Phys. D: Appl. Phys., vol. 20, 1987.

Dow J O, Jones M S and Harwood S A (1990), *A new approach to boundary modelling for finite difference applications in solid mechanics*, International Journal for Numerical Methods in Engineering, vol. 30, 1990.

Enders P and de Cogan D (1993), *The efficiency of Transmission Line Matrix modelling - a rigerous viewpoint*, Int. J. Numerical Modelling : Electronic Networks, Devices and Fields, vol. 6, 1993.

Faria E L and Stoffa P L (1994), *Finite-difference modeling in transversely isotropic media*, Geophysics, vol. 59, no. 2, 1994.

Fenner R T (1975), *Finite element methods for engineers*, Macmillan, 1975.

Harker A H (1988), *Elastic waves in solids with application to nondestructive testing of pipelines*, Bristol : Hilgen, 1988.

Hirst A I (1993), *TLM modelling of the thermal experience of vitreous china ware during firing in a tunnel kiln*, PhD thesis, University of Hull, England, 1993.

Hoefer W R (1989), *The Transmission Line Matrix (TLM) method*, in Numerical Techniques for Microwave and Millimeter-wave passive structures, chap. 10, New York : Wiley, 1989.

Huber C, Krumpholz M and Russer P (1995), *Dispersion in anisotropic media modeled by three-dimensional TLM*, IEEE Trans. Microwave Theory Tech., vol. 43, no. 8, August 1995.

Hudson J A (1980), *The excitation and propagation of elastic waves*, Cambridge University Press, 1980.

Ilan A (1978), *Stability of finite difference schemes for the problem of elastic wave propagation in a quater plane*, Journal of Computational Physics, vol. 29, 1978.

Ilan A and Loewenthal D (1976), *Instability of finite difference schemes due to boundary conditions in elastic media*, Geophysical Prospecting, vol. 24, 1976.

Jaycocks R and Pomeroy S C (1996), *The precise placement of boundaries within a TLM mesh with applications*, in TLM - The Wider Applications, Proceedings of an informal meeting held at the UEA, June 1996.

Johns P B and Beurle R L (1971), *Numerical solution of 2-dimensional scattering problems using a transmission-line matrix*, Proc. IEE, vol. 118, no. 9, 1971.

Johns P B (1974), *The solution of inhomogeneous waveguide problems using a transmission line matrix*, IEEE Trans. Microwave Theory Tech., vol. MTT 22, no. 3, March 1974.

Johns P B (1977), *A simple explicit and unconditionally stable numerical routine for the solution of the diffusion equation*, International Journal for Numerical Methods in Engineering, vol. 11, 1977.

Johns P B (1979), *The art of modelling*, Electronics and Power, IEE, 1979.

Johns P B (1987), *A symmetrical condensed node for the TLM method*, IEEE Transactions on Microwave Theory and Techniques, vol. MTT-35, no. 4, 1987.

Johns P B and Butler G (1983), *The consistency and accuracy of the TLM method for diffusion and its relationship to existing methods*, International Journal for Numerical Methods in Engineering, vol. 19, 1983.

Johns P B and O'Brien M (1980), *Use of the transmission-line modelling (t.l.m) method to solve non-linear lumped networks*, The Radio and Electronic Engineer, vol. 50, no. 1/2, 1980.

Johns P B and Pulko S H (1986), *The modelling of heat and mass transfer in foodstuffs*, Food structure and behaviour : equilibrium and non-equilibrium aspects (ed Blanchard J and Lillford P), Ch. 12, Academic Press, 1986.

Johns P B and Slater G F (1973), *Transient analysis of waveguides with curved boundaries*, Electron. Letters, vol. 9, no. 21, 1973.

Kraus J D (1989), *Electromagnetics*, McGraw-Hill, third edition, 1989.

Langley P, Pulko S H and Wilkinson A J (1996), *A TLM model of transient, two-dimensional stress propagation*, International Journal of Numerical Modelling : Electronic Networks, Devices and Fields, vol. 9, no. 6, 1996.

Langley P, Pulko S H and Wilkinson A J (1994), '*A Three Dimensional Transmission Line Model of Transient Elastic Deformation*' Proceedings of Applied Infomatics, Annecy, 1994.

Langley P, Wilkinson A J and Pulko S H (1995), *A TLM transient elastic deformation model incorporating a frictional contact boundary*, Proceedings of Applied Infomatics, Innsbruck, 1995.

Lee S (1994), *A computational method for the frictional contact problem using finite element method*, International Journal For Numerical Methods In Engineering, vol. 37, 1994.

Leigh J R (1983), *Modelling and simulation*, Peter Peregrinus.

Lekhnitskii S G (1981), *Theory of Elasticity of an Anisotropic Body*, Mir Publishers, 1981.

Mal A K and Singh S J (1991), *Deformation of elastic solids*, Prentice-Hall, 1991.

Mariki G E and Yeh C (1985), *Dynamic three-dimensional TLM analysis of microstriplines on anisotropic substrate*, IEEE Transactions on Microwave Theory and Techniques, vol. MTT-33, no. 9, 1985.

Meliani H, De Cogan D and Johns P B (1988), *The use of orthogonal curvilinear meshes in TLM models*, International Journal of Numerical Modelling : Electronic Networks, Devices and Fields, vol. 1, 1988.

Newton H R (1994), *TLM models of deformation and their application to vitreous china ware during firing*, Ph.D. thesis, University of Hull, England, 1994.

Newton H R and Pulko S H (1991), *A TLM model of drying processes*, Proceedings of the Ninth IASTED International Symposium: Modelling, Identification and Control, Innsbruck, Austria 1991.

Newton H R, Pulko S H, Langley P and Wallis R (1994), *'Modelling the Deformation of Pieces of Vitreous China Ware During Firing'* Modelling and Simulation, IASTED, Pittsburgh, 1994.

Olukoko O A, Becker A A and Fenner R T (1993), *Three benchmark examples for frictional contact modelling using finite element and boundary element methods*, Journal of Strain Analysis, vol. 28, no. 4, 1993.

Orme E A, Johns P B and Arnold J M (1988), *A hybrid modelling technique for underwater acoustic scattering*, Int. J. Numerical Modelling : Electronic Networks, Devices and Fields, vol. 1, 1988.

Parsons P J, Jaques S R, Pulko S H and Rabbi F A (1996), *TLM modeling using distributed computing*, IEEE Microwave and Guided Wave Letters, vol. 6, No. 3, 1996.

Pomeroy S C, Williams H R and Blanchfield P B (1991), *Evaluation of ultrasonic inspection and imaging systems for robotics using TLM Modelling*, Robotica, vol. 9, 1991.

Pulko S H, Gaskell S, Witwit A R M and Chesmore E D (1992), *TLM modelling of the dynamics of populations of simple species*, Proc. 6th IMA Conference on Modelling, Simulation and Control, 1992.

Pulko S H, Halleron I A and Phizacklea C P (1990), *Substructuring of space and time in TLM diffusion applications*, Int. J. Numerical Modelling : Electronic Networks, Devices and Fields, vol. 3, 1990.

Pulko S H and Johns P B (1987), *Modelling of thermal diffusion in three dimensions by the transmission line matrix method and the incorporation of nonlinear thermal properties*, Communications in Applied Numerical Methods, vol. 3, 1987.

Pulko S H, Mallik A, Allen R and Johns P B (1990), *Automatic timestepping in TLM routines for the modelling of thermal diffusion processes*, Int. J. Numerical Modelling : Electronic Networks, Devices and Fields, vol. 3, 1990.

Pulko S H, Mallik A and Johns P B (1986), *Application of transmission line modelling (TLM) to thermal diffusion in bodies of complex geometry*, Int. J. Num. Meth. in Eng., vol. 23, 1986.

Pulko S H and Phizacklea C P (1989), *The application of the TLM numerical technique to mass diffusion processes*, Proc. IASTED, MIC, 1989.

Russell I A D and Webb (1996), *Simulation of the Electrothermal instability in microwave devices using the TLM method*, in TLM - The Wider Applications, Proceedings of an informal meeting held at the UEA, June 1996.

Russer P and Krumpholz M (1993), *The Hilbert Space formulation of the TLM method*, Int. J. Numerical Modelling : Electronic Networks, Devices and Fields, vol. 6, 1993.

Saleh A H M and Blanchfield P (1990), *Analysis of acoustic radiation patterns of array transducers using the TLM method*, Int. J. Numerical Modelling : Electronic Networks, Devices and Fields, vol. 3, 1990.

Schroeder W and Wolff I (1994), *The origin of spurious modes in numerical solutions of electromagnetic field eigenvalue problems*, IEEE Transactions on Microwave Theory and Techniques, vol. 42, no. 4, 1994.

Scott R A and Miklowitz J (1967), *Transient elastic waves in anisotropic plates*, Journal of Applied Mechanics, Transactions of the ASME, (1967).

Selhi H, Christopoulos C and Howe A F (1995), *Development of an induction motor drive phase model based on the TLM method*, Int. J. Numerical Modelling : Electronic Networks, Devices and Fields, vol. 8, 1995.

Shames I H and Cozzarelli F A (1992), *Elastic and inelastic stress analysis*, Prentice-Hall, 1992.

Shibuya T, Nakahara I, Koizumi T and Kaibara K (1975), *Impact stress analysis of a semi-infinite plate by the finite difference method*, Bulletin of the JSME, vol. 18, no. 121, July 1975.

Simons N R S and Bridges E (1991), Equivalence of propogation characteristics for the transmission-line matrix and finite-difference time-domain methods in two dimensions, IEEE Transactions on Microwave Theory and Techniques, vol. 39, no. 2, 1991.

Simons N R S and Sebak A A (1992), *Spatially weighted numerical models for the two-dimensional wave equation: FD algorithm and synthesis of the equivalent TLM model*, International Journal of Numerical Modelling - Electronic Networks, Devices and Fields, vol. 5, 1992.

So P P M, Eswarappa C and Hoefer W J R (1995) , *Parallel and distributed TLM computation with signal processing for electromagnetic field modelling*, Int. J. Numerical Modelling : Electronic Networks, Devices and Fields, vol. 8, no. 3-4, 1995.

Stacey R (1994), *New finite-difference methods for free surfaces with a stability analysis*, Bulletin of the Seismological Society of America, vol. 84, no. 1, February 1994.

Stothard D, Pomeroy S C and Sillitoe I P W (1995), *An application specific processor for TLM*, First International Workshop on Transmission Line Matix (TLM) Modelling - Theory and Applications, Victoria, 1995.

Stubbs D M, Pulko S H and Wilson B (1995), *Extension of the Transmission Line Matrix (TLM) method in its application to lumped networks*, Electron. Letts, 31, 1995.

Stubbs D M, Pulko S H and Wilson B (1996), *Application of Transmission Line Matrix (TLM) method to numerical modelling of a MESFET distributed amplifier*, Electron. Letts, 32, 1996.

Timoshenko S (1934), *Theory of elasticity*, Engineering Societies Monographs, McGraw-Hill, 1934.

Trenkic V, Benson T M and Christopoulos C (1995), *Dispersion analysis of a TLM mesh using a new scattering matrix formulation*, IEEE Microwave and Guided Wave Letters, vol. 5, no. 3, March 1995.

Wang C T (1953), *Applied Elasticity*, McGraw-Hill Book Company, 1953.

Witwit A R M (1994), *Meshing techniques for TLM diffusion problems*, PhD thesis, University of Hull, England, 1994.

Witwit A R M and Pulko S H (1996), *A New boundary treatment for TLM diffusion models and its use with hexagonal meshes*, Numerical Heat Transfer Part B - Fundamentals, vol. 30, no. 3, 1996.

Witwit A R M, Wilkinson A J and Pulko S H (1995), *A method for algebraic analysis of the TLM algorithm*, International Journal of Numerical Modelling - Electronic Networks, Devices and Fields, vol. 8, no. 1, 1995.

Zhang G, Wykes C, Pomeroy S C, 1991, *The application of TLM to the modelling of airborne ultrasonics*, IEE Colloquium on 'Transmission Line Matrix Modelling - TLM', Digest No. 1991/157, 1991.